12-1-2015

Rewetting of Artificially Desiccated Soils: Effect of Gravity on Vapor-Phase Diffusion

Taylor Arland Ball
University of Nevada, Las Vegas

REWETTING OF ARTIFICIALLY DESICCATED SOILS: EFFECT OF GRAVITY ON VAPOR-PHASE DIFFUSION

By

Taylor Arland Ball

Bachelor of Science – Geology

Brigham Young University, 2012

A thesis submitted in partial fulfillment

of the requirements for the

Masters of Science – Geoscience

Department of Geoscience

College of Sciences

The Graduate College

University of Nevada, Las Vegas

December 2015

UNLV | GRADUATE COLLEGE

Thesis Approval

The Graduate College
The University of Nevada, Las Vegas

November 9, 2015

This thesis prepared by

Taylor Ball

entitled

Rewetting of Artificially Desiccated Soils: Effect of Gravity on Vaper-Phase Diffusion

is approved in partial fulfillment of the requirements for the degree of

Master of Science – Geoscience
Department of Geosciences

Michael Nicholl, Ph.D.
Examination Committee Chair

Kathryn Hausbeck Korgan, Ph.D.
Graduate College Interim Dean

David Kreamer, Ph.D.
Examination Committee Member

Zhongbo Yu, Ph.D.
Examination Committee Member

Barbara Luke, Ph.D.
Graduate College Faculty Representative

ABSTRACT

Soil desiccation has been suggested as an economically viable alternative for stabilizing water soluble contaminants in deep vadose zones such as at the Hanford Site. This approach would result in a large volume of the vadose zone being dried out in an effort to eliminate the transport mechanism for aqueous phase contaminants. Protecting the top and sides of the desiccated vadose zone from rewetting is a realistic possibility; however, it would be extremely difficult to restrict the upward migration of water from beneath the desiccated zone. One scenario related to the rewetting of the desiccated soil involves the upward migration of water vapor into the desiccated soil and subsequent adsorption of that vapor onto the soil particles. A series of laboratory experiments was conducted to better understand the processes involved in the migration of water vapor through desiccated soils. Specifically, we considered the relative importance of diffusion and density-driven advection. Water vapor was introduced between a pair of vertically stacked columns filled with desiccated media (empty, BB-, gravel-, and sand-filled columns) to compare the upward and downward migration of the water vapor.

Experiments in all the test media confirm that water vapor migrates preferentially in the upward direction relative to the downward direction. Density differences between humid air (less dense) and dry air (more dense) cause the humid air to rise relative to the dry air (i.e., density-driven advection) in the columns. This combines with vapor phase diffusion leading to increased rates of movement in the upper column. The opposite (i.e., decreased rates) occurs when the vapor moves downward, as density-driven advection works against diffusion. These increased rates of vapor migration in the upward direction led to increased wetting of the media over that in the downward direction.

ACKNOWLEDGEMENTS

First, I would like to thank Dr. Michael Nicholl for allowing me to be a part of this project, for introducing me to the field of vadose zone hydrology, and for advising me throughout this process. It has been a great experience being able to work with you, and I have learned a lot.

It has been a pleasure being part of the UNLV Geoscience community. The faculty, staff, and students here are second to none. A special thanks to everyone that I have met along the way, for making this such a positive time in my life. Thank you to the faculty who have taught me, the office staff who had answers to all of my questions, and fellow students who have become good friends!

I am grateful for the continued love and support of my wife throughout my time as a student. She has had to change more than her fair share of diapers along the way to make sure that I was able to complete this project. I look forward to an exciting future together! The support of our parents, siblings, and extended family has been so valuable to us as well.

Finally, I would also like to give a special thanks to Dr. David Kreamer, Dr. Zhongbo Yu, and Dr. Barbara Luke who agreed to volunteer their time to serve on my committee.

TABLE OF CONTENTS

LIST OF TABLES

LIST OF FIGURES

INTRODUCTION

Soil desiccation has been proposed as a practical means for stabilizing water-soluble contaminants in deep vadose zones (e.g., Oostrom, 2009). This approach entails drying out a large volume of the vadose zone by injecting warm dry air into the contaminated subsurface while simultaneously extracting moist air. It is anticipated that removing liquid water from the vadose zone will eliminate the transport mechanism for aqueous phase contaminants, and thus immobilize them. This process has been suggested as a cost-effective treatment for sites where the contamination is spread over a large area, and is located at depths where excavation costs would be excessive (e.g., Ward, 2008). For example, soil desiccation has been proposed for the highly contaminated Hanford Site in eastern Washington State, where soluble radioactive contaminants have been found at depths of up to 70 m (Fluor Hanford, 2006) over an area of roughly 200 km^2 (DOE, 2008). If successful, the contaminants would be fixed in place, thus reducing the threat to the underlying groundwater and adjacent Columbia River.

A number of studies have been conducted to explore the feasibility of large-scale soil desiccation. The results of numerical simulations (e.g., Ward, 2008), laboratory-scale experiments (e.g., Oostrom, 2009), and field tests (e.g., Truex, 2011) all suggest that creating extremely dry conditions over large volumes of natural soil is possible. However, little attention has been paid to post-treatment rewetting of the desiccated zones that could lead to the remobilization of soluble contaminants. Engineered barriers could be installed around the perimeter of the desiccated zone to protect it from downward infiltration (e.g., surface cap) and lateral flow (e.g., grout curtains). However, it would be extremely difficult to install a physical

barrier that would restrict upward migration of water from beneath the desiccated zone. Mechanisms for the upward migration of liquid water into desiccated soil (i.e., capillary rise) are well understood (e.g., Richards, 1931). Conversely, little is known about the potential for rewetting from the vapor phase. In this scenario, water vapor migrates into the desiccated soil and then adsorbs onto the dry soil particles.

The purpose of this thesis is to better understand the relative importance of vapor-phase diffusion and density-driven advection with respect to the movement of moist air through desiccated soils. It is hypothesized that density-driven advection will combine with vapor-phase diffusion to enhance upward migration, and retard downward migration of water vapor. Simultaneous column experiments are used to evaluate the difference between upward and downward migration of moist air through desiccated media. The experimental media was varied between trials to consider the influence of both pore geometry and adsorptive properties on these processes.

BACKGROUND

Under isothermal and isobaric conditions, the primary mechanisms for the migration of water vapor are diffusion and density-driven advection; both of which result from differences in concentration (C_g; M/L^3). Vapor-phase diffusion occurs when water vapor moves from areas of high concentration to areas of low concentration (e.g., Hillel, 1998). Simple diffusive processes are described by Fick's first and second laws, which relate the diffusive flux to the concentration gradient (e.g., Ho and Webb, 2006). Fick's first law relates mass flux of the diffusive component to the concentration gradient for steady state systems, while the second law addresses time-variant concentration. For both laws, the proportionality constant used to describe the diffusion of a specific gaseous phase (e.g., water vapor) in open air is referred to as the gas diffusion coefficient (d_g; L^2/t), which is dependent on pressure, temperature, and bulk gas composition (e.g., air).

Diffusion through porous media is more complex than in open air. Solid particles block diffusion by: 1) reducing the cross-sectional area; 2) restricting lateral diffusion; and 3) creating longer pathways for longitudinal diffusion. Because these effects depend on properties that are difficult to measure (i.e., pore geometry) they are typically parameterized in terms of the following average measures: 1) porosity (φ; L^3/L^3); 2) pore diameter (d; L); and 3) tortuosity (τ; L/L). Likewise, the gas saturation (S_g; L^3/L^3) is commonly used to account for the presence of liquid in the media (i.e., partially saturated conditions). For a given media, the effective diffusion coefficient (D_g; L^2/t) can be measured through experiment (e.g., Kreamer, 1988), or estimated from d_g and the aforementioned media properties (e.g., Ho and Webb, 2006).

An analytical solution to Fick's second law can be obtained for one-dimensional diffusion of water vapor into a semi-infinite porous media (e.g., Baehr, 1987; Ho and Webb, 2006). The gas occupying the homogeneous and isotropic media is assumed to be uniform in terms of temperature, pressure, and initial vapor concentration (C_i; M/L^3). At t = 0, the vapor concentration at the boundary is instantaneously increased to C_{go} (M/L^3). Under these assumptions, Eq. (1) predicts the water vapor concentration (C_g; M/L^3) as a function of time (t) and distance (x) away from the boundary (modified from Baehr, 1987):

$$\frac{C_g}{C_{go}} = 1 - \left(erfc\left(\frac{x}{2\sqrt{tD_g/R_g}} \right) * \left(1 - \frac{C_i}{C_{go}} \right) \right) \quad (1)$$

where R_g is the dimensionless retardation coefficient that describes the partitioning of the vapor onto the liquid or solid phase by adsorption (e.g., Bouwer, 1991).

Density-driven displacement of one air mass by another in the absence of diffusion and mixing (i.e., piston-type displacement) was considered by Falta (1989) for the case of organic vapors in soil. They adapted Darcy's Law to predict the velocity (V_p; L/t) of the interface between two air masses of different densities. Their result can be restated for the displacement of dry air by humid air in a desiccated soil (no water phase present) as:

$$V_p = \frac{kg}{\varphi \mu_g}(\rho_{hum} - \rho_{dry}) \quad (2)$$

Where k is the intrinsic permeability of the media (L^2), and g is the gravitational constant (L/t^2). Both air masses are assumed to have the same dynamic viscosity (μ_g; M/L-t). The driving force in Eq. (2) is taken to be density differences between the dry and humid air masses ($\rho_{hum} - \rho_{dry}$; M/L^3). For water vapor in air, $\rho_{hum} < \rho_{dry}$, which indicates that the water vapor will flow upward relative to the dry air. Note that the assumption of a sharp interface between the dry and humid air is not physically realistic. However, Eq. (2) can be employed to provide a first-order estimate of density-driven advection.

A simple mathematical analysis was used to compare the relative importance of vapor-phase diffusion (Eq. 1) and density-driven advection (Eq.2) under isothermal and isobaric conditions. For illustrative purposes, we arbitrarily defined a 100 m thick hypothetical vadose zone (Appendix B) composed of well-sorted, medium-to-fine grained sand (porosity of 0.35, mean grain diameter of 0.25 mm). In addition, we assumed the sand to be non-adsorptive ($R_g = 1$) and fully desiccated ($C_i = 0$). Air beneath the desiccated vadose zone (> 100 m) is assumed to be saturated with water vapor (i.e., 100% relative humidity). After 1,000 days, Eq. (2) predicts that the interface between saturated and dry air will move upward from 100 m below land surface to 35.1 m below land surface (Figure A.1-1). Over the same time span, Eq. (1) predicts that diffusion would move small concentrations of water vapor to the land surface, and produce the continuous concentration profile shown in Figure A.1-1. This simple analysis suggests that

vapor-phase diffusion and density-driven advection are of similar importance in the vertical migration of water vapor.

METHODS

Experiments designed to measure the movement of water vapor through desiccated porous media were conducted in two 29.0 cm tall vertical columns (5.08 cm inside diameter) constructed from Schedule 40 PVC pipe (Appendix F). The columns were stacked (Figure A.1-2) to provide a direct measurement of gravitational effects on vapor migration. Gravity was expected to reinforce vapor diffusion in the upper column, and impede it in the lower column. The proximal end of each column connects to a reservoir held at high relative humidity, producing a common boundary condition (Appendix F). The columns were separated from the humidity reservoir by porous membranes (9.6% open area) constructed from plastic and stainless steel (Appendix D). Based on preliminary experiments (Appendix N), the distal end of each column was vented to the laboratory environment using ~1 m of vinyl tubing to simulate a distant atmospheric boundary (Appendix F). The progression of humid air through each column was tracked at 5 cm intervals using individually calibrated relative humidity (RH) sensors (Appendix K, K). The columns and surrounding environment (relative humidity, temperature, and barometric pressure) were monitored at regular intervals using a Campbell Scientific™ CR23X data logger and AM416 Relay Multiplexer (Appendix J).

All experiments were conducted inside a constant temperature enclosure (Appendix I) set to a nominal value of T = 25 ^{o}C. The isothermal condition minimizes the possibility of condensation within the columns, assures that density differences are controlled solely by relative humidity, and allows direct calculation of C_g from measured values (RH, T). The definition of RH (e.g., Lawrence, 2005) relates the vapor pressure for water (P_V) to the saturated vapor pressure (P_{sat}):

$$RH = \frac{P_V}{P_{sat}} X\ 100 \tag{3}$$

where P_{sat} is solely a function of temperature (e.g., Abtew, 2013) and has a value of 3,169 Pascals at our experimental temperature of 25 ^{o}C. A variation of the ideal gas law (e.g., Falta, 1989) can then be used to calculate C_g:

$$C_g = \frac{P_v M}{RT} \tag{4}$$

where M is the molecular weight of water vapor (18 g/mol , e.g., Lide, 2005), R is the ideal gas constant (8.314 J/mol-K), and T is temperature (K).

The procedure for each experiment began with packing dry media into both columns (Appendix M). The filled columns were then sealed to the humidity reservoir, connected to the sensors, and attached to a support (Appendix H) within the constant temperature enclosure (Appendix I). The humidity reservoir was capped and allowed to equilibrate with air in the columns. An ultrasonic fog generator (Figure A.1-2) sealed within a separate humidity chamber (Appendix G) was turned on for ~2 hours. All components of the experiment were then allowed to equilibrate to 25 ^{o}C for 10-12 hours. This process produced ~11.2 *l* of air in the humidity chamber at RH ~ 100%, T = 25 ^{o}C (~10X the air volume of both columns and humidity reservoir when empty). Experiments were then initiated by: 1) opening the constant temperature enclosure, 2) manually connecting the humidity chamber to the humidity reservoir, and 3) resealing the enclosure.

Performing these steps quickly imposes a rapid increase in humidity at the proximal end of each column (i.e., approximates a step change in the relative humidity boundary condition). Experiments were ended when the upper column experienced minimal daily changes in RH. In addition to this procedure, the weight of each column was obtained to a resolution of 0.1 grams immediately prior to the start of an experiment, and immediately upon termination of an experiment. The change in weight during the experiment is attributed to the addition of water onto particle surfaces by adsorption.

The first experiments were performed with the columns empty (largest possible pores, 100% porosity, and negligible adsorption onto the column) to establish a baseline. In subsequent experiments, the pore size (mean, distribution) and adsorptive capability of the media were varied. The first material tested consisted of uniform 6 mm diameter plastic spheres (BB's) packed to ~41% porosity. This hydrophobic media exhibits relatively large, uniform pores and minimal surface adsorption. The second media tested was very fine gravel (2-4 mm diameter, sub-angular to sub-rounded shape). This material produced a similar porosity (~43.5%) as was observed in the BB-filled columns, with smaller and less uniformly distributed pores. The hydrophilic nature of the material was expected to introduce a slight adsorptive capacity. The most complex material considered was a 30-40 mesh (0.42-0.59 mm) washed silica sand. When filled with this rounded/sub-angular material the column had a similar porosity (~42%) to the BB's and gravel, but much smaller pores and greatly increased surface area. Complete descriptions of each media are provided in Appendix M, along with the methods used for preparation and packing the columns.

RESULTS

Measured relative humidity (RH) is shown as a function of time for the four test materials (empty columns, BB's, fine gravel, and 30-40 sand) in Figures 3-6, respectively. Each plot also shows humidity in the laboratory room and at the humidity reservoir (BC1). The initial humidity for each experiment reflects ambient conditions in the laboratory during column assembly. For each test, the start time (t = 0) was taken to be when the humidity chamber (~100% RH) was manually connected to the humidity reservoir (Figure A.1-2). Experiments were ended when temporal changes in column RH became small. As a result, the duration of each experiment varied between test materials (~4 - 91 days). Data was recorded at 1-minute intervals (empty columns, BB's, fine gravel) or 10-minute intervals (30-40 sand). Complete details on the experiments are provided in Appendix N, which also includes results from preliminary experiments (sealed and partially vented columns).

In all four experiments, RH in the humidity reservoir (BC1) rose rapidly to >75%, then quickly leveled off to transition into apparently asymptotic behavior (Figures 3-6). Sensors located along the columns (U1-5, L1-5) responded more slowly than at BC1, producing shallower curves and lower values of RH. Moving away from BC1, the slope of the initial increase became progressively less steep, the transition zone to asymptotic behavior became broader, and the final RH declined. Throughout the duration of each experiment, measured RH was consistently higher in the upper column than in the lower column (i.e., U1 > L1; U2 > L2, etc.). Because columns were vented to the laboratory at U5 and L5, large fluctuations in laboratory RH during the course of an experiment resulted in deviations from the overall upward trajectory of RH. These

deviations decrease in magnitude from the distal end to the proximal end of each column (i.e., U5 to U1, L5 to L1), and are also more noticeable in the lower column than in the upper column. Additionally, changes in room humidity had a smaller effect during the initial rapid rise of RH at the beginning of experiments than during the asymptotic phase. Specific details of experiments in each media are presented below.

In the empty column experiment (Figure A.1-3), RH increase in the upper column closely mimicked the boundary (BC1). At all measurement times, RH decreased slightly with distance from the humidity reservoir (i.e., U1>U2>U3>U4). Conversely, there was considerable differentiation in RH with distance along the lower column. Fluctuations in laboratory RH (16-31%) impacted measurements in the column all the way to the boundary (BC1), but had a noticeably greater effect on the lower column (L1-4) than in the upper column (U1-4). After a period of ~4 days, all sensors in the upper column recorded RH values similar to that of the humidity reservoir, and showed signs of a continued upward trajectory. In comparison, RH values in the lower column did not converge, and were significantly lower than BC1. No adsorption from the humid air occurred during this experiment due to the absence of media within the column.

Filling the columns with coarse media in the form of uniform plastic BB's (Figure A.1-4) retarded the overall advancement of humid air with respect to observations for the empty columns. The advancing humid front showed increased separation between sensor measurements in both columns, as well as wider transition zones. The shape of the recorded RH data in the

upper column (U1-4) did not closely resemble BC1 as in the empty column experiment, although it did eventually reach >75%. The RH in the lower column (L1-4) stabilized at lower values than in the upper column. Measurements in the columns after the initial increase responded to fluctuations in laboratory RH, which ranged from 14 to 31%; such changes are most noticeable in the lower column, but can be seen propagating upward from L4 to U4. One clear example occurred in response to a substantial decrease in laboratory RH beginning near the end of day 2 (Figure A.1-4). This resulted in a downward shift in RH that propagated through the lower column immediately prior to its apparent stabilization; RH in the upper column continued on a slight upward trajectory. This experiment lasted ~6 days, during which time, 0.2 g of water vapor adsorbed onto particle surfaces in both the upper and lower columns.

The added complexity of the fine gravel (non-uniform particles) further retarded vapor movement (Figure A.1-5) with respect to the similarly sized BB's (Figure A.1-4). There was increased separation between all column sensors and BC1, and the advancing humid front was further delayed relative to the BB-filled column. Roughly twice as much time (~12 days) was needed to reach sufficiently high values of RH to end the experiment. Both the upper and lower column ended with RH values that were smaller than in the BB-filled column, although the relative difference between the upper and lower columns in both experiments was similar. The influence of laboratory RH, which ranged from 9 to 19%, altered the RH in the lower column more than in the upper column. The RH at U5 shows an overall increasing trend that follows a diurnal pattern similar to the laboratory, while the RH at L5 is a smooth variation of the

laboratory RH. During this experiment, adsorption of water vapor added 0.2 g to the mass of the lower column and 0.4 g to the upper column.

Vapor movement in columns filled with 30-40 sand (Figure A.1-6) was much slower than in the coarse media (Figures 4, 5). After the initial spike in RH upon connection of the humidity reservoir, values >70% RH were observed at all column locations (1-4) after ~17 days, at which point there was a significant decline in the rate of increase. Values of RH >75% were observed at all column locations (1-4) after 27 days. At this point, we opted to let the experiment continue to run for several more weeks. This experiment showed a significant decrease in separation between the recorded RH in the humidity reservoir (BC1) and both test columns, relative to the other experiments. The length of the experiment increased substantially to ~91 days. Even with this increase, the difference in RH between U1 and BC1 at the end of the experiment was greater than at the end of previous experiments. This experiment differed from the others in that it yielded the most similarly looking results between the upper and lower columns. In addition, both the upper and lower columns responded in a similar fashion (including at sensors U5 and L5) to laboratory fluctuations, which had a much higher range than in the other experiments (10 to 63%). Despite the apparent similarity between the two, the upper column did exhibit consistently higher values of RH than the lower column throughout the experiment. As with the previous experiments, response to laboratory fluctuations was greater in the lower column than in the upper column. During this experiment, 1.6 g of water adsorbed onto particles in the upper column, and 0.9 g was added to the lower column.

The average vapor concentration in the first 20 cm of each column (Figure A.1-7) was estimated by converting measured RH at the proximal four sensors (U1-4, L1-4) to concentration (g/m^3) using Eq. (3) and (4). It was assumed that measured RH was representative of a 5 cm segment of each column (2.5 cm above/below each sensor). The distal 9 cm of each column was ignored because laboratory conditions clearly influenced measurements at sensors U5 and L5. Curves associated with the average vapor concentration (Figure A.1-7) begin with concave upward slopes before transitioning to slopes that are concave downward. Measured RH in the empty column responded "immediately" (< 1 minute) to the initial introduction of water vapor; as media complexity increased, the initial response became more and more delayed, including between the BB and gravel-filled columns despite the similarity in pore volume. By design, all experiments ended with similar average concentrations in the upper column, although the time it took to reach these values varied significantly. At all measurement times, and in all experiments, the average concentration in the lower column was lower than in the upper column. The addition of media with higher adsorptive capacities decreased the initial differences between the average concentration in the upper and lower columns. Additionally, the average vapor concentrations in the columns involving the coarsest media (BB's and gravel) diverge over time, while the others (empty and 30-40 sand) converge.

DISCUSSION

In all experiments, water vapor moved preferentially into the upper column with respect to the lower column, confirming that density-driven advection reinforces diffusion in the upward direction and opposes it in the downward direction. This is why the RH in the upper column was consistently higher than in the lower column for a given time in each experiment. To help illustrate this, the average concentration of water vapor (derived from the RH) in the proximal 20 cm of the lower column is plotted as a function of the average concentration in the upper column as Figure A.1-8. All experiments began at equilibrium, resulting in data that plots on the 1:1 line. As the vapor preferentially migrates upward, the average vapor concentration in the upper column exceeds that of the lower column producing data that plots below the 1:1 line. This effect appears to diminish with increasing media complexity, but is still present in the sand-filled column. In two of the experiments (the empty and sand-filled columns), the data eventually re-converges towards the 1:1 line (Figure A.1-8). This occurs in the empty column experiment because the upper column quickly reached near equilibrium with the vapor source (humidity reservoir), while the lower column slowly increased throughout the duration of the experiment (Figure A.1-3). In the sand-filled column experiment (Figure A.1-6), both the upper and lower column approached a near equilibrium condition with the humidity reservoir due to the extended length of the experiment. Conversely, the difference in concentration between the upper and lower columns increased as the experiments progressed for both of the coarse media experiments (BB's and fine gravel). This is the result of the RH stabilization that occurred in the lower column during these experiments (Figures 4 and 5). This stabilization is attributed to the

opposing forces of density-driven flow (upward) and vapor-phase diffusion (downward) in the lower columns.

The empty column experiment (Figure A.1-3) represents the simplest system possible for unimpeded vapor migration, yielding the fastest rates of vapor movement in both columns. The highest recorded values of RH occur at the proximal end (U1 and L1) of each column, and gradually decrease with a slight time delay towards the distal end without overlap, suggesting that vapor movement is dominated by diffusion with no mixing. Evidence of density-driven advection is present in the form of early decreases in RH (especially in the lower column) that occur as humid air (less dense) within the columns rises, and is replaced by dry air (more dense) from the box (Appendix I) during the initial connection of the humidity chamber. Additionally, density-driven advection is displayed in the instantaneous response of individual sensors along the upper and lower columns to changing laboratory RH. As less dense humid air within the columns rises, it is replaced by air from the laboratory entering the system at L5. The cycle is repeated as this air in turn interacts with water vapor inside of the column, becomes less dense, and rises. The rising air mass can be seen across all sensors (L4 to U4). The opposing force of density-driven advection to diffusion in the lower column decreases the rate of vapor movement relative to the upper column.

The addition of the uniform BB's to the test columns limited vapor movement to pore openings, leading to a reduction in the overall rate of vapor migration in both directions. The experiment was allowed to run longer than the empty column experiment to compensate for the decreased

rate of vapor movement. The hydrophobic nature of this media limited the adsorption of water vapor. The downward movement of the already "slow" vapor (i.e., lower column) was reduced to a point that a state of equilibrium was reached in the lower column after a few days. This stabilization, not observed in the upper column, is evidence of the competing forces of diffusion and density-driven advection in the lower column. Near the end of day 2 during the experiment (Figure A.1-4), a slight increase in laboratory RH was followed by a large decrease in RH that propagated almost instantaneously through the lower column, but had little effect on the upper column. Similar to what occurred in the empty column experiment, air in the laboratory entered the system at L5 creating a smooth variation of laboratory RH. The air became less dense, then rose within the lower column until it entered into the humidity reservoir where it interacted with water vapor. Once in the humidity reservoir (highly humid environment), the air mass became similar to the air in the humidity chamber, explaining the absence of sensor response in the upper column.

Vapor movement was further slowed with the addition of the gravel to the test columns. This media had particles that varied in size and shape, which reduced the overall permeability of the system and increased the vapor pathways. Additionally, the hydrophilic nature of the gravel relative to the BB's, acted to both slow the advancing vapor as well as decrease the overall RH within the system by removing water vapor from the air. The increased adsorption that occurred in the upper column of this experiment relative to the lower column suggests that more water vapor was present in the upper column than in the lower column. This supports the notion that vapor movement is enhanced in the upward direction. As in the BB-filled column experiment,

stabilization in the lower column occurred as laboratory air entered the system at L5 and moved upward through the lower column due to density differences. After passing through the humidity reservoir, the air had little effect on the RH in the upper column.

During the sand-filled column experiment, the rate of vapor movement was impeded in both directions to the point that all sensors (upper and lower columns) were heavily influenced by fluctuations in laboratory RH. This is due to the increased tortuosity and decreased permeability that came from significantly decreasing the size of the media. The decrease in media size also caused a significant increase in the total media surface area. This led to greater adsorption of the vapor onto the media, which further impeded its movement by removing moisture from the air. The impact of fluctuating RH in the laboratory on the slow moving vapor masked the effects of density-driven advection that were observed in previous experiments (i.e., upward moving vapor in the lower column). In fact, individual sensors responded differently to these fluctuations than observed previously. Figure A.1-9 compares the sensor responses in both the upper and lower columns (U4 to L4) during the last five major laboratory fluctuations of the experiment. These have been identified in Figure A.1-6 for convenience. Air from the laboratory enters the system at the distal ends of the columns, U5 and L5 (exhibited by the smoothing variation of laboratory RH), and then propagates towards the proximal ends of the columns. For a given event, sensors toward the distal ends of the column changed more than at the proximal end, which was nearest to the humid boundary (Figure A.1-9). In addition, sensors in the lower column had a greater response (i.e. larger changes) to changes in laboratory RH than in the upper column (Figure A.1-9) suggesting that vapor movement was slower in the lower column than in the upper column

(i.e., effects of density-driven advection). In addition, as with the gravel, increased adsorption of water vapor in the upper column from the presence of more water vapor in the pore spaces provides further evidence of density-driven advection.

As water vapor migrated through the test columns it interacted with the desiccated media, leading to adsorption. Molecular interactions between the migrating water vapor and the desiccated media attract the vapor to the particle surfaces (e.g., Ruiz, 1998). The amount of adsorption in each column is a function of the wetting characteristics of the media (hydrophilic or hydrophobic), the surface area of the media, and the amount of water vapor in the open pore spaces. The experiments involving hydrophilic media (especially the 30-40 sand), show the wetting potential of water vapor. Even small amounts of water vapor can contribute to adsorption. For example, the estimated mass of the water vapor in the columns (derived by multiplying the average concentration by pore volume) was orders of magnitude smaller than the mass adsorbed onto the media. In the sand-filled columns, the mass of the vapor in each column was about 0.003 g at the end of the experiment, leading to 1.6 g adsorbed in the upper column, and 0.9 g in the lower column (< 2 orders of magnitude difference).

CONCLUSIONS

Density plays an important role in the movement of water vapor through porous media. Water vapor migration through desiccated media occurs preferentially in the upward direction than in the downward direction. In the upward direction, movement is driven by a combination of vapor-phase diffusion and density-driven advection. Conversely, in the downward direction these forces oppose each other. Although changes to the size, shape, uniformity, and hydrophobicity of the media can diminish or even hide these effects by physically impeding the pathway of the migrating vapor, different rates of movement were consistently observed, even in the most complex media considered (i.e., 30-40 sand). Additionally, small amounts of water vapor that may seem insignificant can rewet desiccated media as it adsorbs onto its surface. Enhanced vapor movement in the upward direction led to higher amounts of adsorption in the upper column. Conversely, slower vapor movement in the downward direction led to lower amounts of adsorption in the lower column. Although this study focused specifically on the upward and downward movement of water vapor through desiccated media, vapor density should be considered when describing subsurface vapor migration independent of direction.

APPENDIX A: FIGURES

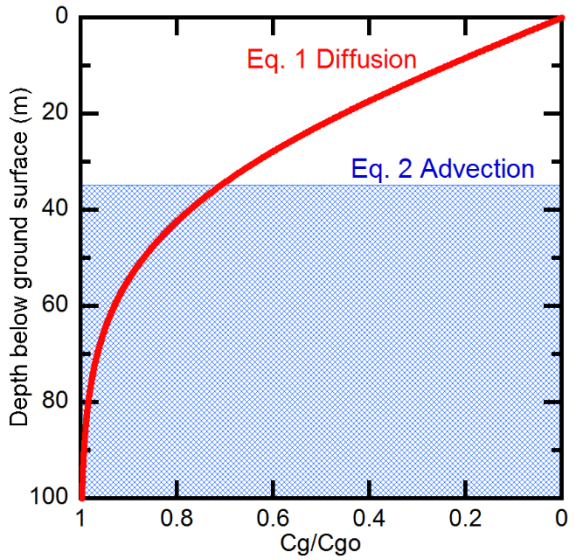

Figure A.1-1: Pre-experimental estimation of diffusion and density-driven advection. An order of magnitude estimate of the relative importance of vapor-phase diffusion (Eq. 1) and density-driven advection (Eq. 2) in a hypothetical vadose zone (100 m thick) at 1,000 days post desiccation. The red line shows the concentration profile associated with vapor-phase diffusion. The blue crosshatch pattern shows the humid/dry air interface for density-driven advection and represents pore spaces that are fully saturated with water vapor, while the white zone remains fully desiccated. In both instances, the closer C_g/C_{go} is to 1, the higher the water vapor concentration at a particular depth. Estimation of input parameters from the assumed properties of the vadose zone is described in Appendix B.

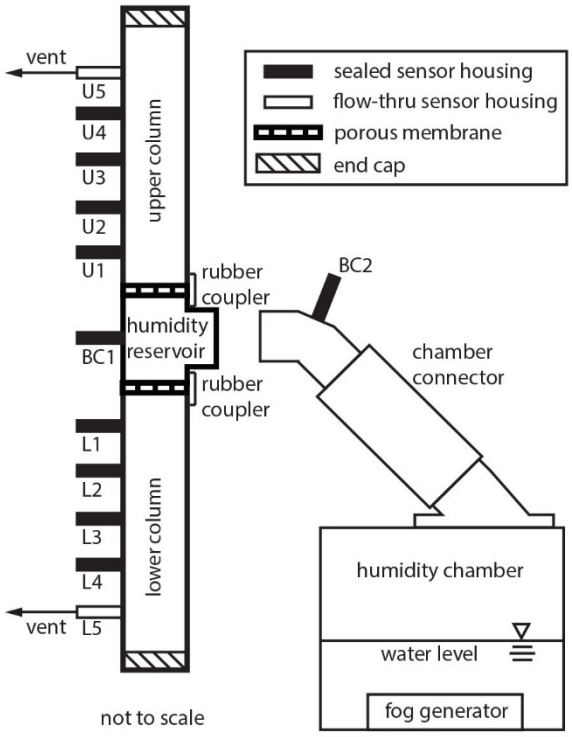

Figure A.1-2: Experimental design. A conceptual model of the experimental design shows columns stacked above and below a humidity reservoir. Sensor housings are aligned along each column with U1 and L1 placed 2.5 cm from porous membranes that separate the media from the humidity reservoir. Additional sensor housings (U2-5 and L2-5) are spaced at 5 cm intervals from U1 and L1. Humidity sensors are affixed to sensor housings U1-5, L1-5, and BC1-2, with thermocouples at U2, U4, L2, L4, and BC1. The distal end of each column (U5 and L5) is vented to the laboratory environment. Humid air is generated in the humidity chamber. The apparatus shown here is located in a temperature-controlled enclosure (Appendix I). All construction details are found in Appendices C through H.

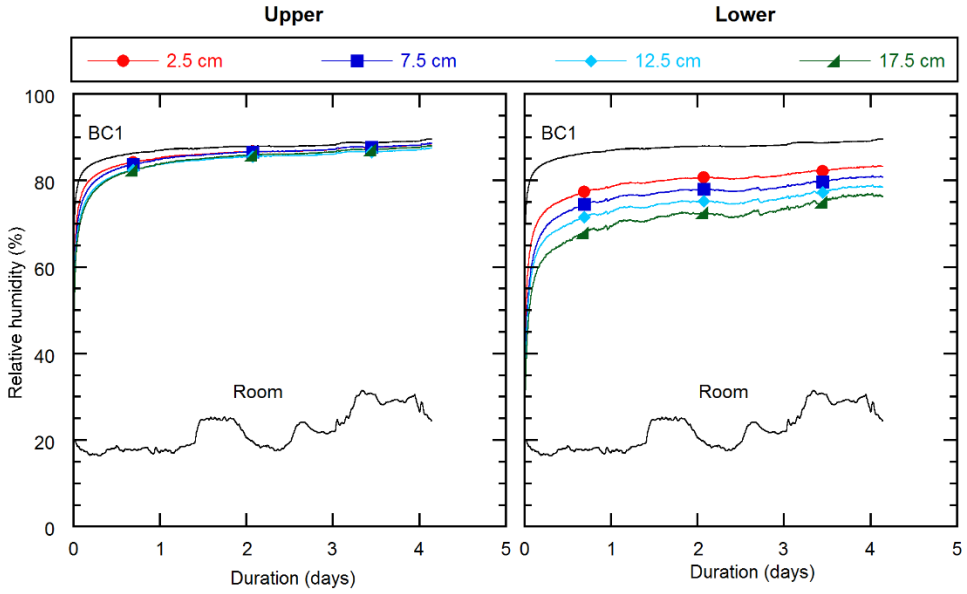

Figure A.1-3: Empty column. Relative humidity in the upper and lower columns at distances of 2.5 cm (U1/L1), 7.5 cm (U2/L2), 12.5 cm (U3/L3), and 17.5 cm (U4/L4) from the respective porous membrane when both columns were empty. This test did not capture data at 22.5 cm (U5/L5). Data from the upper column (left) is shown beside data from the lower column (right). In each plot, relative humidity in the humidity reservoir (BC1) and laboratory (Room) are shown for reference. The total duration of this experiment after connecting the humidity chamber to the humidity reservoir was 4 days, 3 hours, and 20 minutes.

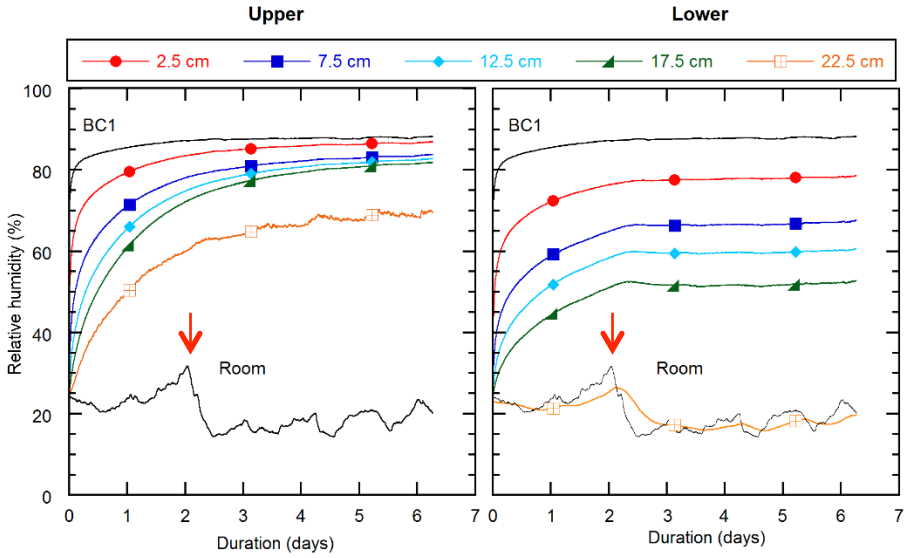

Figure A.1-4: Plastic BB's. Relative humidity in the upper and lower columns at distances of 2.5 cm (U1/L1), 7.5 cm (U2/L2), 12.5 cm (U3/L3), 17.5 cm (U4/L4), and 22.5 cm (U5/L5) from the respective porous membrane when both columns were filled with plastic BB's. Data from the upper column (left) is shown beside data from the lower column (right). In each plot, relative humidity in the humidity reservoir (BC1) and laboratory (Room) are shown for reference. The red arrow shows a particular point of interest when RH in the laboratory decreased suddenly, which was followed by stabilization of RH values in the lower column. The total duration of this experiment after connecting the humidity chamber to the humidity reservoir was 6 days, 6 hours, and 16 minutes.

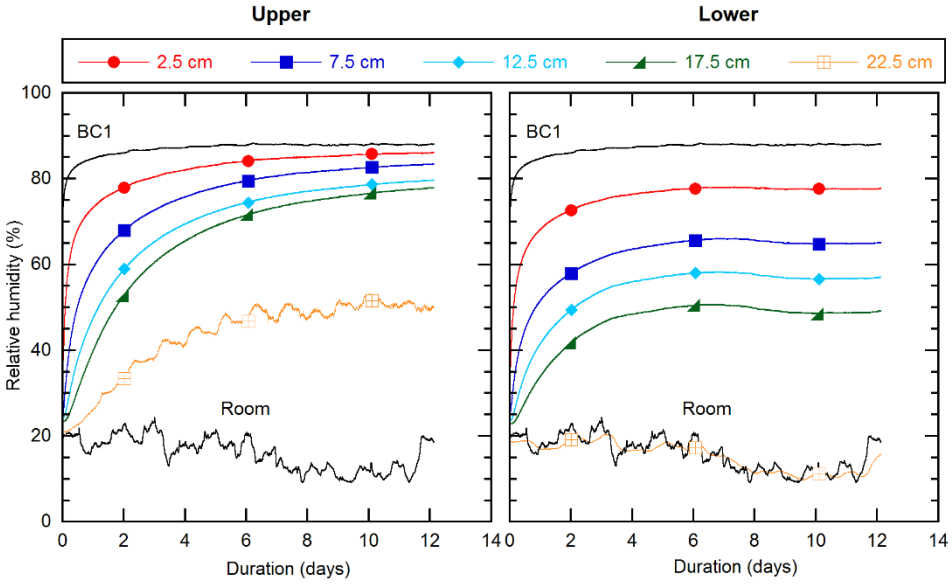

Figure A.1-5: Fine gravel. Relative humidity in the upper and lower columns at distances of 2.5 cm (U1/L1), 7.5 cm (U2/L2), 12.5 cm (U3/L3), 17.5 cm (U4/L4), and 22.5 cm (U5/L5) from the respective porous membrane when both columns were filled with fine gravel. Data from the upper column (left) is shown beside data from the lower column (right). In each plot, relative humidity in the humidity reservoir (BC1) and laboratory (Room) are shown for reference. The total duration of this experiment after connecting the humidity chamber to the humidity reservoir was 12 days, 2 hours, and 57 minutes.

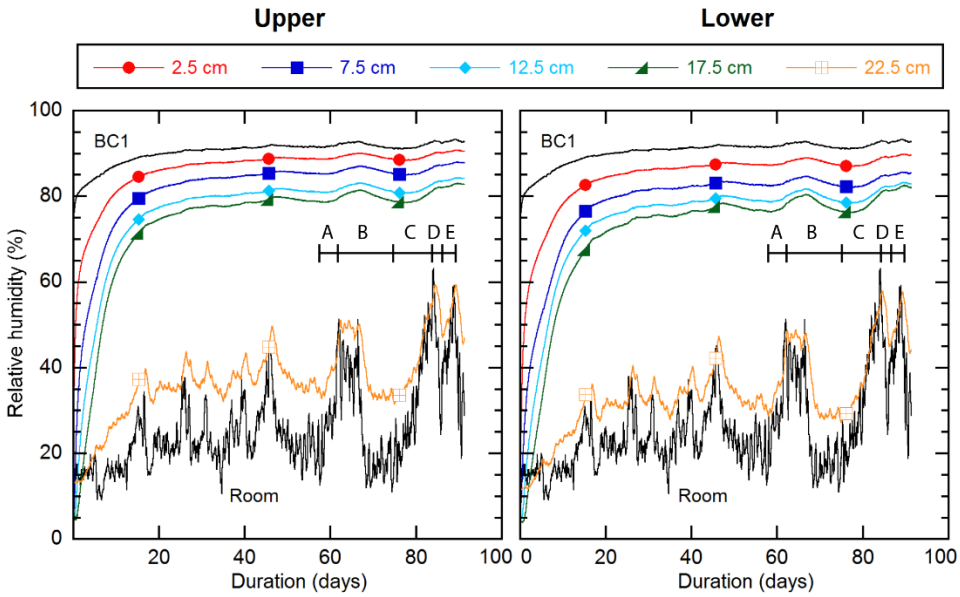

Figure A.1-6: 30-40 sand. Relative humidity in the upper and lower columns at distances of 2.5 cm (U1/L1), 7.5 cm (U2/L2), 12.5 cm (U3/L3), 17.5 cm (U4/L4), and 22.5 cm (U5/L5) from the respective porous membrane when both columns were filled with 30-40 sand. Data from the upper column (left) is shown beside data from the lower column (right). In each plot, relative humidity in the humidity reservoir (BC1) and laboratory (Room) are shown for reference. Letters A-E are associated with local maxima and minima that occur from fluctuating RH in the laboratory. The total duration of this experiment after connecting the humidity chamber to the humidity reservoir was 91 days, 7 hours, and 50 minutes.

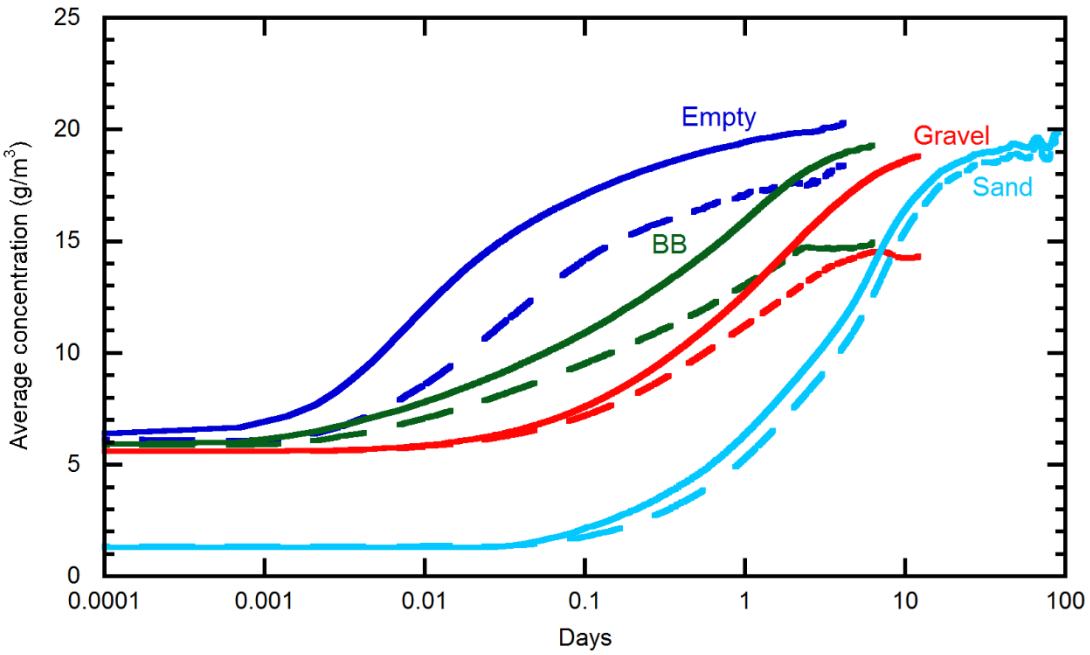

Figure A.1-7: Average concentration of water vapor over time. Estimated vapor concentration (g/m^3) of water vapor within the distal 20 cm of each column (solid – upper; dashed – lower) for all four experiments. Time is shown on a log-scale to facilitate comparison between experiments of vastly different duration (4-91 days).

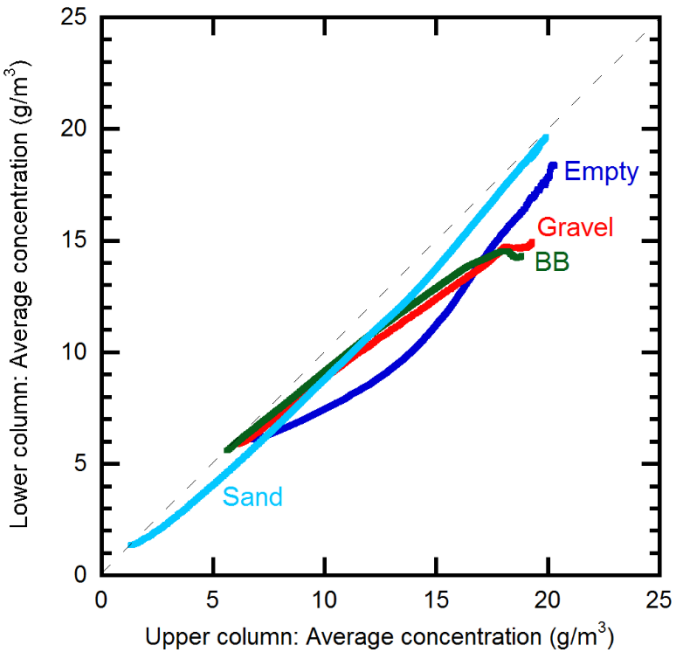

Figure A.1-8: Average vapor concentration in the upper and lower columns. A comparison of the average vapor concentration (g/m^3) in the upper column relative to the lower column for each experiment. Vapor movement in each experiment appears to preferentially move into the upper column (i.e., higher vapor concentrations) relative to the lower column.

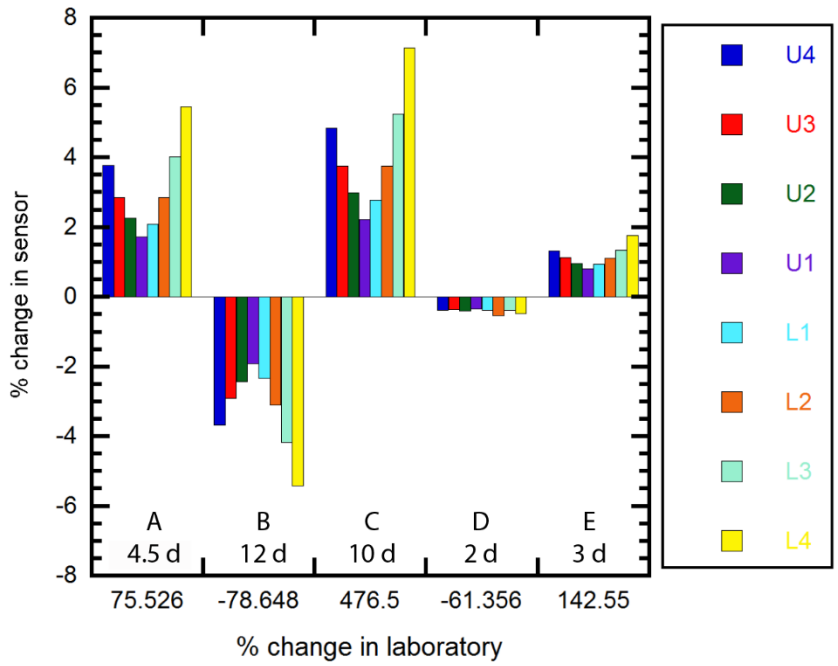

Figure A.1-9: Sensor response to fluctuating laboratory RH. Sensor response to the last five major changes in laboratory RH during the sand-filled column experiment (beginning with the increase after day 60 in Figure A.1-6). In all instances, sensors in the lower column were most affected by laboratory changes. The percent increase/decrease of the RH in the laboratory was obtained using local maxima/minima over a specific time. The time was calculated to be the amount of time from one local maxima/minima to the following minima/maxima. These are labeled as A-E in Figure A.1-6.

APPENDIX B: HYPOTHETICAL SOIL

B.1 Assumptions

The relative importance of vapor-phase diffusion and density-driven advection were evaluated by comparing predictions based on Eq. (1) to those from Eq. (2). Important assumptions and derived parameters used in the analysis are described in this appendix. General assumptions related to the ambient conditions and soil composition is presented in Table B.1-1.

PARAMETER	VARIABLE	ASSUMED VALUE	UNITS
Temperature	T	25	^{o}C
Pressure	P	1	atm.
Initial water vapor concentration	C_i	0	kg/m^3
Vadose zone depth	x	100	m
Average grain diameter	D	0.25	mm
Porosity	φ	0.35	---
Retardation factor	R_g	1	---
Gas phase saturation	S_g	1	---
Time	t	8.64X10^7	sec.

Table B.1-1: Assumptions for hypothetical soil. Important assumptions associated with both equations.

B.2 Vapor-phase diffusion

Equation 1 for vapor-phase diffusion was used to create a concentration profile that showed the changing concentration of water vapor in the pore spaces relative to the saturation concentration as a function of both time and distance away from the boundary:

$$\frac{C_g}{C_{go}} = 1 - \left(\text{erfc}\left(\frac{x}{2\left(tD_g/R_g\right)^{\frac{1}{2}}} \right) * \left(1 - \frac{C_i}{C_{go}}\right) \right) \quad (1)$$

where C_i is the initial water vapor concentration (kg/m^3) , C_{go} is the saturated water vapor concentration (kg/m^3) , R_g is the dimensionless retardation factor, and D_g is the effective diffusion coefficient (6.41X10^{-6} m^3/kg).

The saturated water vapor concentration was determined from the ideal gas law (e.g., Falta, 1989):

$$\mathrm{C_{go}} = \frac{\mathrm{P^0 M}}{\mathrm{RT}} \quad (A\ 1)$$

where $\mathrm{P^0}$ is the saturated water vapor pressure (3.169 kPa), $M$is the molecular weight of the water vapor (18.015 g/mole), R is the universal gas constant (8314 kg-kPa/mole-^{o}C), and T is the temperature (^{o}C). The saturated vapor pressure is 0.02 kg/m^3 at a temperature of 25 ^{o}C and 1 atmosphere (101.325 kPa) pressure using values obtained from Lide (2005).

The effective diffusion coefficient (Ho and Webb, 2006) was obtained by multiplying the gas diffusion coefficient (d_g), which is the proportionality constant used in Fick's first and second laws, by properties of the porous media: porosity (φ), gas saturation (S_g), and tortuosity (τ).

$$D_g = d_g * \varphi * S_g * \tau \quad (A\ 2)$$

The gas diffusion coefficient for water vapor in air is $2.56X10^{-5}$ (Hillel, 1998), the porosity and gas saturation were assumed (Table 1). Tortuosity, which describes the curved path of vapor movement through the pore space in soil, was estimated using porosity and gas saturation estimates as follows (e.g., Falta, 1989):

$$\tau = \varphi^{1/3} * {S_g}^{7/3} \quad \text{(A 3)}$$

In instances when adsorption is considered due to the partitioning of water vapor into the liquid or solid phase, the retardation factor can be calculated by (e.g., Bouwer, 1991):

$$R_g = \frac{\rho_b K_D}{\varphi} + 1 \quad \text{(A 4)}$$

where ρ_b is the soil dry bulk density (M/L^3), and K_D is the partitioning coefficient (L^3/M) between the gas phase and the solid soil particles, and φ is porosity. Here, we chose not to consider adsorption of water vapor onto the desiccated soil, and therefore the value of 1 was used.

B.3 Density-driven advection

Equation 2 for density-driven advection (Falta, 1989) shows the displacement of one air mass by another in the absence of diffusion and mixing (i.e., piston-type displacement) due to density differences between water vapor and dry air under the assumption that the dynamic viscosity (Roy, 1970) of each air mass is equal ($1.83 X 10^{-5}$ kg/ms)

$$V_p = \frac{kg}{\varphi \mu_g}(\rho_{hum} - \rho_{dry}). \quad (2)$$

In this equation, k is the intrinsic permeability (3.52 X 10^{-11} m^2), g is the gravitational constant (9.806 m/s^2), and $\rho_{hum} - \rho_{dry}$ is the density difference between humid and dry air (1.18 kg/m^3 – 1.17 kg/m^3, respectively).

The intrinsic permeability was estimated using the following equation (Nield, 2006):

$$k = \frac{D^2 \varphi^3}{180(1-\varphi)^2} \quad (A\ 5)$$

where D is the average grain diameter and φ is porosity. For our hypothetical soil, the diameter of 0.25 mm was chosen because it represents the diameter boundary of the medium-fine grained sand interface.

The density of each air mass (water vapor and dry air) was estimated mathematically in a similar way (e.g., Falta, 1989):

$$\rho_{hum} - \rho_{dry} = \frac{P^0(M_{hum} - M_{dry})}{RT} \quad (A\ 6)$$

and is dependent on the conditions of the environment such as the saturated vapor pressure ((P^0), molecular weights of both humid air and dry air (M_{hum} and M_{dry}), the universal gas constant (R), and temperature (T).

APPENDIX C: OVERVIEW OF EXPERIMENTAL DESIGN

C.1: Overview

The basic design of the experiment is to connect two vertical sand columns to a single reservoir that contains air at nearly 100% relative humidity (Figure C.1-1). One column is situated above the reservoir, and the other sits below it. The reservoir is connected to a common humidity source, and vented to the laboratory. The entire column assembly was fabricated from 2" Schedule 40 PVC pipe and associated fittings. The column was designed to house calibrated humidity and temperature sensors (Appendix K, K) to help monitor the movement of humid air within the sand-filled columns. The column design was based on the desire to treat both columns identically throughout the duration of the experiment, except that water vapor enters one column from below and the other from above.

The success of the experiment rests upon the ability to support a sand-filled column (Appendix M) with an open bottom to allow water vapor to diffuse upwards into that column. Sand filters (Appendix D) were fabricated to support the sand and to allow water vapor to interact with that sand. The movement of water vapor through the pore spaces within the columns is monitored using a variety of sensors (Appendix K) that are protected from the sand and attached to the sand columns in specially designed sensor housings (Appendix E). Based on preliminary experiments (Appendix N), the distal end of each column was vented to the laboratory environment using ~1 m of vinyl tubing to simulate a distant atmospheric boundary (Appendix F). A humidity reservoir (Appendix F) was fabricated to provide a constant humidity boundary for both upper and lower columns (Appendix F) and interacting with the sand. The water vapor was generated in a

separate humidity source (Appendix G), which was connected to the main columns at the beginning of the experiment. A stand (Appendix H) was fabricated to make sure that the columns are supported and level during the experiment. The entire procedure was performed at constant temperature (Appendix I) and data from the sensors (Appendix K) was collected by a data logger and multiplexer (Appendix J). In order to obtain comparable results, a procedure (Appendix X) has been established and was followed for each trial.

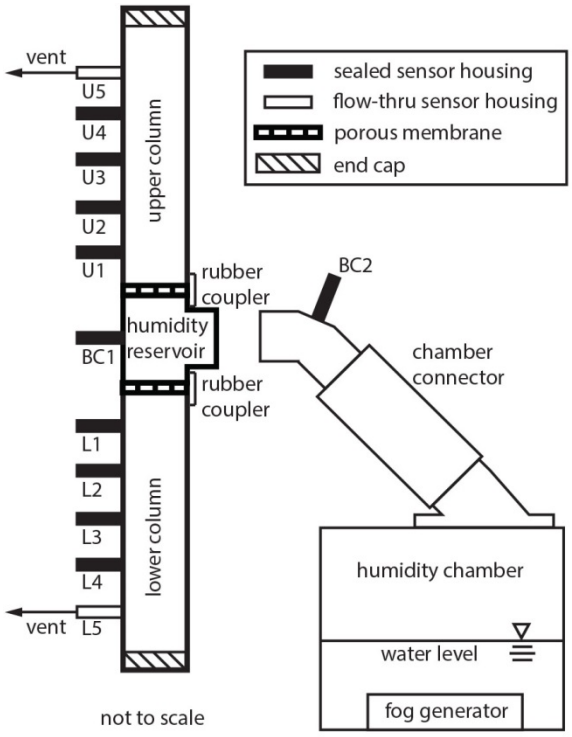

Figure C.1-1: Experimental design. Illustration showing the basic components of the experiment. The stacked experimental columns are shown on the left-hand side and the humidity source is on the right. Not to scale. For more details on specific elements of the overall experiment, refer to the list of appendices above.

APPENDIX D: SAND FILTERS

D.1 Filter supports

The base of the upper column must: 1) support the weight of the sand inside, and 2) provide open space that allows vapor to pass into the sand. Filter supports were fabricated for this purpose. Identical supports were used for both columns, noting that function (1) above is not required for the lower column. The supports were created using the following steps:

1. The process began with a 2" X ½" Lasco© PVC reducing bushing (Figure D.1-1).
2. A PVC saw was used to remove the outer ring from the ½" side of the bushing and expose the bushing frame (Figure D.1-2).
3. A lathe was used to trim the outside edges of the bushing frame (Figure D.1-3) to fit snuggly inside a 2" diameter PVC knockout plug.
4. The internal threads at the center of the bushing were removed on the lathe (Figure D.1-4) to increase the diameter of the central hole. This acts to increase the amount of open space.
5. The bottom half of the reducing bushing was sawn off to separate the internal frame (Figure D.1-5).
6. A hole was drilled perpendicular to the central hole of the bushing frame (not shown). In the event that separating the filter support from the column becomes difficult, a wire can be inserted through these holes, and used as a handle to apply pressure.
7. The inside of a 2" diameter PVC knockout plug was removed (Figure D.1-6) by applying pressure.

8. The internal bushing frame was solvent welded into the outer ring of the 2” knockout using Weld-On™ 790 Multi-purpose PVC cement. For uniformity, the smooth original surface of the bushing was glued flush with the large diameter end of the knockout ring (not shown as a separate figure).
9. A lathe was used to cut down the combined piece to a total thickness of 1.1 cm (Figure D.1-7), producing a smooth surface that supported wire mesh. Of the total thickness, 0.9 cm was inside the completed column.
10. The completed filter support is shown along with pieces in various stages of fabrication as Figure D.1-8.

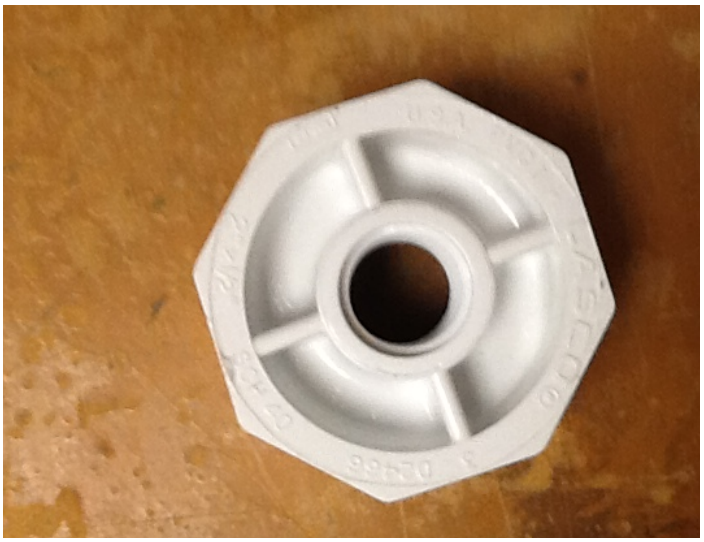

Figure D.1-1: Fabrication of filter supports step 1. 2” X ½” Lasco© PVC reducing bushing.

Figure D.1-2: Fabrication of filter supports step 2. Bushing with the outer ring removed. The central ring and four crosspieces are referred to as the bushing frame. Pencil is shown for scale.

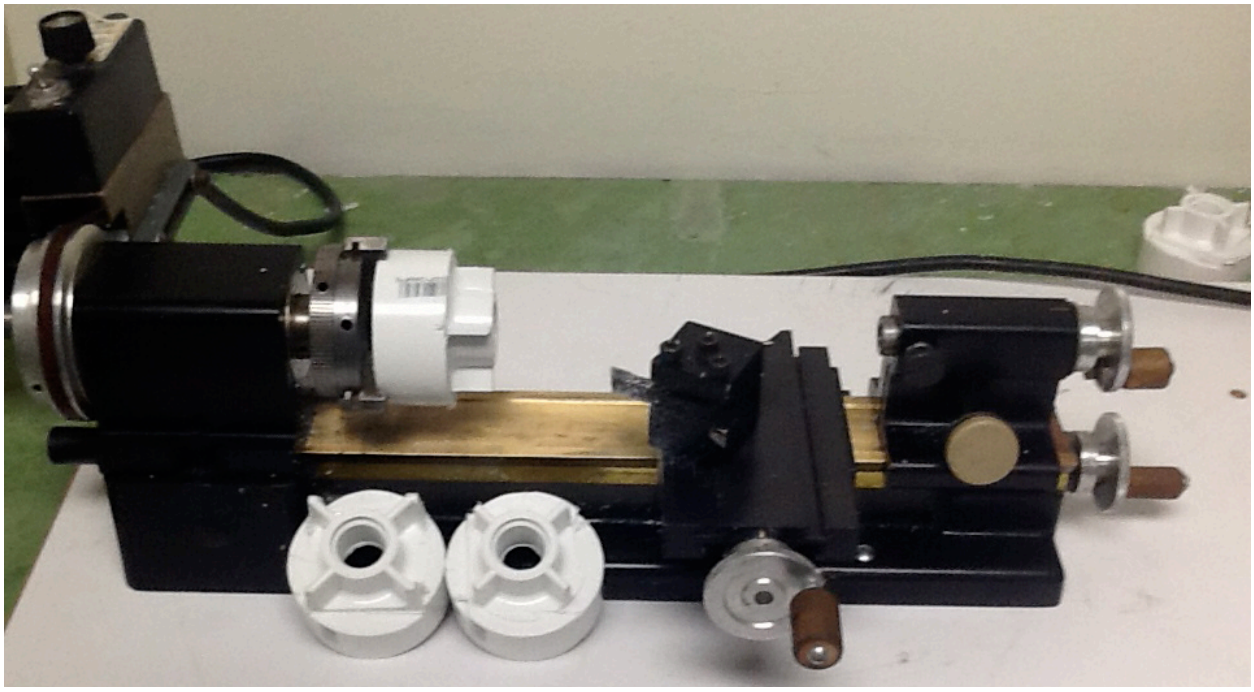

Figure D.1-3: Fabrication of filter supports step 3. A lathe was used to turn the outside of the bushing frame to fit inside a 2” PVC knockout plug. Examples of finished (right) and unfinished (left) pieces are shown against the lathe.

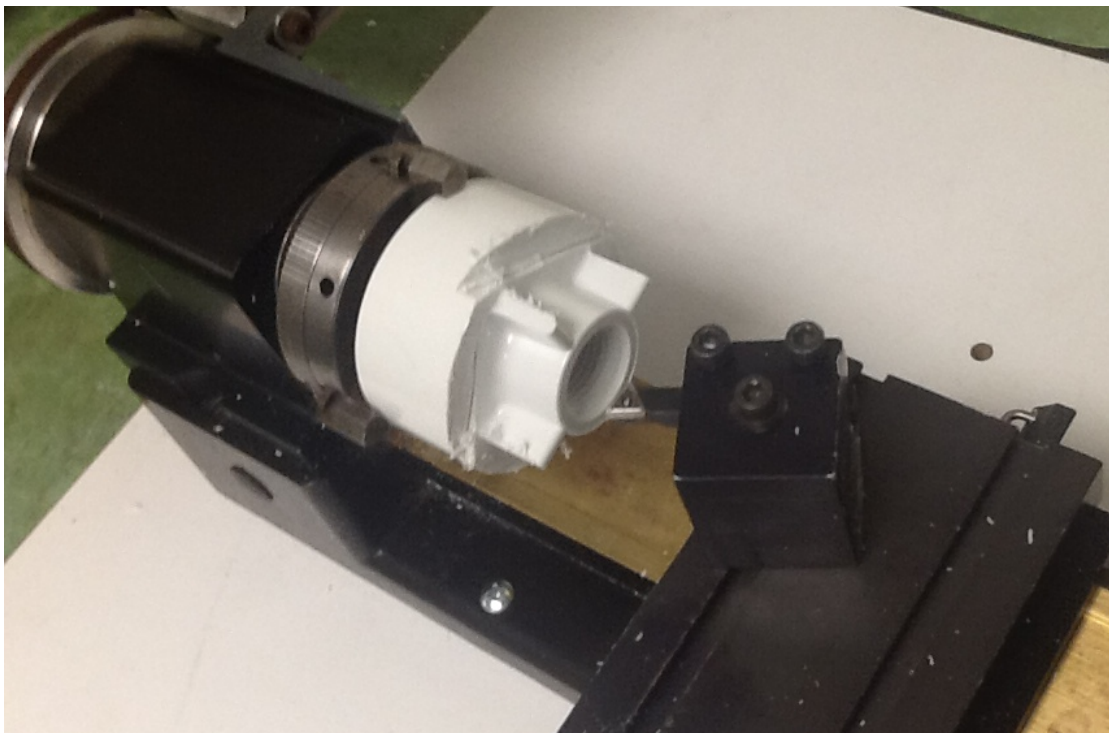

Figure D.1-4: Fabrication of filter supports step 4. Lathe set up to remove the threads and expand the center diameter of the bushing frame.

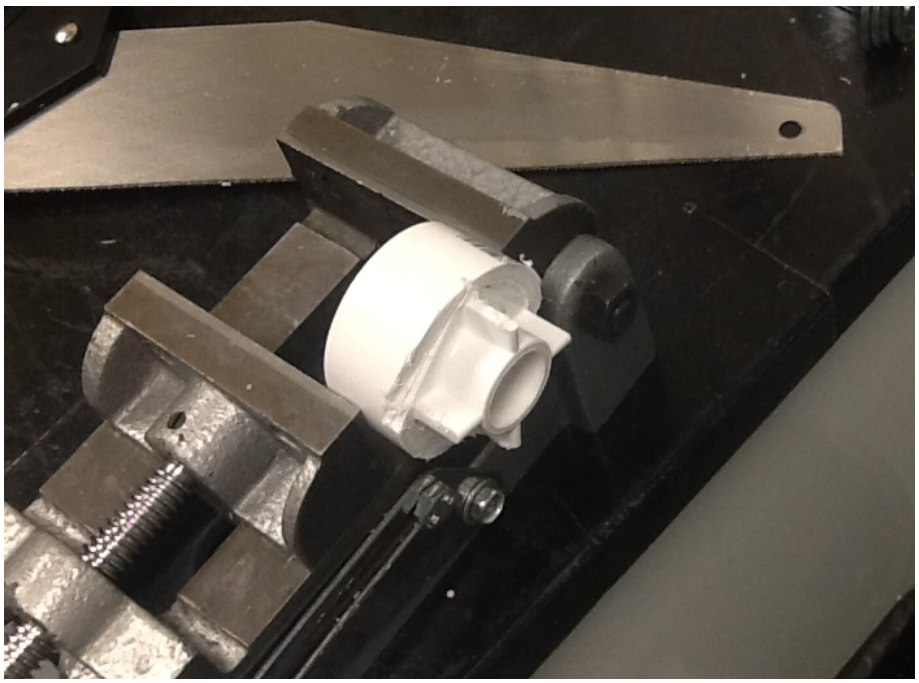

Figure D.1-5: Fabrication of filter supports step 5. The bushing was clamped into a vice so that the frame could be removed with a PVC saw. Note that the outer edge of the frame has a smooth surface remaining from the original manufacture.

Figure D.1-6: Fabrication of filter supports step 6. A 2” PVC knockout plug before and after removing the center.

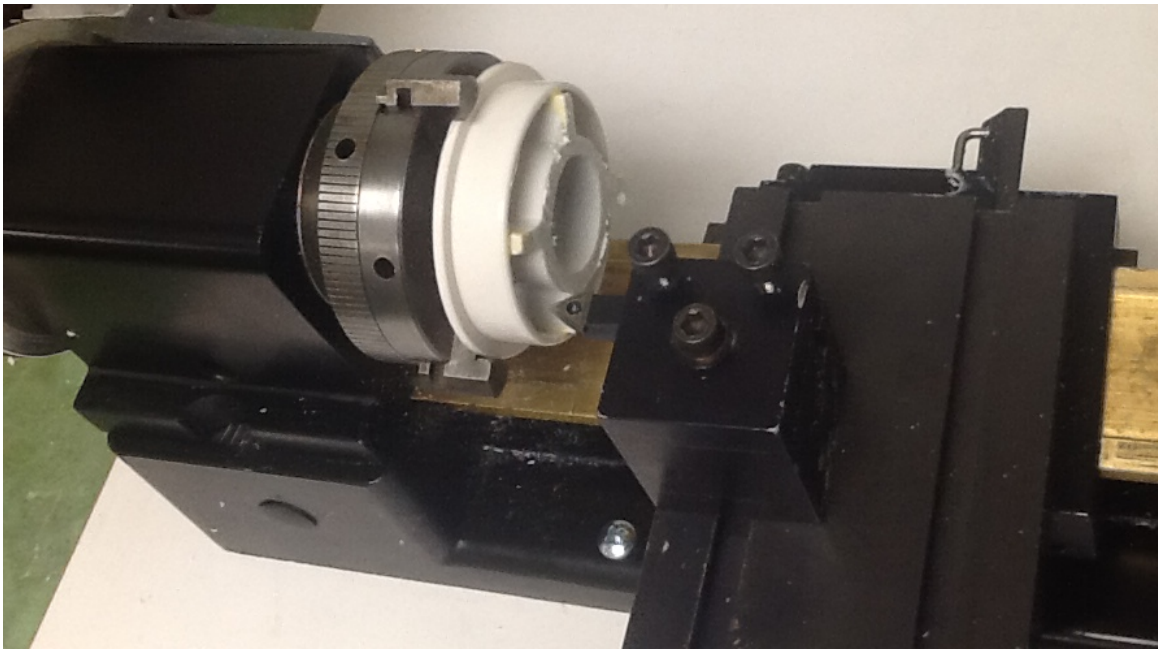

Figure D.1-7: Fabrication of filter supports step 7. The bushing frame was glued into the outer ring of the knockout plug with the rough saw-cut surface protruding. A lathe was used to complete the filter support by cutting it to a constant thickness and producing a smooth surface.

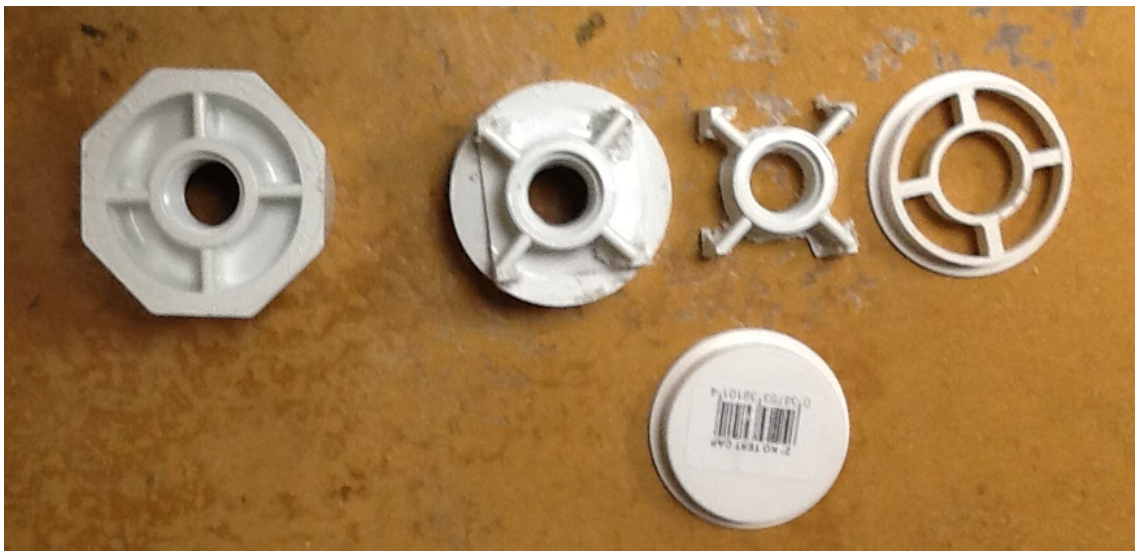

Figure D.1-8: Fabrication of filter supports step 8. Finished filter support (far right) is shown alongside raw materials (far left) and partially completed parts.

D.2 Completed sand filters

Two different stainless steel mesh screens are sandwiched between the sand and filter support. The purpose of these screens is to: 1) hold the sand in the column during the experiment, and 2) provide open space for vapor diffusion and advection. A precut 2" diameter 20 X 20 mesh screen (Figure D.2-1) with an opening size of 0.034" and open area of 46% is placed on top of the filter support to transfer the weight of the sand onto the filter support. A finer 80 X 80 screen (Figure D.2-2) is placed on top of the 20 X 20 screen to prevent movement of the sand particles. This precut 2" diameter screen has an opening size of 0.0055" and 31% open area. The sand filters were completed using the following steps:

1. The coarse mesh screen was tacked to the filter support using JB Weld™. A toothpick was used to apply droplets of JB Weld™ to locations where the internal frame meets the outer ring (Figure D.2-3). The mesh screen was then centered on the filter support. A stack of fender washers was placed on top of the screen to hold it in place while the epoxy hardened for 24 hours.
2. The fine screen was placed on top of the coarse screen and centered. A stack of fender washers was placed on top of the screen to hold it in place. A toothpick was used to apply droplets of JB Weld™ at regular intervals around the outer ring (Figure D.2-4). The epoxy was allowed to harden for 24 hours.
3. Any additional epoxy that prevented the completed filter support from smoothly fitting inside the 2" PVC diameter columns was cleaned off with a razor knife.

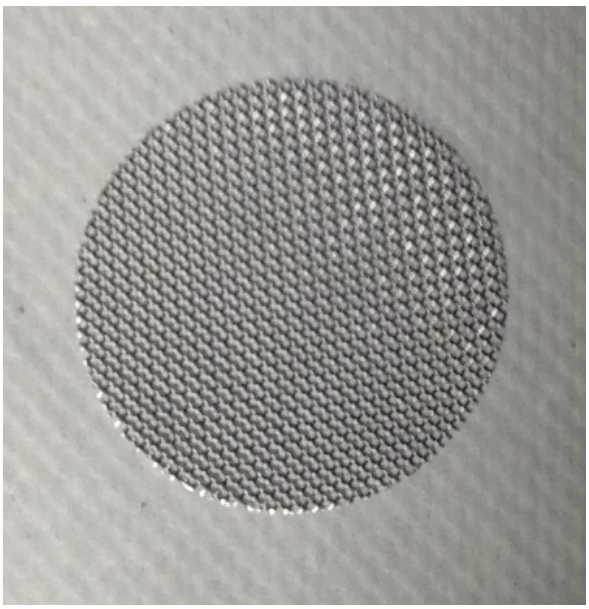

Figure D.2-1: Fabrication of filter supports step 9. This coarse 20 X 20 mesh screen was used to support the weight of particles within the column.

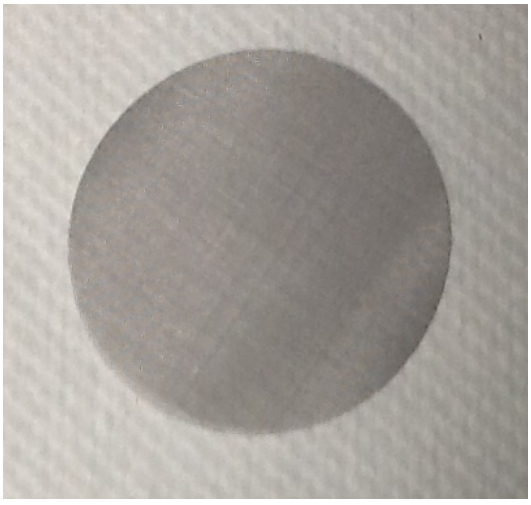

Figure D.2-2: Fabrication of filter supports step 10. This fine 80 X 80 mesh screen was used to keep sand particles in the column.

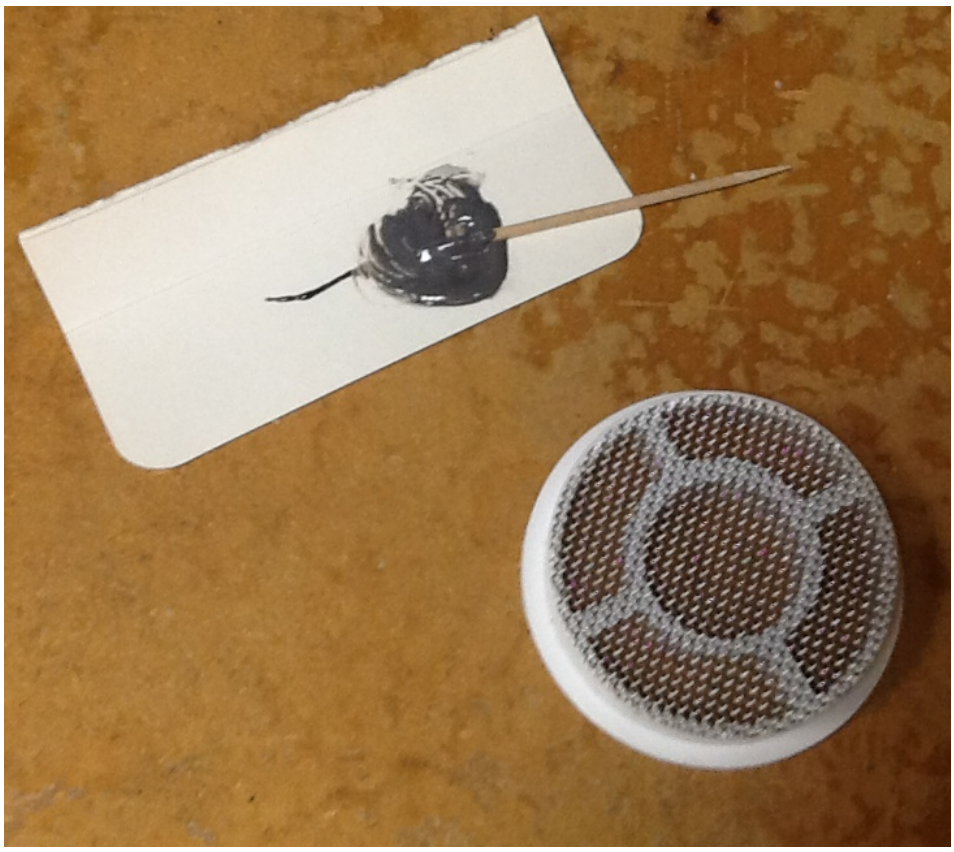

Figure D.2-3: Fabrication of filter supports step 11. JB Weld™ epoxy was applied using a toothpick to hold the coarse mesh screen in place.

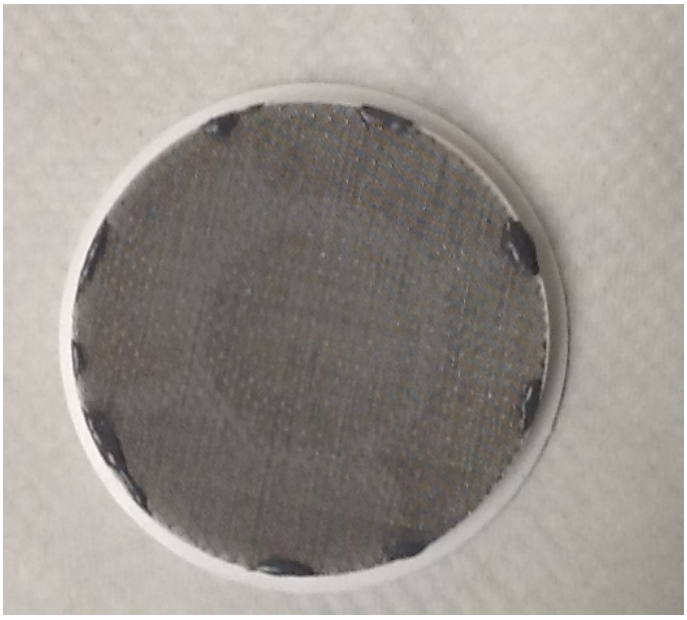

Figure D.2-4: Fabrication of filter supports step 12. The completed sand filter. The filter support is at the base, coarse mesh screen in the middle, and fine mesh screen on top.

D.3 Percent open area of the filter support and completed sand filter

The percent open area of the filter support was calculated by determining the area of the outer ring, inner ring, and four rectangular connectors (Figure D.3-1). Data shown in Table D.3-1 below are the averages of three independent measurements made to a precision of 0.001 inches with a dial caliper.

Measurement	Length
Outer ring – Outside diameter	2.031 in
Outer ring – Inside diameter	1.872 in
Inner ring – Outside diameter	1.149 in
Inner ring – Inside diameter	0.926 in
Connector – Length*	0.3615 in
Connector - Width	0.139 in

*Length obtained by subtracting Inside Diameter (Outer ring) from Outside diameter (Inner ring) and dividing by 2.

Table D.3-1: Average measurements of filter support. Measurements taken by averaging three independent measurements made to a precision of 0.001 inches with a dial caliper.

The area of a circle is defined by $A = \pi r^2$. The area of a rectangle is defined by $A = L * H$.

Given these 2 simple formulas, the open area and closed area of the support structure were calculated:

1. Area of the outer ring: $\pi * (1.0155\ in)^2 - \pi * (0.936\ in)^2 = 0.4874\ in^2$
2. Area of the inner ring: $\pi * (0.5745\ in)^2 - \pi * (0.463\ in)^2 = 0.3634\ in^2$
3. Area of the four connectors: $4 * 0.723 * 0.139 = 0.201\ in^2$
4. Total Area: $\pi * (1.0155\ in)^2 = 3.2397\ in^2$

The areas obtained for the outer ring, inner ring, and connectors represent the closed area of the filter support. The sum of the closed area comes out to be 1.0518 in^2, or 32.5%. Therefore, the open area comprises 67.5% of the interior of the filter support.

The fine and coarse stainless steel wire mesh placed on top of the support has open areas of 31% and 46% respectively. The JB Weld™ epoxy was only placed on solid portions of the filter support and therefore does not reduce the open area of either screen. The total percent open area

for the sand filter is approximated as the product of the three components (filter support, fine mesh, and coarse mesh): 0.31*0.46*0.675 = 0.096 or 9.6% total open area.

Because both sand filters were created following the same procedures, the open area for each is assumed to be equal.

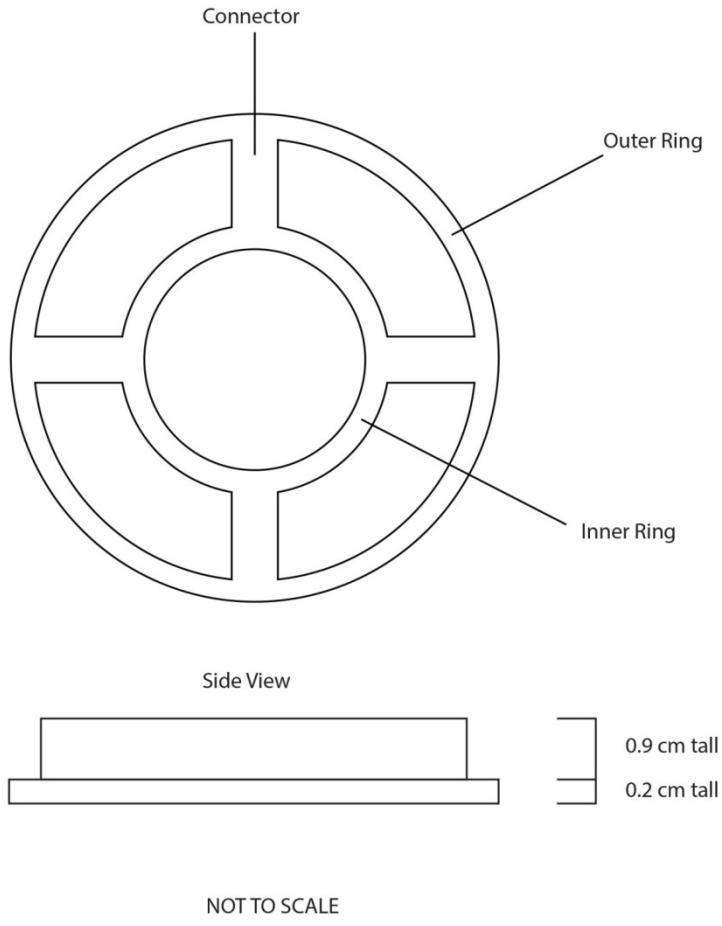

Figure D.3-1: Cartoon drawing of the filter support.

APPENDIX E: SENSOR HOUSINGS

E.1 Sensor housings

Sensor housings were fabricated to mount humidity and temperature sensors at intervals along the columns. Housings were designed to allow sensors to be separated from the columns between experiments. Each housing consists of two sections fabricated from ½" PVC rod, a socket and a plug (Figure E.1-1 and Table E.1-1). The sockets are meant to be permanently attached to the test columns, while the plugs are removable.

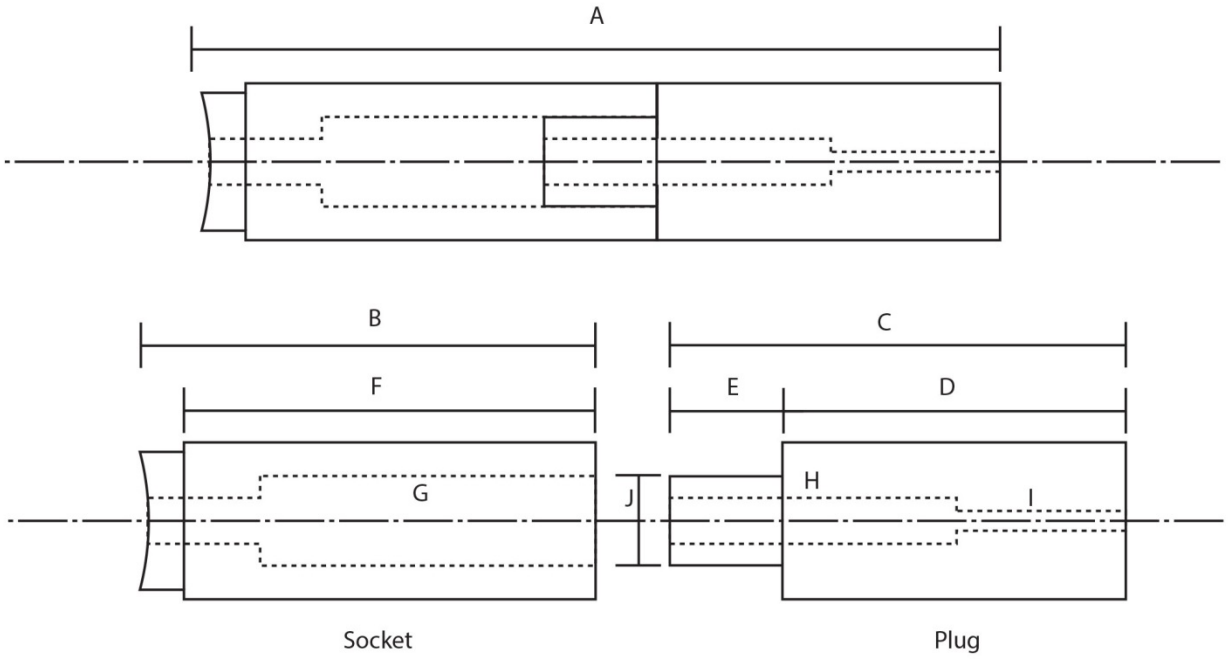

Figure E.1-1: Cartoon drawing of sensor housings. The top drawing represents the assembled plug and socket. The lower left-hand drawing is the socket. The lower right-hand drawing is the plug. Drawing is not to scale. Letters correspond to dimensions shown in Table E.1-1. Dashed lines indicate drilled sections of the interior and corresponding measurements. Semi-dashed lines indicate the centerline.

Figure E.1-1 Label	Name of Measurement	Measurement #1 (inches)	Measurement #2 (inches)	Measurement #3 (inches)	Measurement Average (inches)
A	Attached Length	1.895	1.892	1.879	1.889
B	Socket Length	0.990	0.988	0.989	0.989
C	Plug Length	1.164	1.169	1.166	1.166
D	Plug Base Length	0.905	0.895	0.890	0.897
E*	Male end Length	0.259	0.184	0.276	0.240
F	Trimmed socket Length	0.844	0.856	0.859	0.853
G	Depth of 3/8” Hole in socket	0.845	0.855	0.850	0.850
H	Depth of 3/16” Hole in plug	0.737	0.852	0.708	0.766
I**	Depth of 5/32” Hole in plug	0.427	0.317	0.458	0.401
J	Diameter of Male Connection	0.377	0.380	0.371	0.376

*Derived by taking the difference of C and D. **Derived by taking the difference of C and H.

Table E.1-1: Includes the measurements taken with a dial caliper to a precision of 0.001 inches of three randomly selected sensor sockets and plugs.

E.1a Sensor housings – socket fabrication

The process for creating a socket is as follows:

1. Pieces of ½” PVC rod were cut to a length of roughly 1-1/4” using a PVC saw and miter box (Figure E.1a-1).
2. A lathe was used to square both ends of each piece and bring the overall length to roughly 1” (Figure E.1a-2).

3. One end of each piece was turned on the lathe (Figure E.1a-3) to remove roughly 0.01” of material so that it would fit snuggly within a hole drilled into the column with a ½” drill bit. Note that the drilled holes were slightly less than 0.500” in diameter.
4. A 3/8” end mill was used to bore a flat-bottomed hole to a depth of 0.85” in the center of the unturned side of the socket. This operation was carried out on a milling machine (Figure E.1a-4). The resulting cavity houses the sensor(s) and provides a female connection for the plug.
5. A 3/16” drill bit was used to center drill through the rest of the socket on the lathe so that vapor from the column could reach the sensor head (Figure E.1a-5).
6. The turned end from step 3 was sanded to match the interior curvature of the PVC pipe. The socket was inserted into a section of 2” PVC pipe so that it was held perpendicular to a 2” diameter brass cylinder with sandpaper attached to the surface (Figure E.1a-6). The socket was then sanded flush with the pipe section to produce a matching curve.
7. Tin snips were used to trim precut ½” circles of 80 X 80 stainless steel mesh screen (0.0055” openings, 31% open area) to a diameter of 3/8” (Figure E.1a-7) for attachment to the socket. The purpose of the screen is to allow vapor communication between the sand and sensor, while preventing sand from contacting the sensor head.
8. The screen was attached to the sensor socket using JB Weld™ (Figure E.1a-8). The screen was bent to match the curvature of the socket, and then placed in the center. A toothpick was used to apply pressure to the center of the screen, while another toothpick was used to place the epoxy around the outer circumference of the screen. The epoxy was allowed to dry for 24 hours.

9. A lathe was used to remove any excess epoxy that dripped from the top of the column to the area where the sensor was glued to the PVC column (see step 3, above).

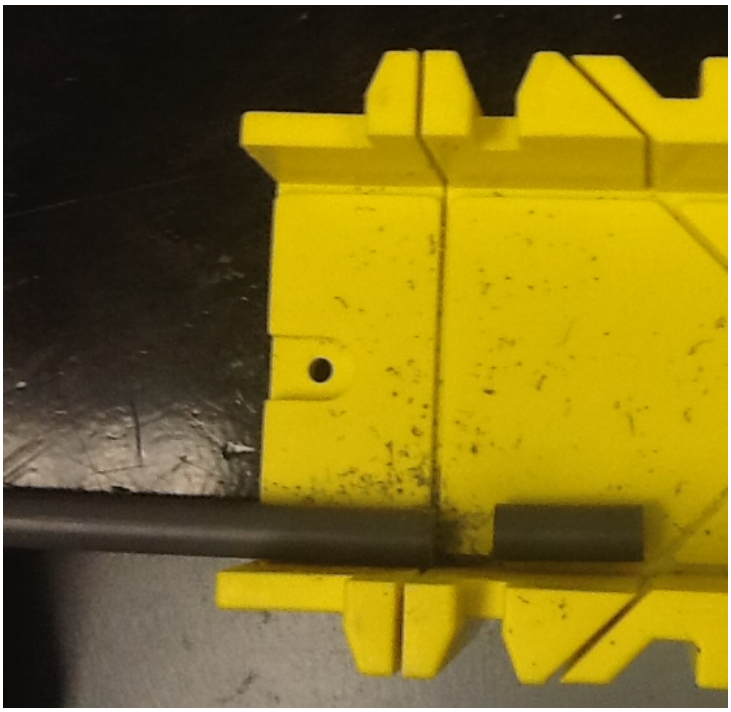

Figure E.1a-1: Fabrication of socket step 1. The PVC rod was cut into 1-1/4” pieces using a PVC saw and miter box.

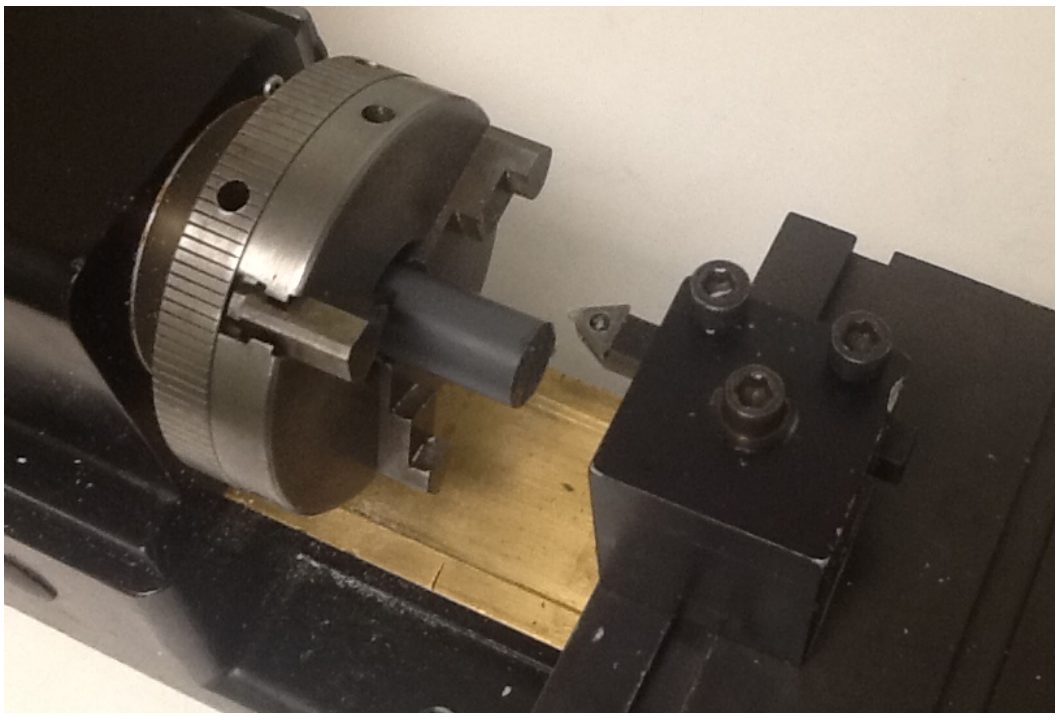

Figure E.1a-2: Fabrication of socket step 2. Both ends were squared off using a lathe and trimmed to a length of 1.00 inches.

Figure E.1a-3: Fabrication of socket step 3. One end of the sensor housing was turned on a lathe in order to fit a ½” hole drilled into the side of the column.

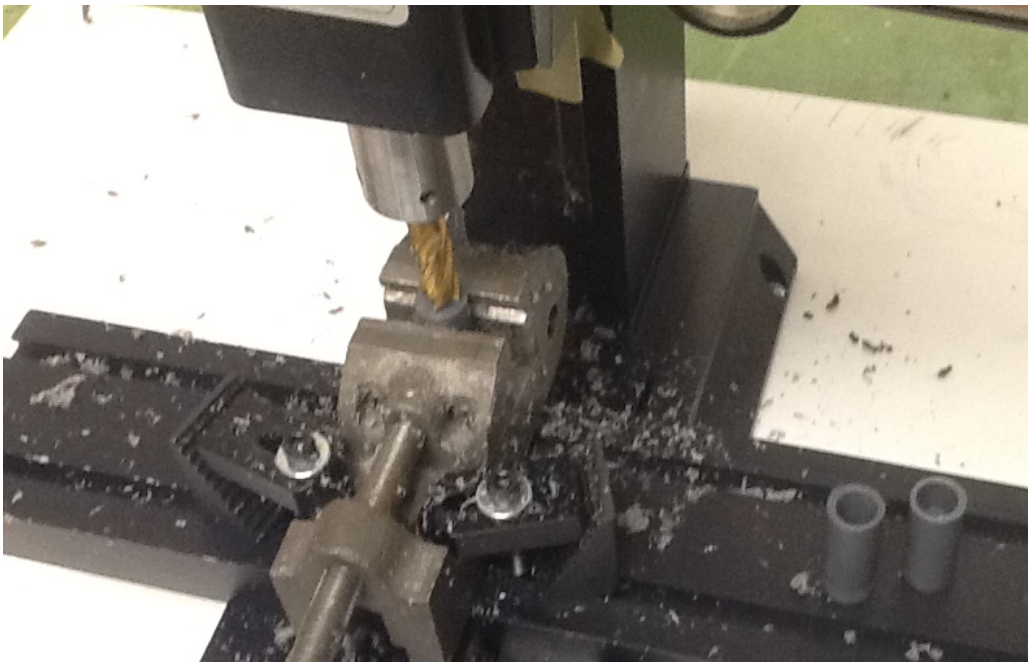

Figure E.1a-4: Fabrication of socket step 4. A mill was used to bore a 3/8” hole on the unturned side of the socket. Two bored pieces can be seen in the lower right corner.

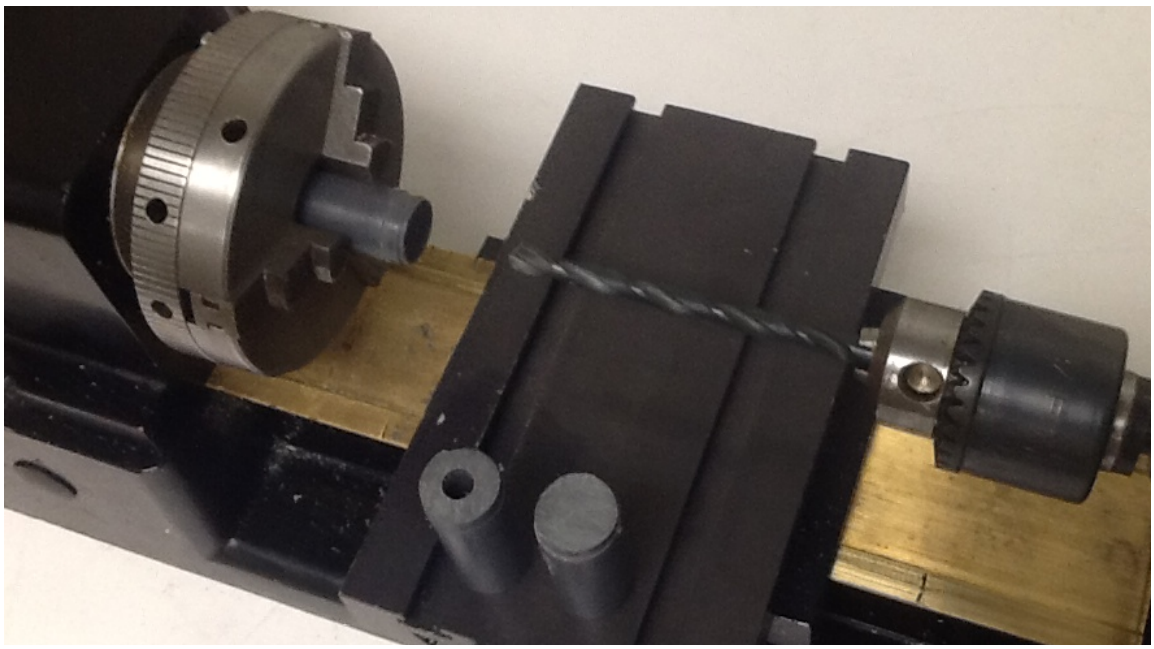

Figure E.1a-5: Fabrication of socket step 5. A 3/16” hole is center drilled on the turned side from step 3. This enabled water vapor to reach the sensor.

Figure E.1a-6: Fabrication of socket step 6. The turned end is sanded down to fit the inner curvature of the column.

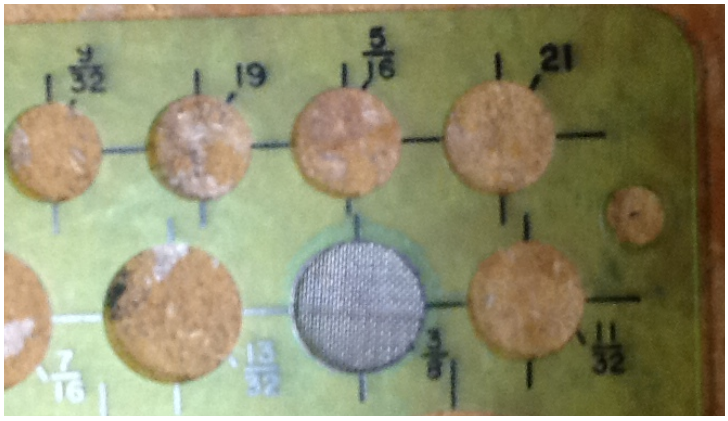

Figure E.1a-7: Fabrication of socket step 7. A ½” precut 80 X 80 mesh screen is trimmed to a diameter of 3/8”.

Figure E.1a-8: Fabrication of socket step 8. A toothpick was used to apply JB Weld™ to secure an 80 X 80 stainless steel screen to the turned end of the socket.

E.1b Sensor housings – plug fabrication

Each plug was created using the following steps:

1. Pieces of ½" PVC rod were cut to a length of roughly 1-1/4" using a PVC saw and miter box (Figure E.1b-1).
2. A lathe was used to square the ends of each piece and bring the overall length to 1.1" (Figure E.1b-2).

3. A 1/8” hole was center drilled through the entire piece using a lathe. This hole provides a passage for the sensor wires (Figure E.1b-3).
4. The outside of one end was turned on the lathe in order to make the male connection for the socket (Figure E.1b-4). This male connection has a diameter of 0.37”.
5. A 3/16” hole was center drilled on the lathe to a depth of 0.78” on the freshly turned (0.37” diameter) side of the plug in order to make room for wire connections to the sensor (Figure E.1b-5)
6. A completed sensor housing is shown in Figure E.1b-6 along with an illustration of the internal configuration.

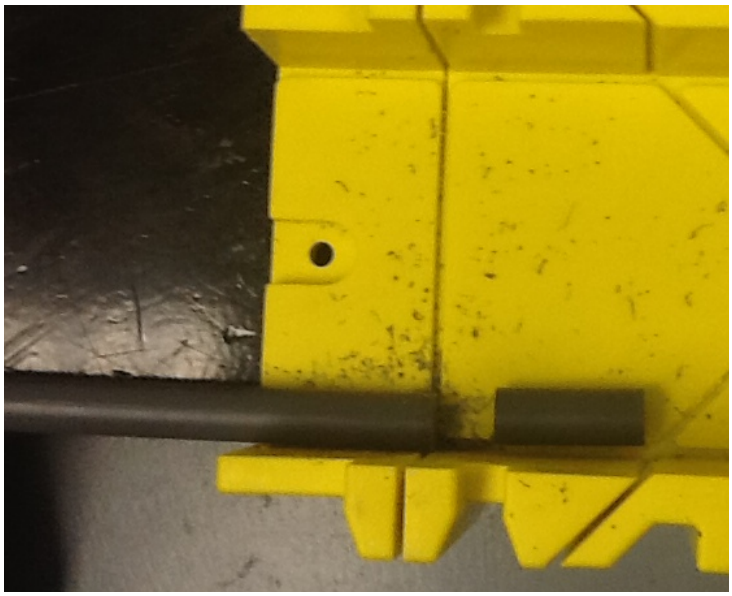

Figure E.1b-1: Fabrication of plug step 1. The PVC rod was cut into 1-3/16” pieces using a PVC saw.

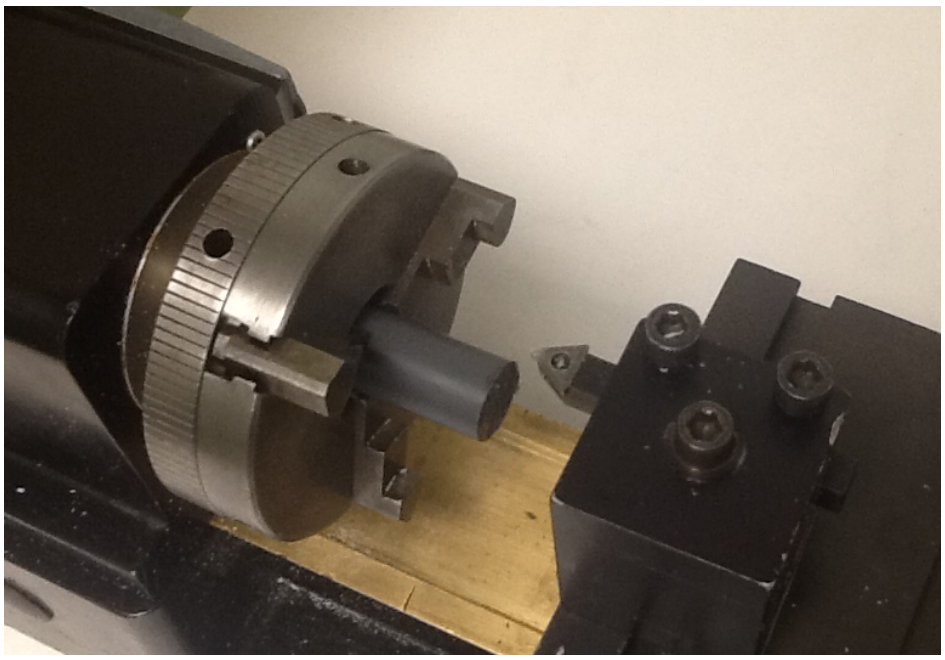

Figure E.1b-2: Fabrication of plug step 2. Both ends were squared off using a lathe.

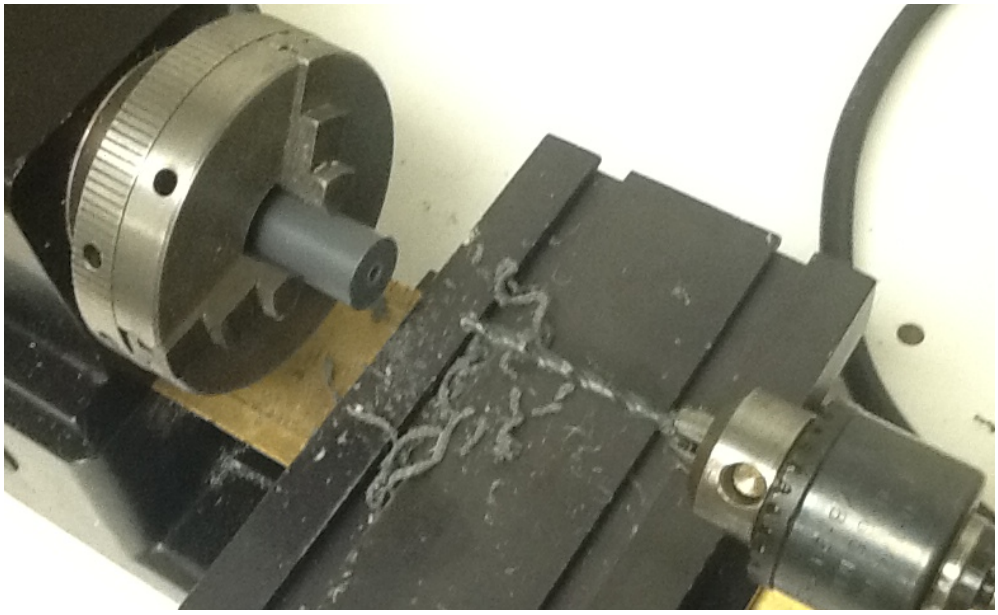

Figure E.1b-3: Fabrication of plug step 3. A 1/8” drill bit was center drilled through the entire piece for the sensor wires.

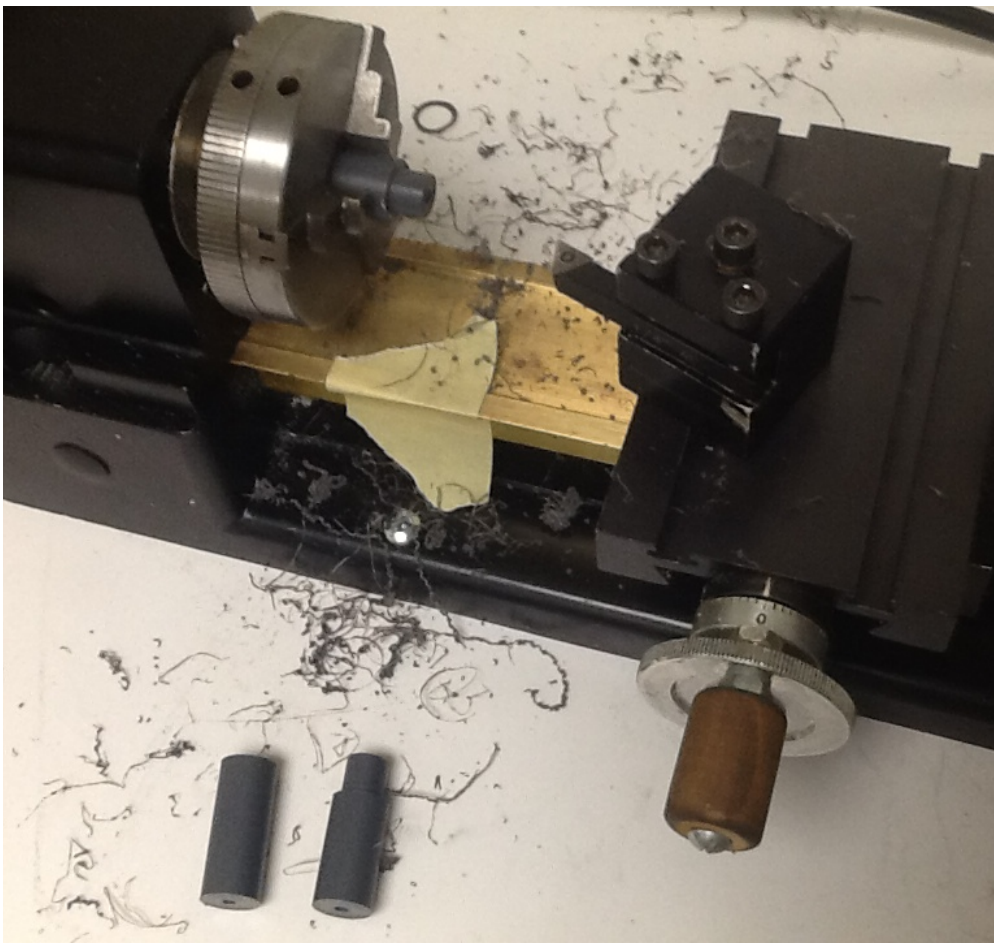

Figure E.1b-4: Fabrication of plug step 4. The male connection of the plug is made on the lathe. Finished and unfinished pieces are shown.

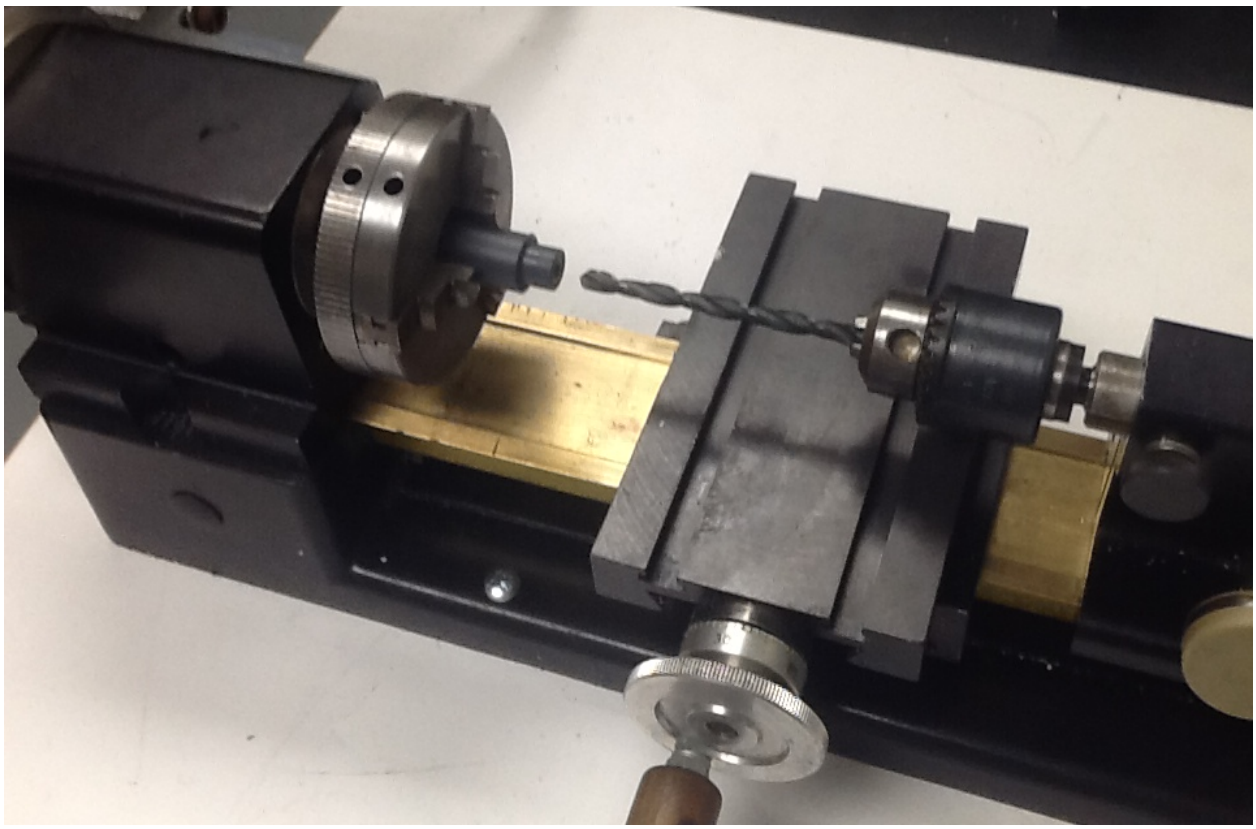

Figure E.1b-5: Fabrication of plug step 5. A 3/16” drill bit is used to center drill through the male end of the plug.

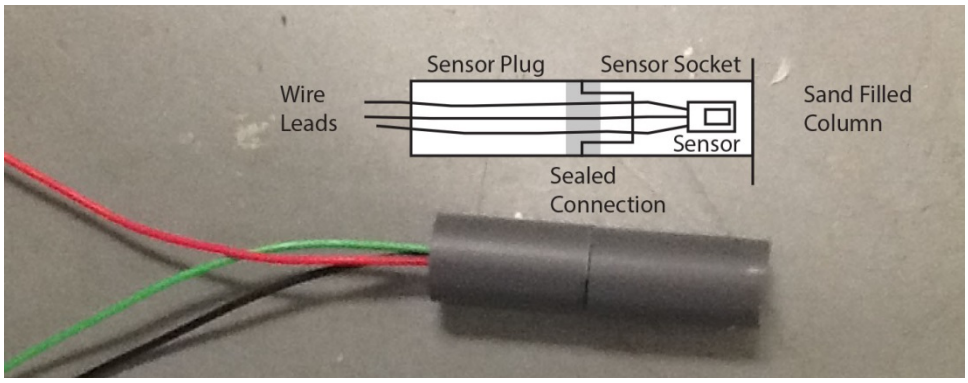

Figure E.1b-6: Actual socket and plug beside a cartoon. Side by side comparison of the finished piece and an illustration showing the socket and plug. The joint between the two pieces was sealed with silicone tape when the sensors are installed in the columns.

E.2 Sealing sensors into plugs

Sensors were sealed into the sensor housing plugs (Appendix E.1) using GE™ Waterproof silicone sealant. Because of the short working time (5 minutes) of the sealant, some of the steps were not documented with pictures; instead completed sensors are shown (Figure E.2-3)

1. Prior to assembly, humidity sensors (Appendix K) were soldered onto 12" unshielded wire leads (22 gauge) and the connections were protected with heat-shrink tubing (Figure E.2-1). All humidity sensors were tested after attaching the wire leads. Also prior to assembly, the bi-metal junction of the Omega™ thermocouples (Appendix K) was sealed with four coats of clear acrylic nail polish.
2. Humidity Sensors were placed in all plugs (Figure E.2-2) and capped with sockets to make sure that they fit together.
3. Thermocouples were placed in five sockets (housed jointly with the humidity sensors).
4. Silicon sealant was applied using a toothpick along the wire leads (about 1 inch below) nearest the sensor heads. These wire leads were then pulled into the plug, dragging the silicone into the hole. Additional sealant was applied to the wire entry, being careful to not come in contact with the sensor. Any residual sealant was carefully removed from around the plug with a towel before hardening. The sealant was allowed to dry for 24 hours.
5. A toothpick was used to apply silicon sealant to the opposite end of the plug where the wire leads exit. The sealant was allowed to dry for 24 hours.

6. The wire leads of the sealed sensor plugs (for humidity sensors only) were soldered to 64” lengths of 22 gauge shielded 4-conductor cable. Heat shrink tubing was used to protect the solder joints.

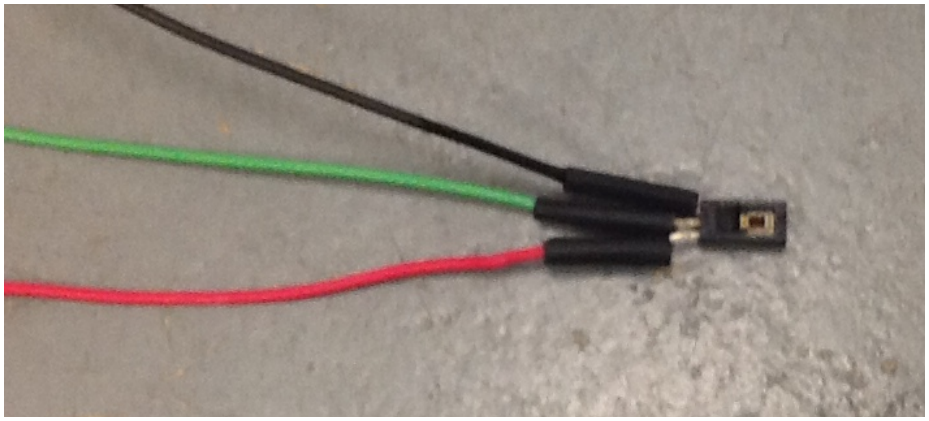

Figure E.2-1: Humidity sensor. Humidity sensor with 12” wire leads.

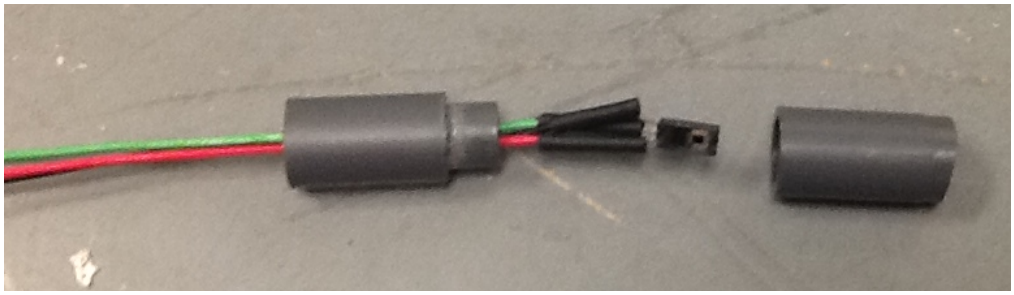

Figure E.2-2: Connecting humidity sensor to sensor housing. Humidity sensors were placed into plugs, and capped with sockets to make sure they fit before sealing began.

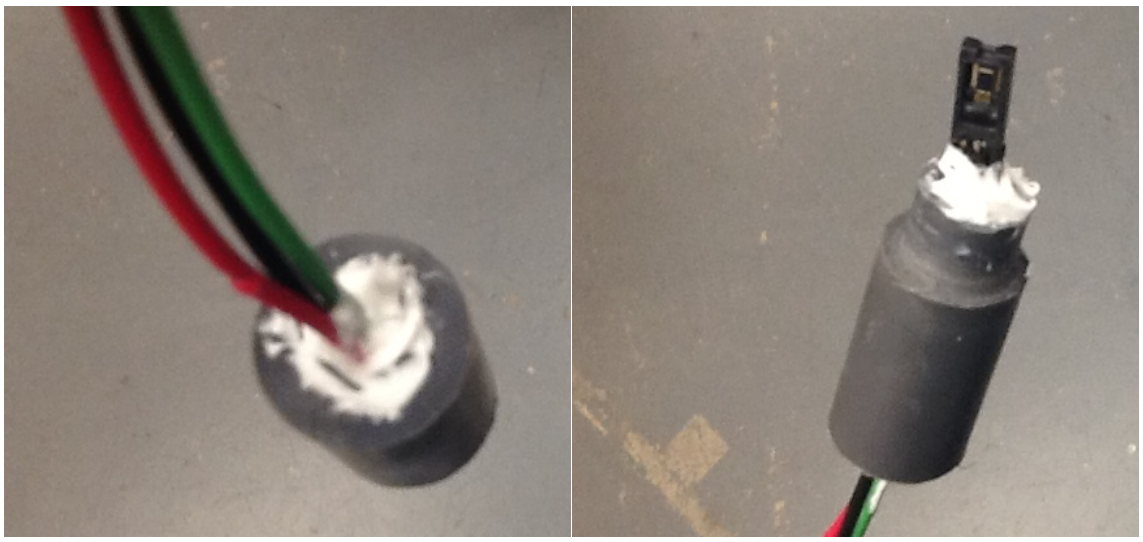

Figure E.2-3: Sealing humidity sensor in place. The top and bottom of a completely sealed plug.

APPENDIX F: COLUMNS AND HUMIDITY RESERVOIR

F.1 Upper and lower columns

Both upper and lower columns were cut to a length of 29 cm from 2" diameter Schedule 40 PVC pipe. The design was to consider a 25 cm sand pack. An additional 4 cm was included on the column, and is associated with boundary conditions. The sand pack starts about 1 cm into the column length and the last 3 cm of sand distance is present to minimize the impact from boundary conditions. In preliminary experiments this boundary was the sealed end of the columns; in the main set of experiments, columns were left open to the laboratory to simulate an open atmosphere. In the latter case, relative humidity fluctuations occurring in the laboratory during experiments may influence measurements. This choice for column length also allowed the entire apparatus (Figure D.1-1) to fit within an existing constant temperature chamber (see Appendix I). The following steps were performed to fabricate the columns:

1. Segments of 2" Schedule 40 pipe were cut to a length of 29 cm using a power miter saw (not pictured). Stop blocks on the power saw assured that both columns would be the same length. The saw produced smooth square ends that did not require additional finishing.
2. Holes were drilled in each column with a ½" drill bit at 5 cm intervals for the sensor holders (Figure F.1-1). Each column was clamped to a length of Unistrut™ 1-5/8" slotted channel, which in turn was clamped into a vice. A wiggler was inserted into the drill press and used to align the vice so that the column could be drilled on the exact centerline. The first hole was placed 3.4 cm from one end of each column. This value was used to account for the 0.9 cm taken up by the sand filter (Appendix D), resulting in the

first sensor being placed 2.5 cm from the start of the sand within the column. Subsequent holes were drilled at 5 cm intervals. For each hole, a small pilot hole was drilled, and then successively larger bits were used to enlarge the hole. The drilled columns were stacked as mirror images of each other. Therefore, the lower column is oriented with the holes drilled from the top down, while the upper column is oriented with the holes drilled from the bottom up.

3. Sensor housing sockets (Appendix E) were solvent welded to the PVC column using Christy's Red Hot Blue Glue™, a brand of PVC Cement (Figure F.1-2). In order to make sure that the cement did not affect the screen on the socket, it was applied using an artist's paintbrush. Cement was first applied to the test column, then to the turned end of the socket. The socket was inserted and twisted 90^{o} for a tight seal. Sockets were pre-marked to indicate the top of the socket. This was to ensure that the curved part of the socket is aligned with the curvature of the column. After cementing the sockets in place, the artist's brush was used to apply cement around the joint between the outside of the column and the socket. The purpose of this 2^{nd} cementing operation was to ensure an impermeable seal. Vinyl tubing (~1 m) was inserted into the distal socket of each column and left open to the atmosphere during experiments (Figure F.1-3).
4. A 2" knockout plug was cemented to the bottom end of the lower column to support the weight of the sand. The upper column was capped after being filled.
5. Both columns were water tested to verify that there was no leakage. All sockets were plugged with rubber stoppers and a temporary rubber end cap was placed on one end of

the upper column. Both columns were found to be water tight, and are assumed to be airtight as well.

6. Completed columns were washed in distilled water using Mr. Clean™ Multipurpose cleaner soap. Columns were scrubbed with a washcloth both inside and out to remove any oils from handling. Columns were rinsed in a separate bin of distilled water to remove soap. Process was repeated. Columns were left to air dry.

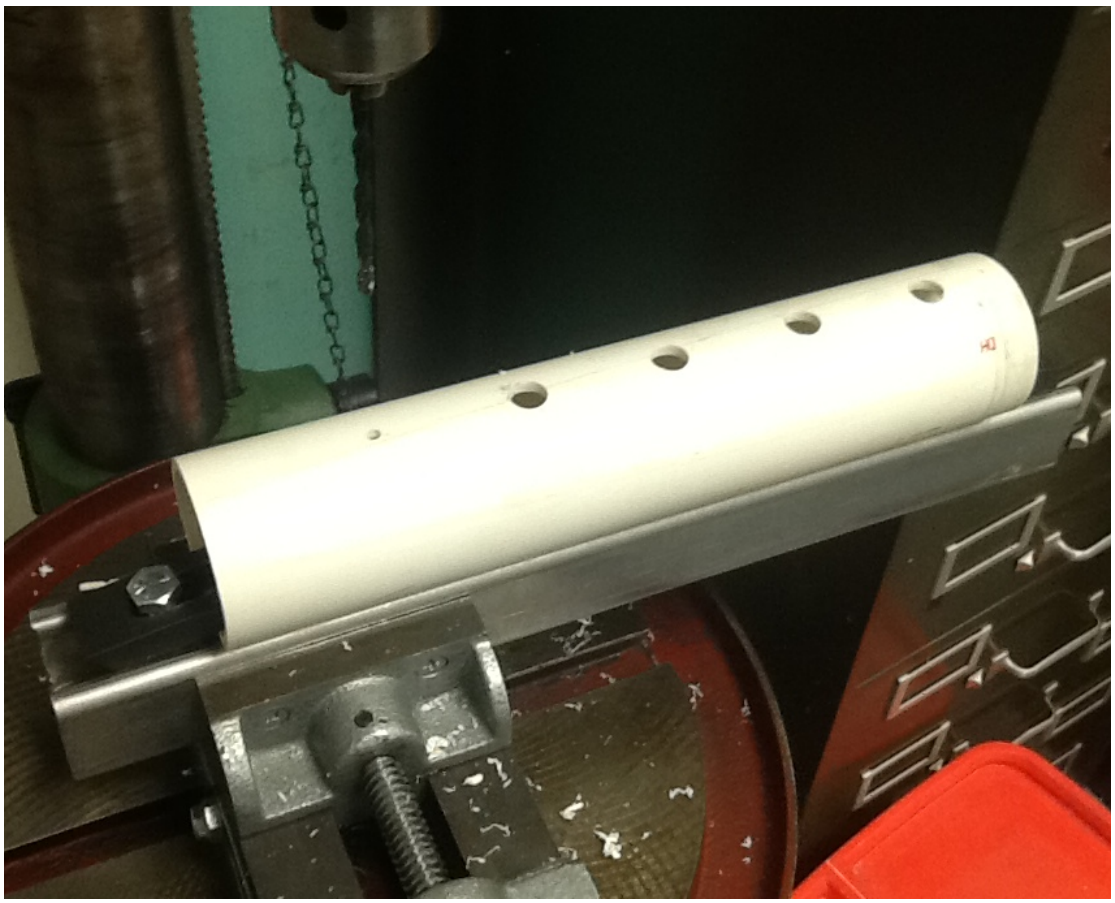

Figure F.1-1: Column fabrication step 1. Once the centerline was found using a wiggler, the PVC pipe was slid across the vice to make sure that all holes were drilled on the centerline of the column at 5 cm intervals.

Figure F.1-2: Column fabrication step 2. Columns with sensor sockets cemented in place. A knockout plug was cemented into the lower column only. Blue coloration is from the cement used to solvent weld the PVC.

Figure F.1-3: Column fabrication step 3. Vinyl tubing was inserted into the distal end of each column and routed out of the constant temperature box (Appendix I) during the main experiments to simulate an open atmosphere. The corresponding distal sensor (U5-H, L5-H) was slightly removed from the column in this instance, and attached using a barbed tee fitting.

F.2 Humidity reservoir

The humidity reservoir consists of a 2" PVC Tee-fitting that joins both test columns to the humidity source. The stock Tee-fitting was modified to shorten distances between the sand columns and the humidity source, which has the effect of assuring that boundary conditions are nearly identical between the two upper and lower columns. It was constructed in the following manner:

1. The “arms” of the Tee-fitting were shortened using a power miter saw to minimize distances between the columns and the humidity source (Figure F.2-1). The original distance from end-to-end of the tee was 5.713 inches from the manufacturer. The use of the saw reduced the end-to-end distance to 3.335 inches as measured with a dial caliper to 0.001-inch precision.
2. A hole was drilled with a ½” drill bit to place a sensor socket into the PVC Tee-fitting (Figure F.2-2). The hole was placed in the center of the fitting.
3. Two roughly 1.45” long pieces of 2” PVC were solvent welded with Christy’s Red Hot Blue Glue™ to the shortened ends of the PVC-Tee fitting (Figure F.2-3). The purpose of these pieces is to connect the humidity reservoir to the columns using a rubber coupler. The use of a rubber coupler facilitated the detachment of the columns between experiments.
4. A sensor housing socket (Appendix D) was solvent welded to the PVC Tee-fitting using the same process as for the columns (See Appendix F.1 above).
5. The humidity reservoir was washed using the same procedure as in F.1.

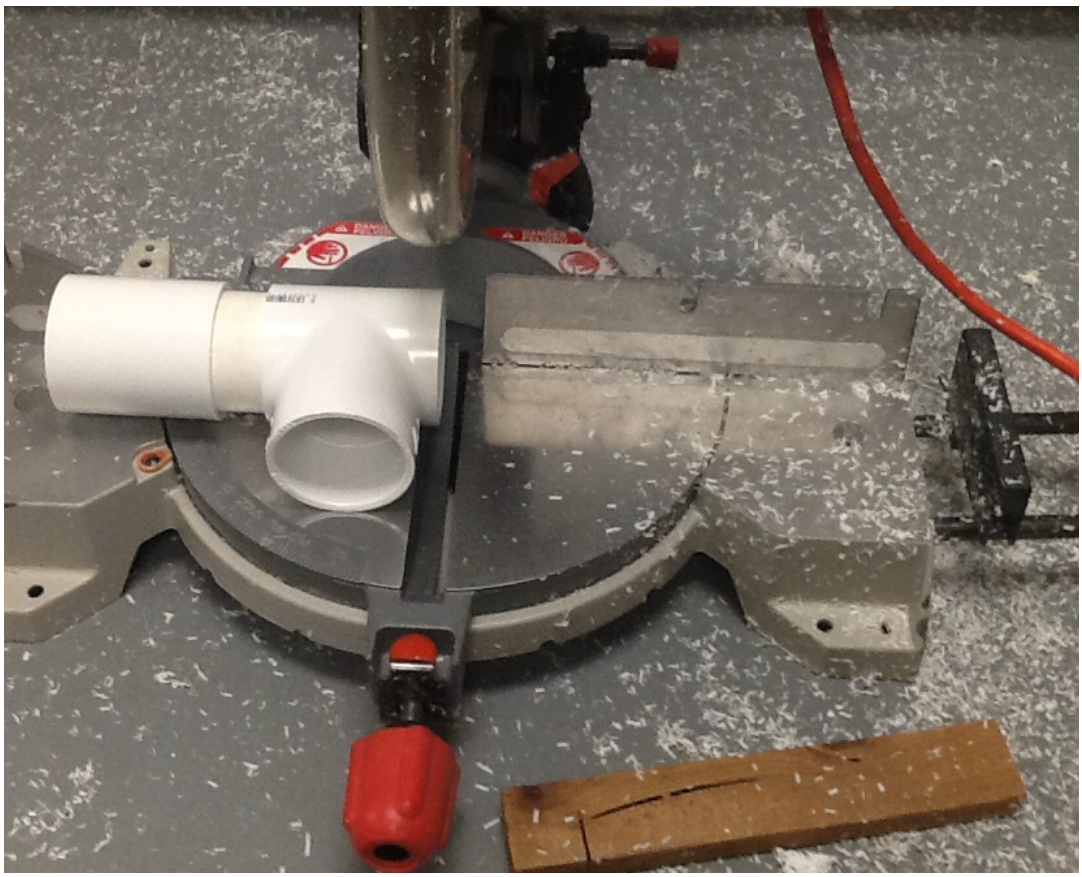

Figure F.2-1: Humidity reservoir fabrication step 1. The arms of a 2” PVC Tee-fitting were shortened using a power miter saw in order to bring the sand closer to the humidity source. The PVC fittings seen on the left side of the image were temporarily attached in order to facilitate clamping the Tee-fitting to the saw table and assuring the cuts were square. The wood block seen in the foreground was used as a spacer to set the location of the cuts.

Figure F.2-2: Humidity reservoir fabrication step 2. A ½” hole was drilled along the center line of the Tee-fitting in order to mount a sensor socket.

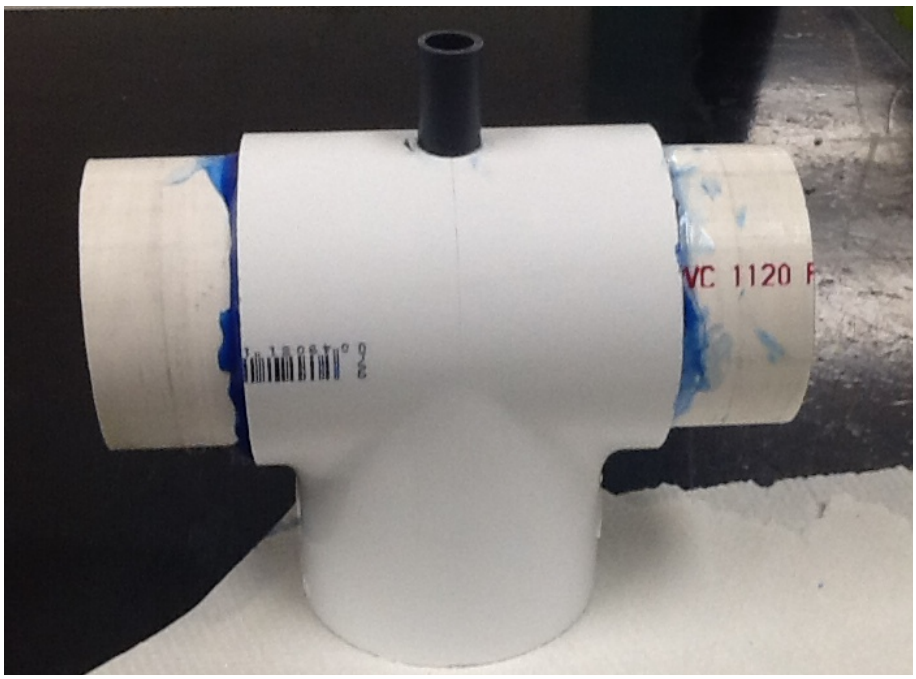

Figure F.2-3: Humidity reservoir fabrication step 3. The completed humidity reservoir with sensor socket and mounting points for the rubber coupler cemented in place. The blue coloration is residue from the solvent cement.

APPENDIX G: HUMIDITY SOURCE

A humidity source was constructed in order to provide air to the experiment at near 100% relative humidity, and at the same temperature as the sand columns. The humidity source consists of two major components; a humidity chamber and a connector (Figure C.1-1). The humidity chamber holds liquid water and a 24V ultrasonic fog generator. The fog generator ejects fine droplets of water vapor into the upper portion of the humidity chamber. The increased surface area of the water facilitates evaporation into vapor. The upper half of the humidity chamber also serves as a reservoir for water vapor. In addition to routing water vapor from the humidity chamber to the experiment, the connector provides additional storage for water vapor.

G.1 Humidity chamber

A humidity chamber was constructed by placing a 24V ultrasonic fog generator in a covered 12-quart polyethylene food storage bucket (Figure G.1-1). Humid air exits the lid of the food storage bucket through a 4" angled dust port. The humidity chamber was constructed using the following steps:

1. Handles on the bucket and the lower part of the lid were removed and filed smooth in order to create a sealable surface (Not pictured).
2. A rectangular piece of ¼" thick polycarbonate sheet (5.25" X 7.5") was cut to provide a backing plate for a 4" angled dust port. An oblong hole (4" X 3.75") was cut from the center of the polycarbonate sheet to match the opening on the bottom of the dust port. The hole was rough cut with a jigsaw and finished using a sanding drum mounted in a Dremel™ tool (Figure G.1-2).

3. The corners of the polycarbonate sheet were rounded off with a Dremel™ tool (Process not pictured, but rounded corners can be seen in Figure G.1-3).
4. A hole was cut on a flat part of the bucket lid to match the holes in the 4" angled dust port and the polycarbonate sheet.
5. Four holes were drilled onto the base of the 4" angled dust port to fit #10-32x¾ machine screws. Two larger holes were present on the piece from the manufacturer (Figure G.1-3).
6. Six holes were drilled into the polycarbonate sheet to match the holes on the angled dust port (Figure G.1-3).
7. Two - 2" PVC knockout plugs were center drilled on the lathe for a 3/8" NPT liquid-tight cord grip. The cord grip allows the electrical cord from the ultrasonic fog generator to reach a power source (Figure G.1-4).
8. Three small holes were drilled around the center hole of the knockout for passage of #10-32x3/8 machine screws (Figure G.1-4). The screws apply clamping pressure to seal against leakage.
9. After determining the final placement of the angled dust port and electrical cord opening, holes were drilled onto the bucket lid to match those already drilled for the #10-32x3/8 machine screws on the polycarbonate sheet, dust port, and knockout plugs (Figure G.1-5 & Figure G.1-6).
10. All potential sealing surfaces were lightly sanded to get rid of high spots and increase the surface area. This included removing the manufacturer's logo and printing on the top of the food storage bucket and bottom of the angled dust port.
11. All sanded gluing surfaces were cleaned using soap and distilled water.

12. The ultrasonic fog generator (Figure G.1-7) was placed inside the bucket, and its electrical cord passed through the liquid-tight cord grip immediately prior to sealing the chamber. This allowed the ultrasonic fog generator to be supplied with power (120VAC to 5VDC converter) while maintaining a sealed system that did not leak. The electrical cord ran through the lid of the chamber, out the front of the constant temperature box (Appendix I), and is plugged into a power strip.
13. The lid of the chamber was assembled using GE™ waterproof silicone sealant, and attached using #10-32x¾ stainless steel machine screws. Sealant was generously applied to any potential leaking point including around the perimeter of fabricated pieces, around stainless steel screws, and around the electrical cord within the liquid-tight cord grip (Figures G.1-8 and G.1-9).
14. The lid of the humidity chamber was snapped in place and sealed with silicone tape before the ultrasonic fog generator is turned on to further prevent any leaking.
15. The finished humidity chamber is shown (Figures G.1-10). The ultrasonic fog generator is located within the chamber.

G.1-1: Polyethylene food storage bucket prior to modifications. Lid is not shown. Image taken from public domain.

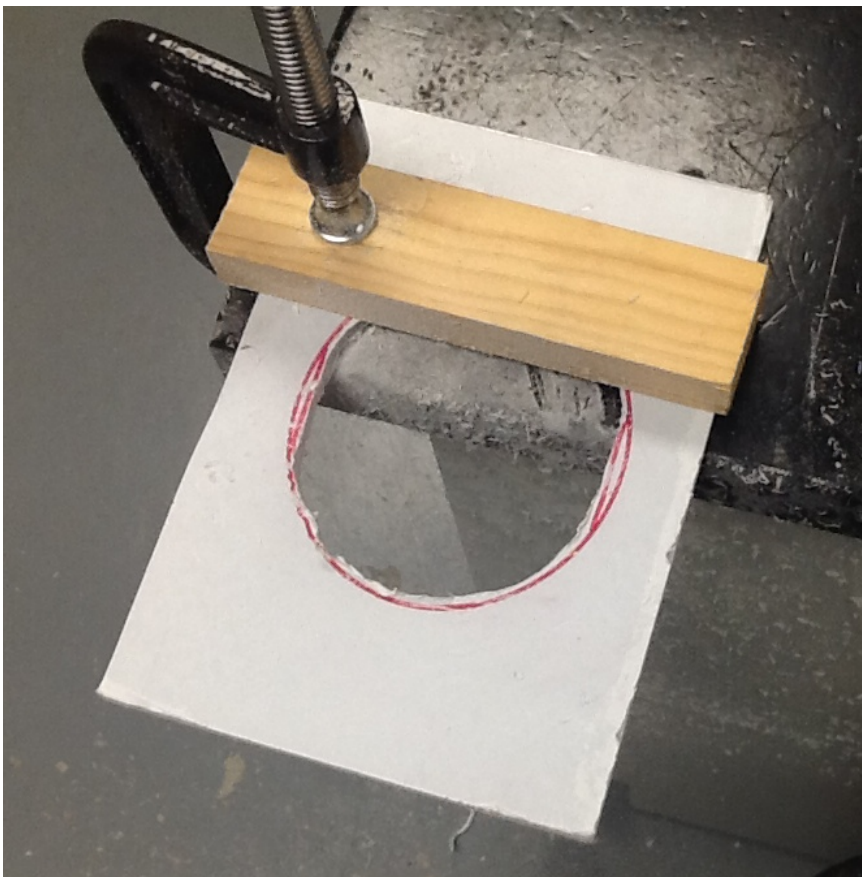

Figure G.1-2: Humidity chamber fabrication step 1. A hole (4” longest diameter, 3.75” shortest diameter) was rough cut into a rectangular piece of polycarbonate sheet using a jigsaw, and then finished with a sanding drum mounted in a Dremel™ tool. The outside corners were later rounded using the Dremel™ tool. This piece served as a firm surface to both seal and attach the 4” angled dust port.

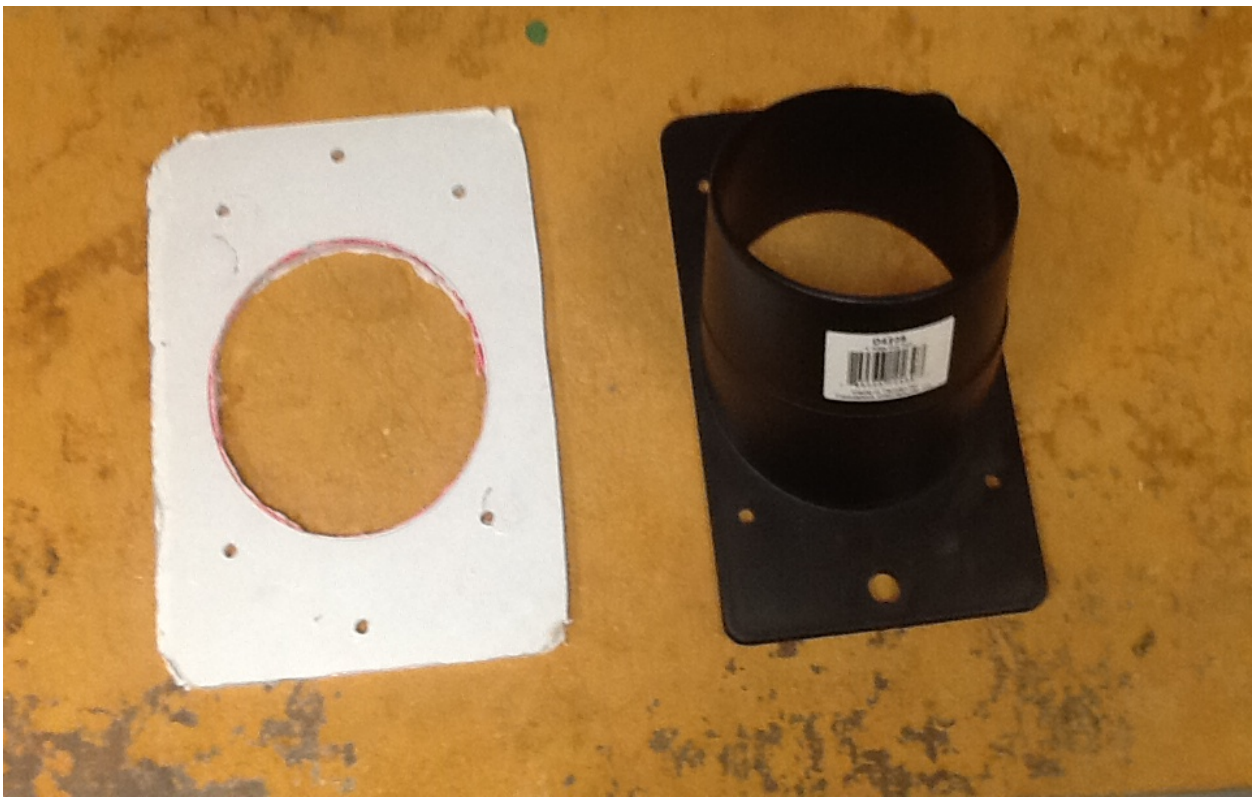

Figure G.1-3: Humidity chamber fabrication step 2. Four inch angled dust port and matching polycarbonate base plate. Both pieces have matching holes that allowed them to be attached using stainless steel machine screws.

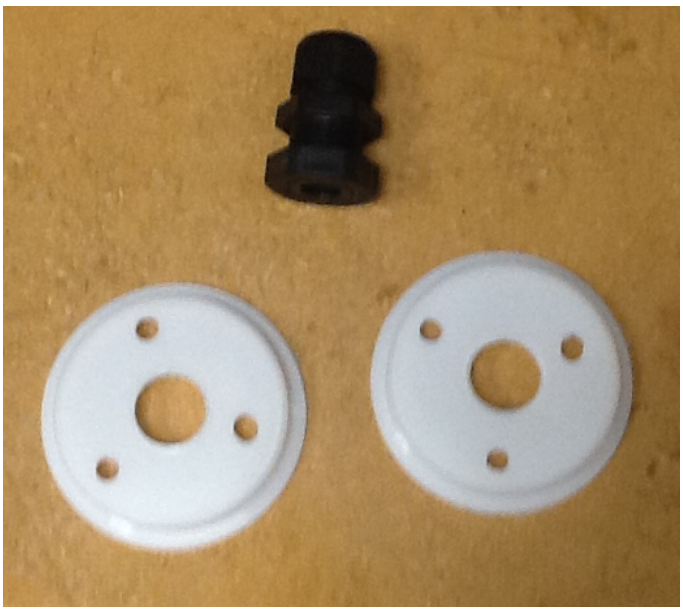

Figure G.1-4: Humidity chamber fabrication step 3. 2” PVC knockout plugs and a liquid-tight cord grip were connected to the chamber lid to provide an air-tight passage for the electrical cord to the ultrasonic fog generator.

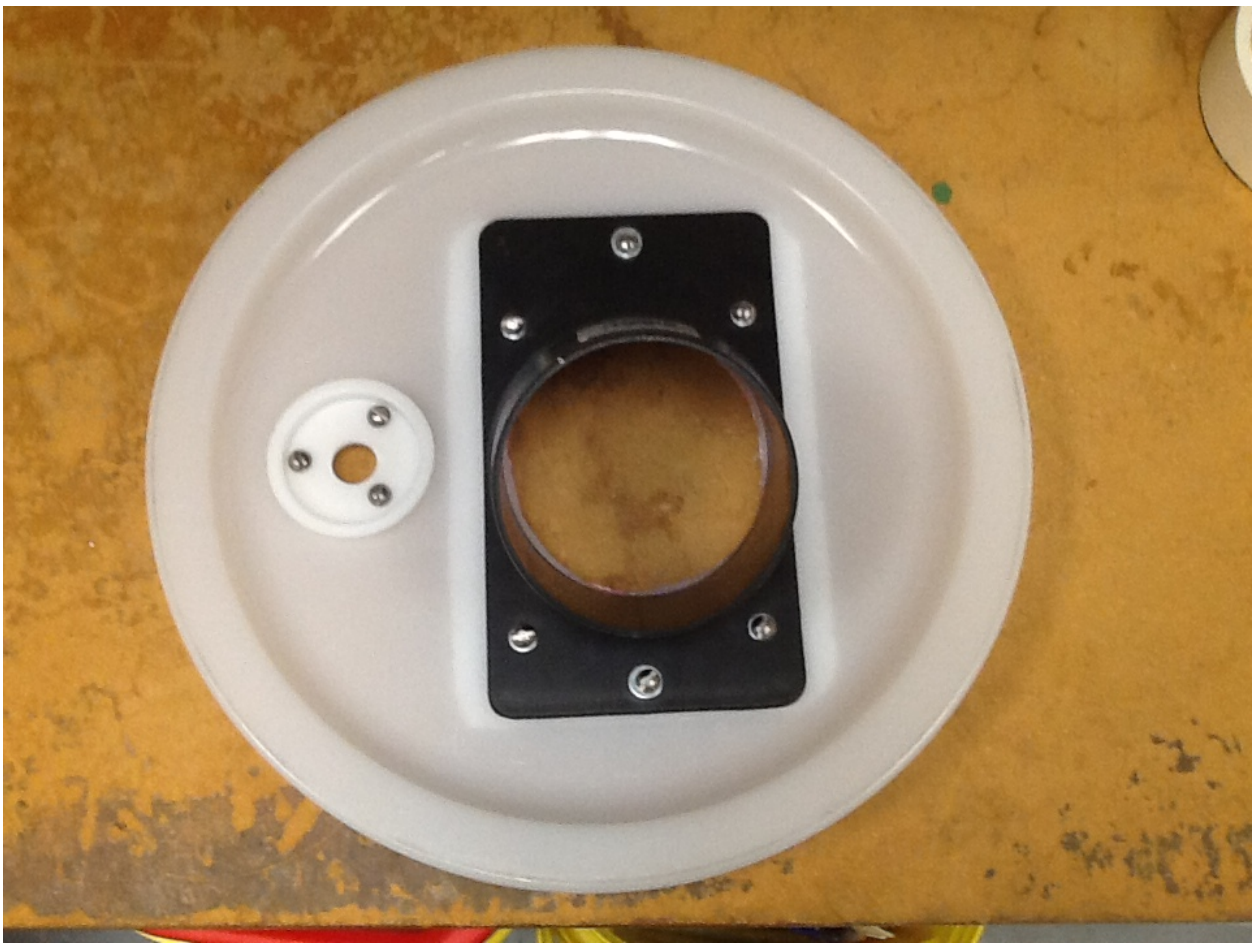

Figure G.1-5: Humidity chamber fabrication step 4. Top of the chamber lid. Pieces were assembled prior to sealing to make sure that everything fit in its appropriate place and to develop a strategy for applying the sealant.

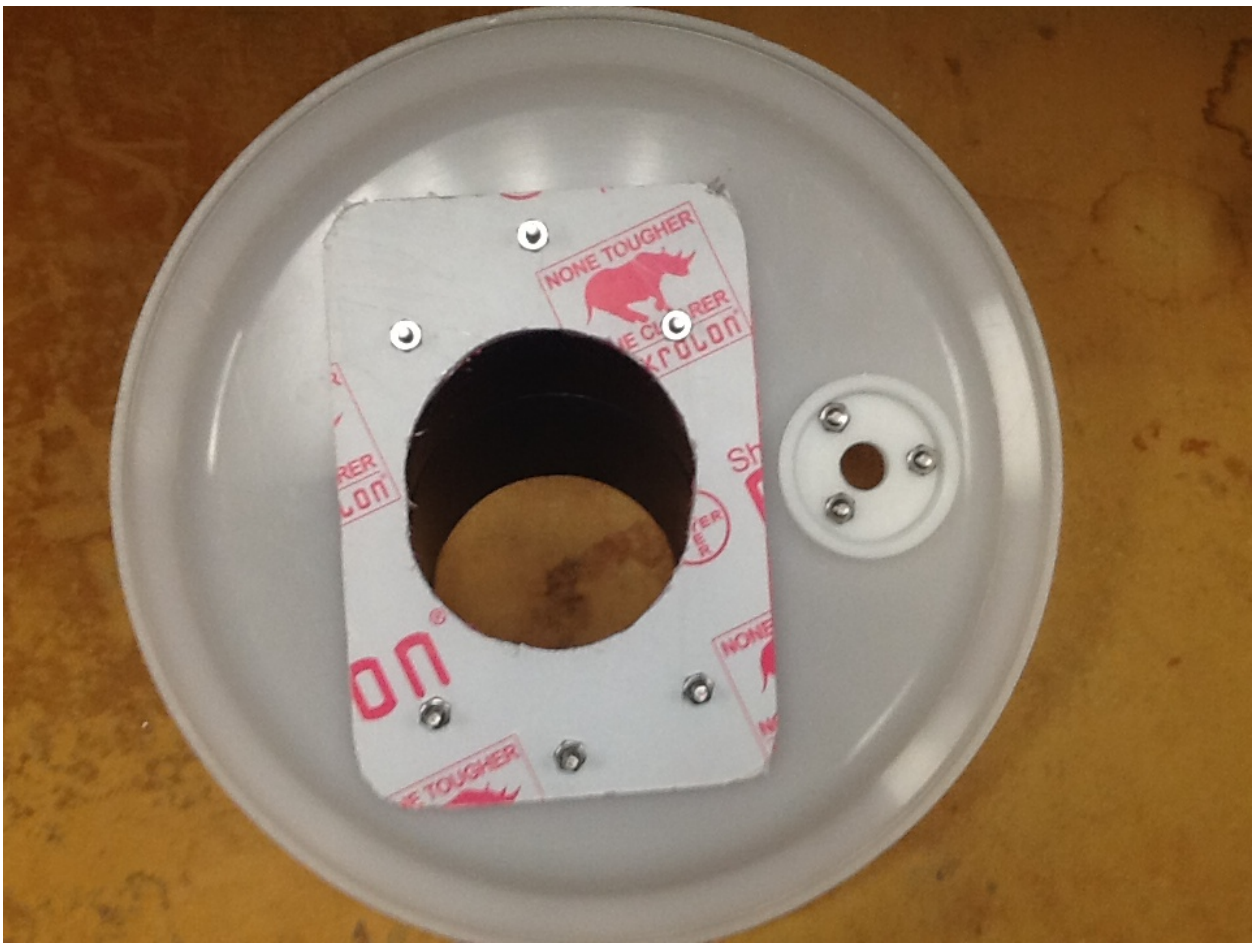

Figure G.1-6: Humidity chamber fabrication step 5. Bottom of the chamber lid. Pieces were assembled prior to sealing to make sure that everything fit in its appropriate place and to develop a strategy for applying the sealant.

Figure G.1-7: Completed humidity chamber base. A picture showing the completed humidity chamber base open and closed. The cord of the ultrasonic fog generator passes through the lid of the completed bucket so that it can be housed inside when the reservoir is sealed.

Figure G.1-8: Top of the humidity chamber lid. GE™ waterproof silicone sealant was generously applied to create an air tight seal.

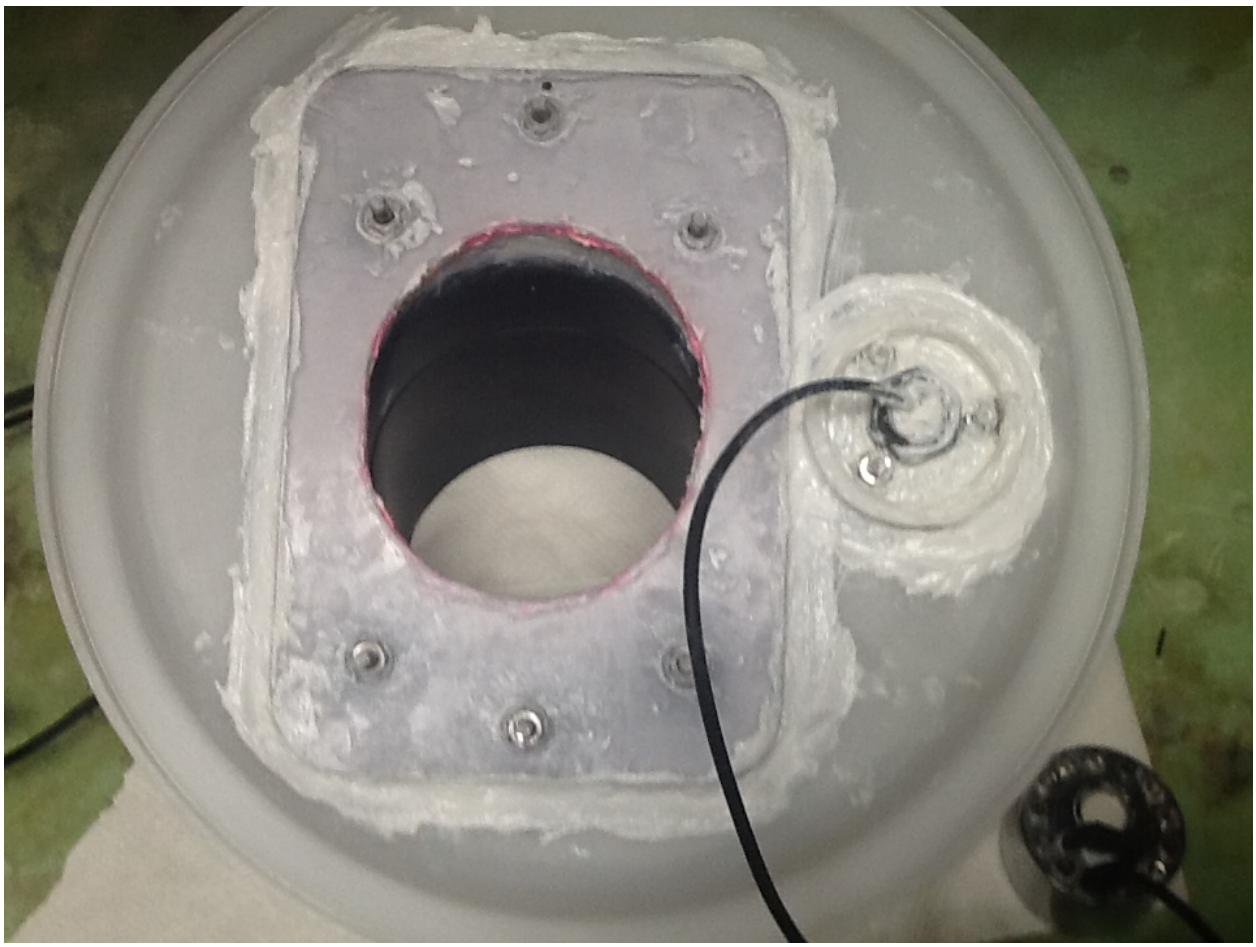

Figure G.1-9: Bottom of the humidity chamber lid. GE™ waterproof silicone sealant was generously applied to create an air tight seal. The ultrasonic fog generator can be seen in the lower right corner of the image.

Figure G.1-10: Completed humidity chamber base. The ultrasonic fog generator is housed within the chamber.

G.2 Chamber connector

The chamber connector served as the bridge between the humidity chamber and the experimental columns. It was fashioned out of 4” diameter flex hose in order to also serve as a reservoir for humid air. It was created in the following manner:

1. A PVC saw and miter box was used to shorten a 2” to 1–½” Schedule 40 PVC adapter by 0.6” (Figure G.2-1).
2. Both ends of the adapter were squared on the lathe (Figure G.2-2).
3. The center opening of the adapter was widened slightly on the lathe so that it would friction-fit on a 2” to 4” dust reducer (Figure G.2-3).
4. The adapter was solvent welded to the dust reducer with Christy’s Red Hot Blue Glue™, a type of PVC cement (Figure G.2-4).
5. The protruding portion of the reducer on the newly created piece was sawn off using a PVC saw and miter box (Figure G.2-5).
6. A hole was step drilled eventually reaching a ½” drill bit on a 2” PVC 45^{o} angled connector to fit a sensor socket (Figure G.2-6).
7. The 2” PVC angled connector was solvent welded with Christy’s Red Hot Blue Glue™ to the 2” to 4” dust reducer. The newly created piece is capable of providing a connection to both PVC and dust port pipes (Figure G.2-7).
8. A sensor socket was solvent welded to the PVC 45^{o} angled connector with Christy’s Red Hot Blue Glue™. An artist’s paintbrush was used to apply the cement around the joint between the outside of the connector and the socket to make the connection leak proof.
9. The completed connector is shown (Figure G.2-8).
10. A 12” length of 4” flex hose was attached using hose clamps to both the connector and chamber. It was then sealed with red silicone tape to complete the humidity sensor (Figure G.2-9).

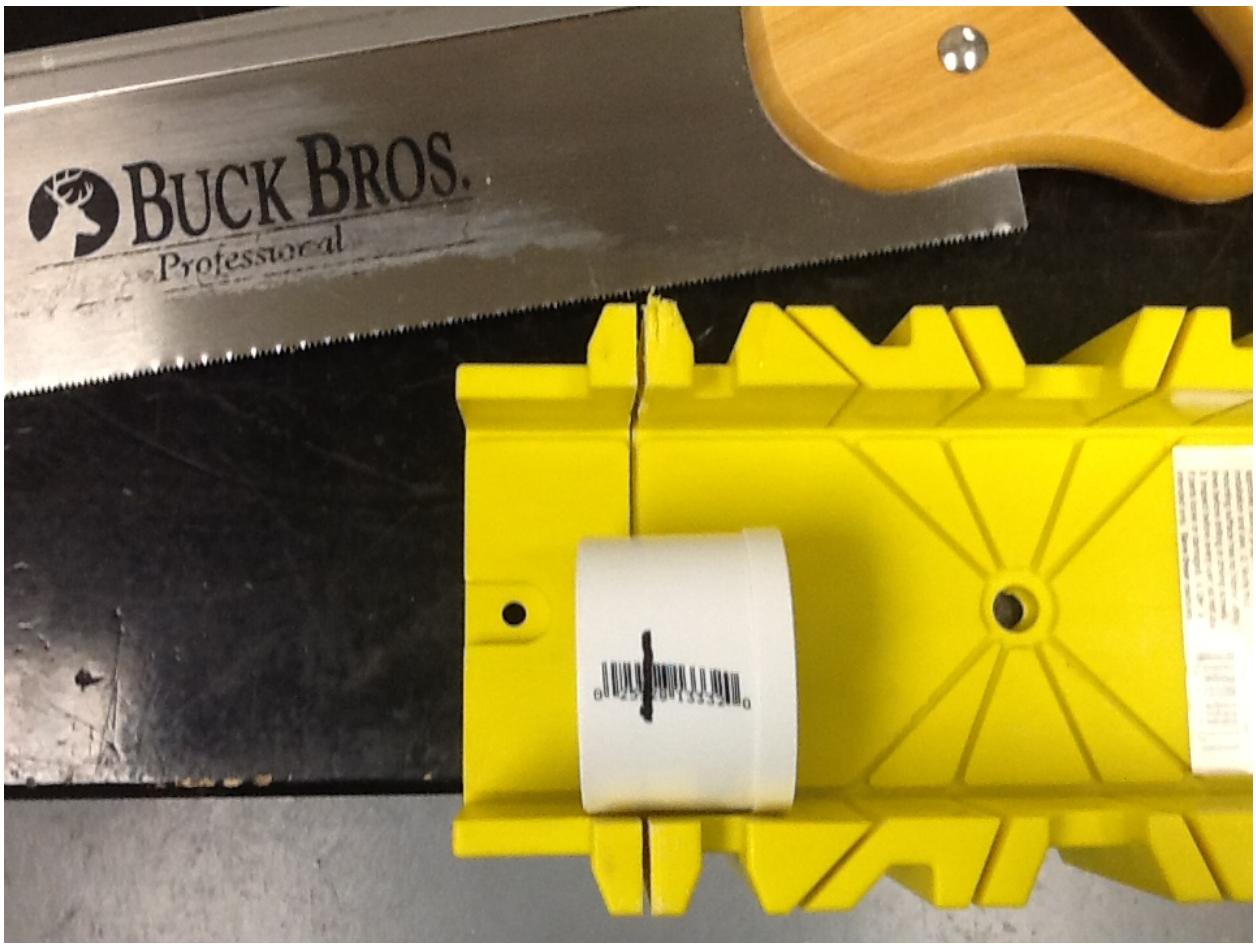

Figure G.2-1: Chamber connector fabrication step 1. A PVC saw and miter box was used to remove 0.6” from one end of a 2” to 1–½” adapter.

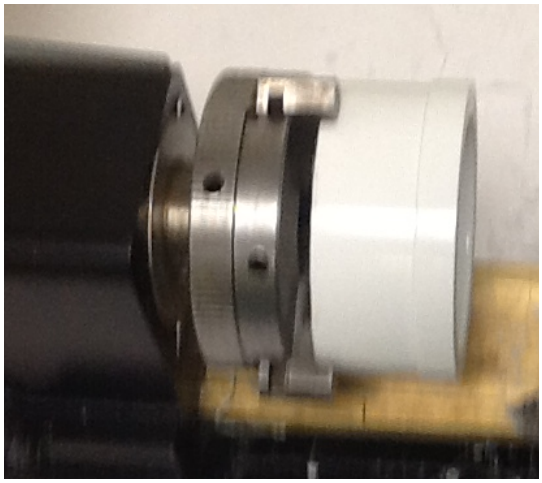

Figure G.2-2: Chamber connector fabrication step 2. Both ends of the adapter were squared on the lathe.

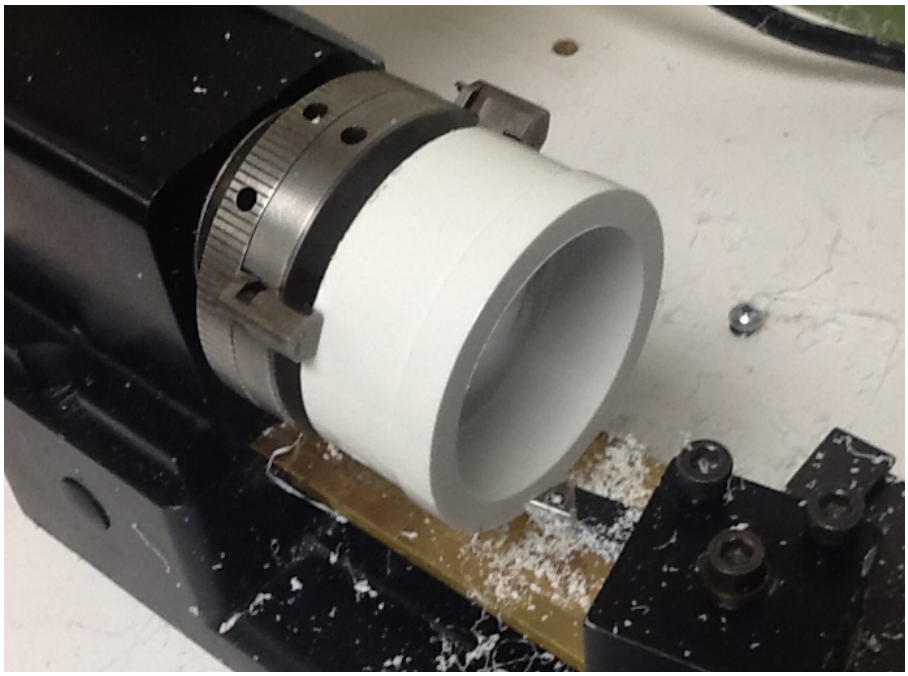

Figure G.2-3: Chamber connector fabrication step 3. The center opening of the adapter was widened on the lathe to be able to slide onto a 2” to 4” dust reducer

Figure G.2-4: Chamber connector fabrication step 4. The adapter was solvent welded with Christy's Red Hot Blue Glue™ to the dust reducer.

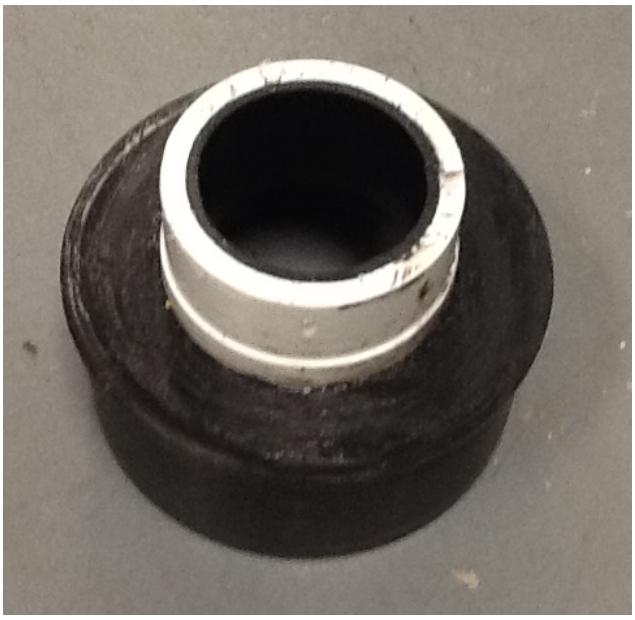

Figure G.2-5: Chamber connector fabrication step 5. The protruding portion of the reducer was sawn flush with the adapter.

Figure G.2-6: Chamber connector fabrication step 6. A hole was step drilled, eventually reaching a ½” drill bit on a 2” PVC 45^{o} angled connector to house a sensor socket.

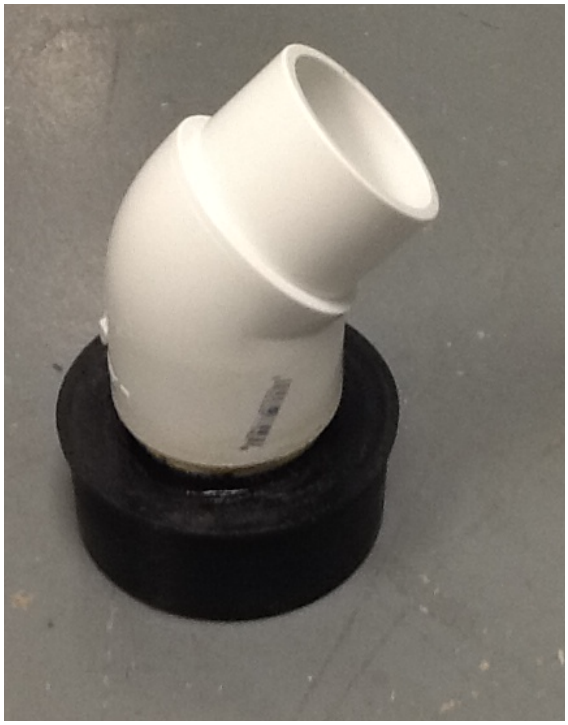

Figure G.2-7: Chamber connector fabrication step 7. The 2” PVC angled connector was glued to the 2” to 4” dust reducer.

Figure G.2-8: Chamber connector fabrication step 8. The completed connector is shown. This piece was attached to the humidity chamber.

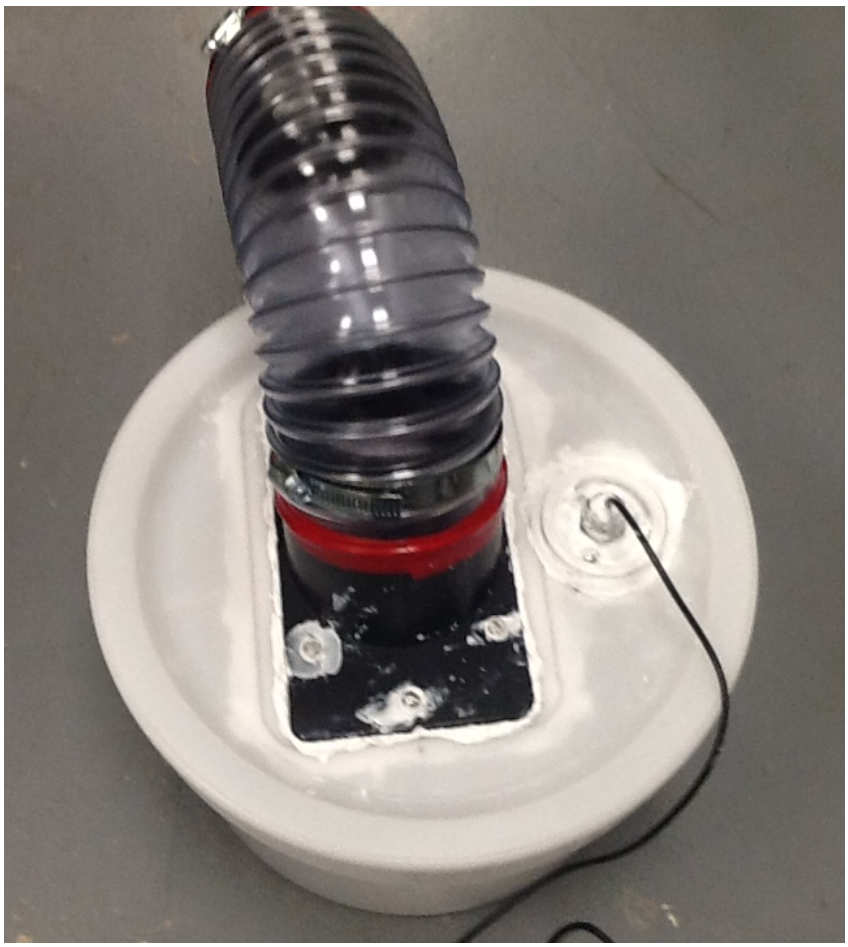

Figure G.2-9: Completed humidity chamber. The finished humidity source is shown.

APPENDIX H: COLUMN STAND

H.1 Column stand

A rigid fixture was constructed from Unistrut™ 1-5/8" slotted channel (Figure H.1-1) to hold the experiment in place. Note that the column stand is asymmetrical so that the column mass is centered (Figure H.1-2). The primary components of the column stand are:

1. Two uprights consisting of 21" long pieces of channel.
2. Two 12" long pieces of channel for horizontal crossbars.
3. One 12" long piece of channel mounted perpendicular to the base of an upright. This horizontal piece serves to create a tripod base for stability.
4. Various Unistrut™ connectors attached with 3/8-16x1 hex bolts and Unistrut™ spring nuts.
5. Three carriage bolts (3/8-16x1.5), one for each corner of the stand, are attached to a Unistrut™ connector in a way that allows easy leveling of the experiment (Figure H.1-2). A 3/8-16 nut located on the bottom side controls the height of the leg, and an identical nut on top locks the leg in place. Fender washers are used to cover large slots in the Unistrut™ connector.
6. The test column is attached to the crossbars of the column stand with Unistrut™ pipe clamps for 2" Schedule 40 PVC (Figure H.1-3).

Figure H.1-1: Column stand fabricated from Unistrut™ 1-5/8” slotted channel.

Figure H.1-2: Column stand feet. Carriage bolts (3/8-16x1.5) were used as feet for the column stand to allow for easy leveling of the column.

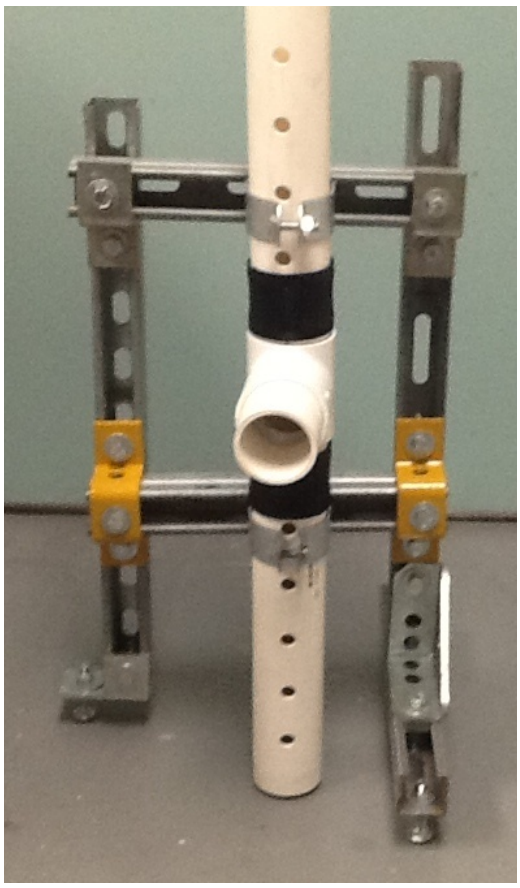

Figure H.1-3: Column stand is shown holding a partially completed column.

APPENDIX I: CONSTANT TEMPERATURE BOX

I.1 Constant temperature box

Relative humidity is highly dependent on temperature. An increase in temperature decreases the relative humidity by increasing the ability of the air to absorb water vapor, while a decrease in temperature can lead to condensation, especially in an environment where the relative humidity is near 100%. To avoid condensation, the experiment was performed within a constant temperature box that was fabricated for a previous project. The interior of the constant temperature box (Figure I.1-1) measures 31.5" X 48" X 30" (depth X length X height) and is made of two-inch thick Styrofoam insulation that has been joined with drywall screws and construction cement. The Styrofoam has an effective R value of 10.50 at 75 ^{o}F. The front of the box is a removable piece of 2" thick styrofoam that is held in place with elastic cord (Figure I.1-2). A piece of ¾" thick Styrofoam sheet fits within the box and behind the front to help create a better seal (Figure I.1-3). This sheet has an R value of 5.0. The constant temperature box rests on top of a heavy steel desk and is thermally isolated from the desk with a piece of ¾" thick particle board and another sheet of 2" Styrofoam insulation (Figure I.1-1).

Temperature inside the box is controlled by a Pharmacia Biotech Multitemp III™ water bath (Figure I.1-4). The water bath generates constant temperature water, and circulates it to two Lytron™ radiators (part #4121G3) within the box through 3/8" diameter tubing (Figure I.1-5). The radiators are supported by bricks (Figure I.1-6) to provide unrestricted airflow to two 120 mm Comair Rotron™ 24VDC fans (model #MC24B3) located on the underside of each radiator. The power supply for the fans is located outside of the box. This arrangement circulates constant

temperature air within the insulated box. From experimentation, it was found that setting the water bath to a temperature of 21.8 ^{o}C keeps the box at 25 ^{o}C. In addition to the water circulation hoses, sensor wires and power supply cables also pass through the walls of the box. These holes are not completely sealed. A plastic cafeteria tray placed below the column stand (Appendix H) prevents the legs from sinking into the Styrofoam box and provides a stable surface for leveling the column (Figure I.1-7).

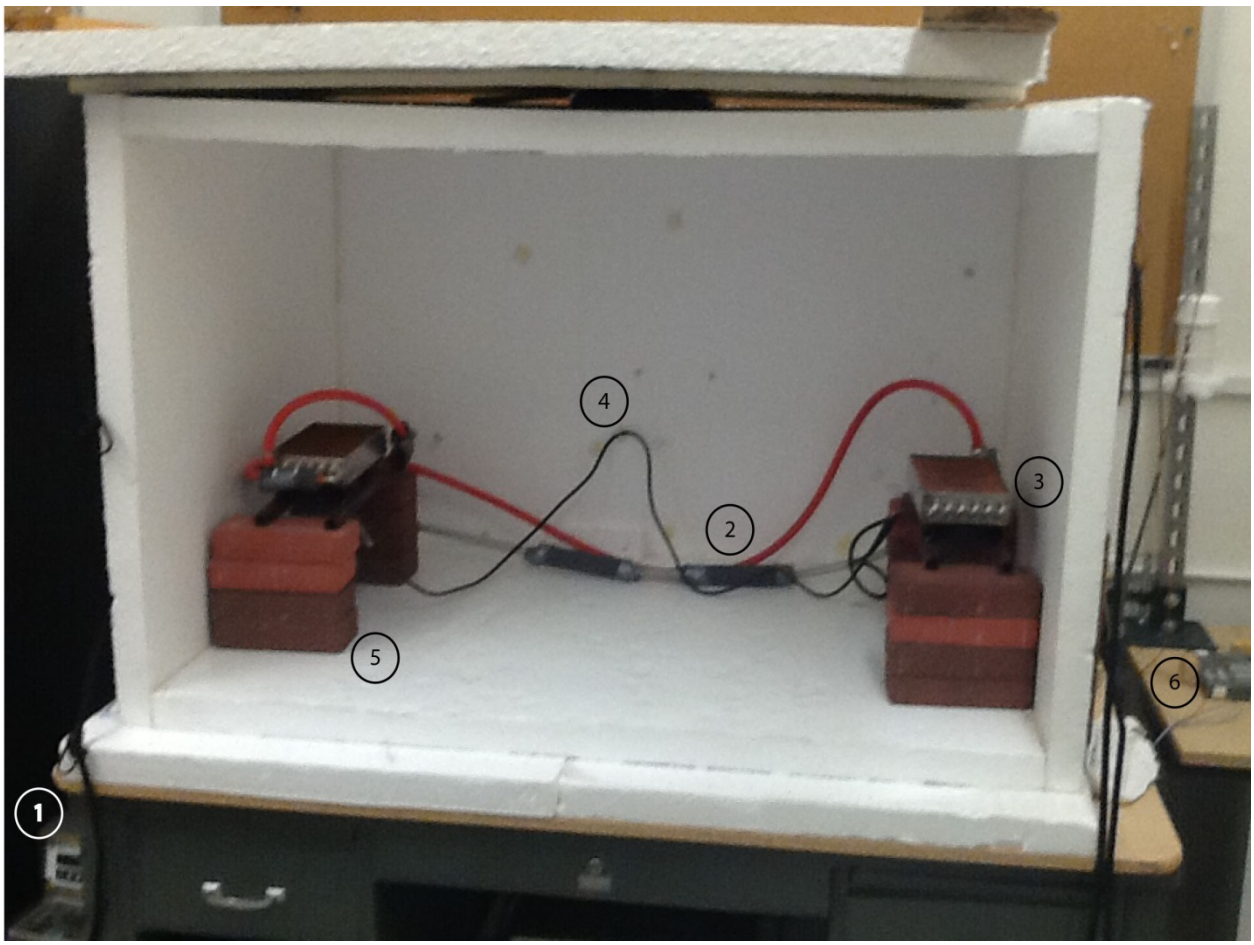

Figure I.1-1: Constant temperature box. Data logging equipment is to the right of the box. Water bath is to the left. The front of the box is lying on top in this picture.

The numbers correspond to:

1) The water bath used to circulate water at 21.8 ^{o}C to keep the temperature within the box at 25 ^{o}C.

2) 3/8" diameter tubing used to circulate the water. The orange tubes take water from the water bath to the radiators, while the clear tubes return the water to be recirculated.

3) Radiator/fan combination. The stainless steel radiators with copper fins each have two 120 mm diameter fans located beneath them.

4) Power cords for the fans. This power cord is held by a tie to the side of the box to prevent contact with water in the event of a leak.

5) Bricks used to support the radiators/fans and facilitate free circulation of air.

6) Data logger and power supply equipment

Figure I.1-2: Closed constant temperature box. A 2” thick piece of Styrofoam was used to close the constant temperature box. Wooden planks on each side of the front piece help to prevent the elastic cord from digging into the styrofoam.

Figure I.1-3: Partially closed constant temperature box. A piece of ¾" thick Styrofoam sheet fits within the box and behind the front to help create a better seal. Part of the experimental column can be seen within the box. The power cord for the ultrasonic fog generator (Appendix G) is seen exiting the cut-out square.

Figure I.1-4: Water bath. A water bath is used to circulate water within the sealed box to keep temperature constant.

Figure I.1-5: Tubes entering constant temperature box. Holes in the walls of the box allow water tubes, electrical cords, sensor lead wires, and the tubing attached to the column at U5 and L5 to enter and exit the closed environment.

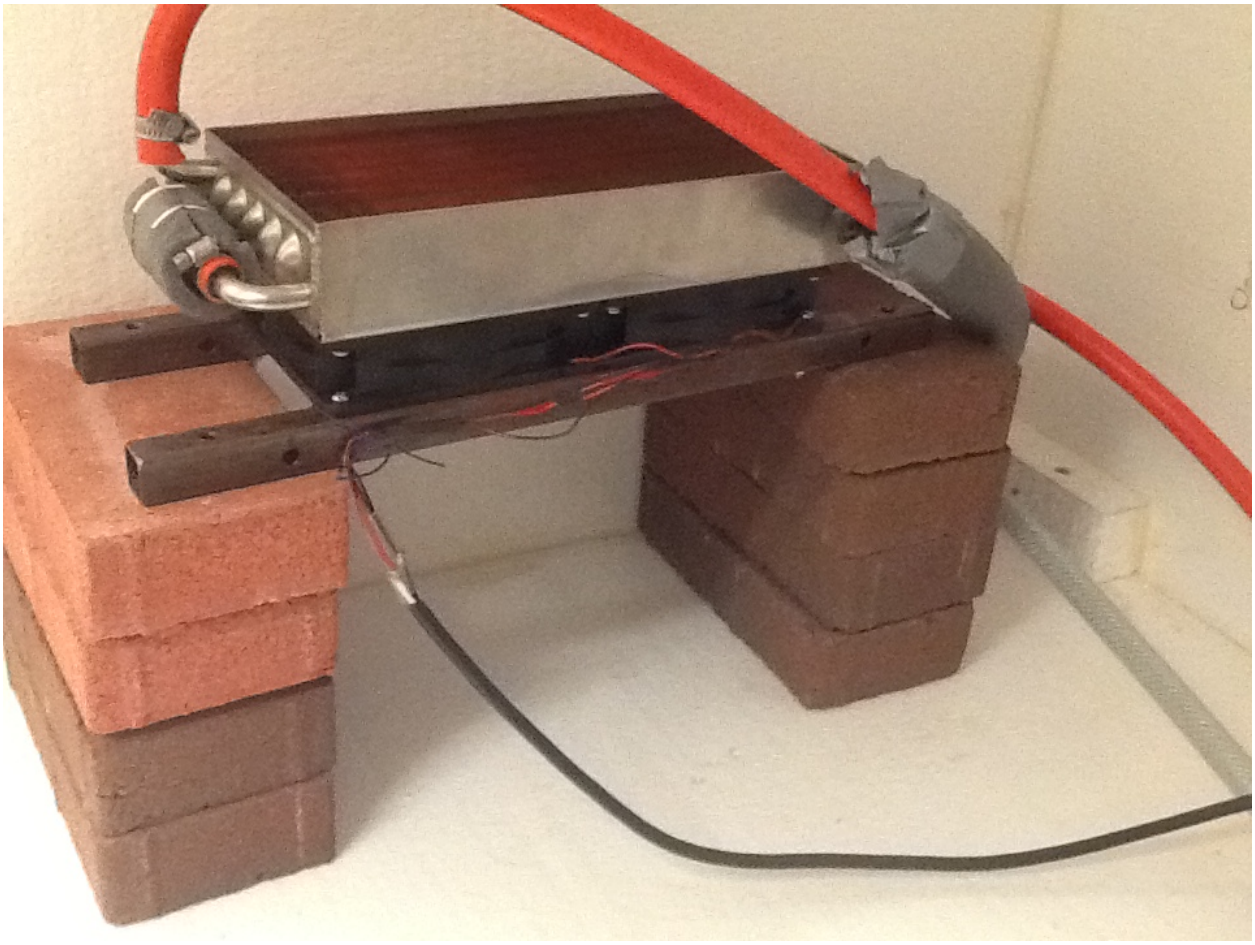

Figure I.1-6: Fans. Fans are placed on bricks to facilitate air circulation.

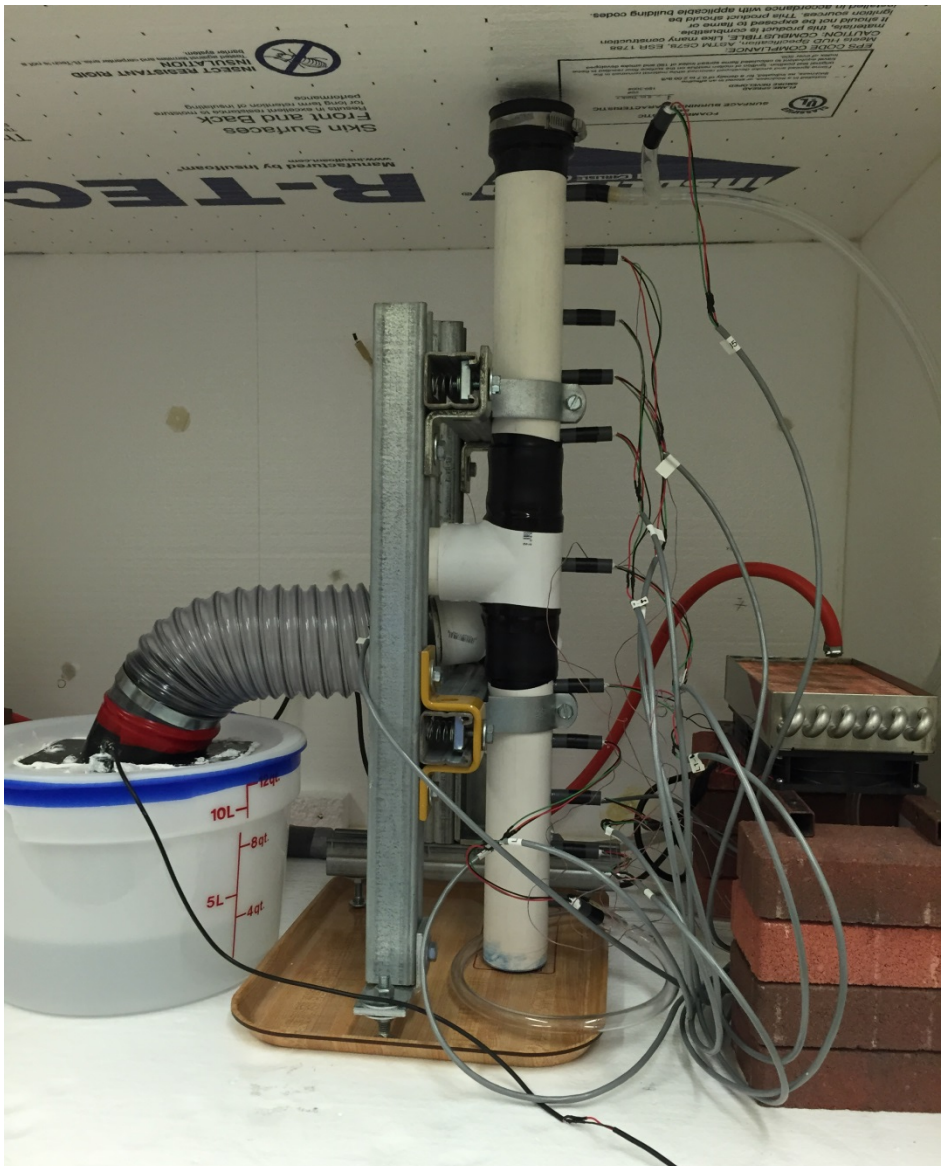

Figure I.1-7: Completed experiment inside of the constant temperature box. A cafeteria tray is used to support the weight of the test columns and not damage the Styrofoam. All sensors are routed through the side of the box and connected the data logger to the right of the image (not shown).

APPENDIX J: DATA ACQUISITION AND POWER SUPPLY

J.1: Equipment and setup

In addition to the water bath, a number of external components are employed to: 1) acquire data from the experiment; and 2) provide power for the sensors and fans. These components are mounted on a table next to the constant temperature box (Figure J.1-1).

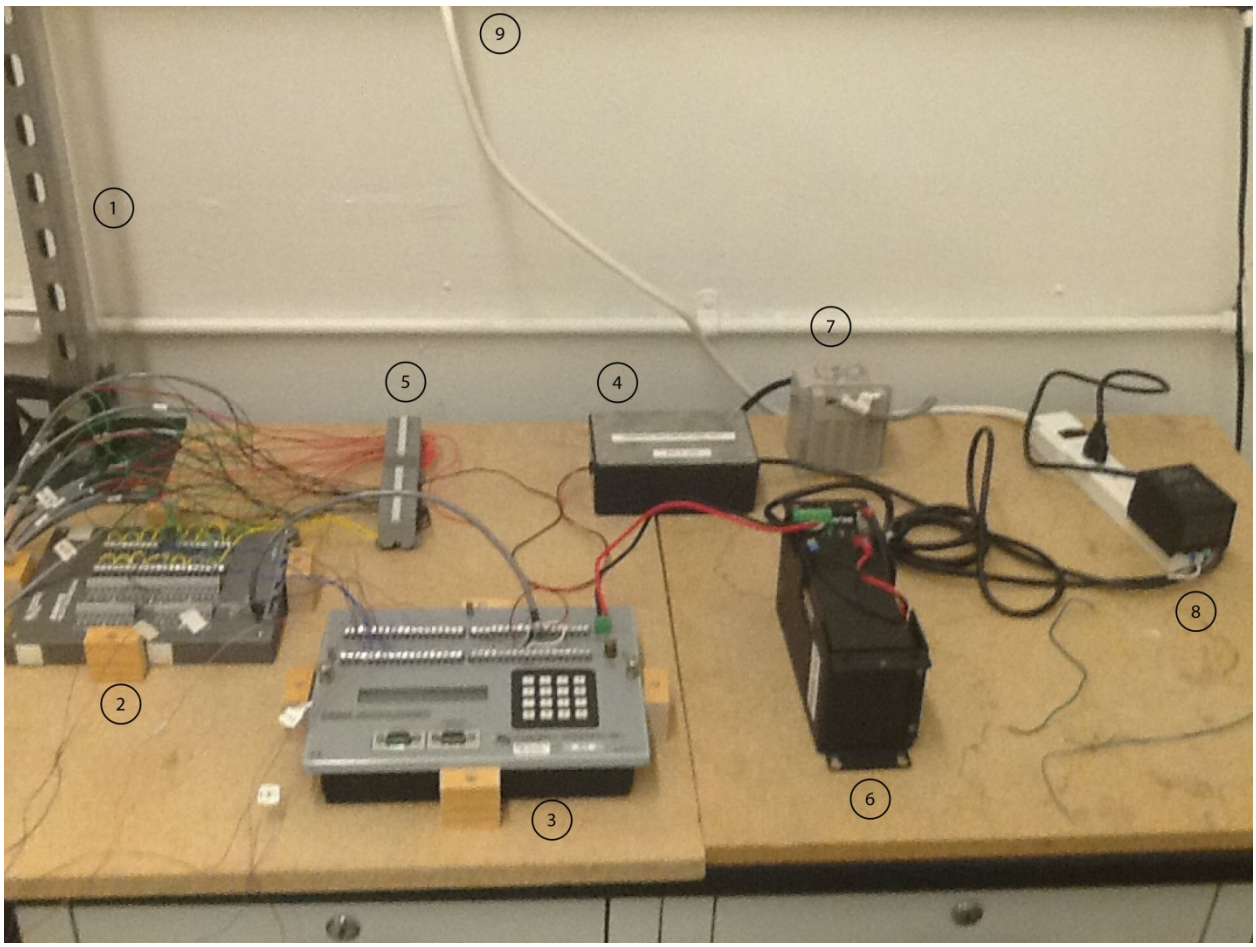

Figure J.1-1: A numbered image of the important electrical components of the experiment.

1) Weather station: This station (Figure J.1-2) records room temperature conditions during the experiment. A vertical post made from Unistrut™ 1-5/8" slotted channel holds a barometer, thermocouple, and humidity sensor (Appendix K) in close proximity to the outside of the constant temperature box (FigureJ.1-2). The barometer and thermocouple are enclosed within a partially sealed length of PVC pipe to negate the effects of local air currents (e.g. people walking by, room door opening, etc.).

2) Campbell Scientific™ AM416 Relay Multiplexer: The multiplexer increases the number of sensors that can be monitored by a data logger. All of the powered sensors (humidity and barometer) are connected to the multiplexer. The multiplexer is controlled by the data logger (see below).

3) Campbell Scientific™ CR23X Data logger: The CR23X is used to control the measurements made during the experiment. It is programmed to measure the output from

all sensors sequentially. All thermocouples used in the experiment are connected directly to the data logger.

4) Omega™ PST-5 Regulated Power supply: This power supply provides a stable 5 volt DC output for the humidity sensors and barometer. Voltage output from the PST-5 is monitored by the multiplexer on the same schedule as the experiment.

5) Power distribution blocks: Provide multiple connection points for the powered sensors (humidity and barometer) to connect with the positive and negative terminals of the PST-5. The negative side is also routed to the data logger to provide a reference voltage for the same sensors.

6) Campbell Scientific™ PS100 12 volt battery supply: Power supply for the CR23X data logger includes a 12 volt battery to serve as a backup in the event of a power outage.

7) Omron™ S82K-03024 24 Volt DC power supply: This 24 Volt power supply is used to supply power to the radiator fans in the constant temperature box.

8) Power Strip: Used to increase the available sockets for equipment to be powered.

9) Main power supply: Wall outlets used to feed power to the power strip.

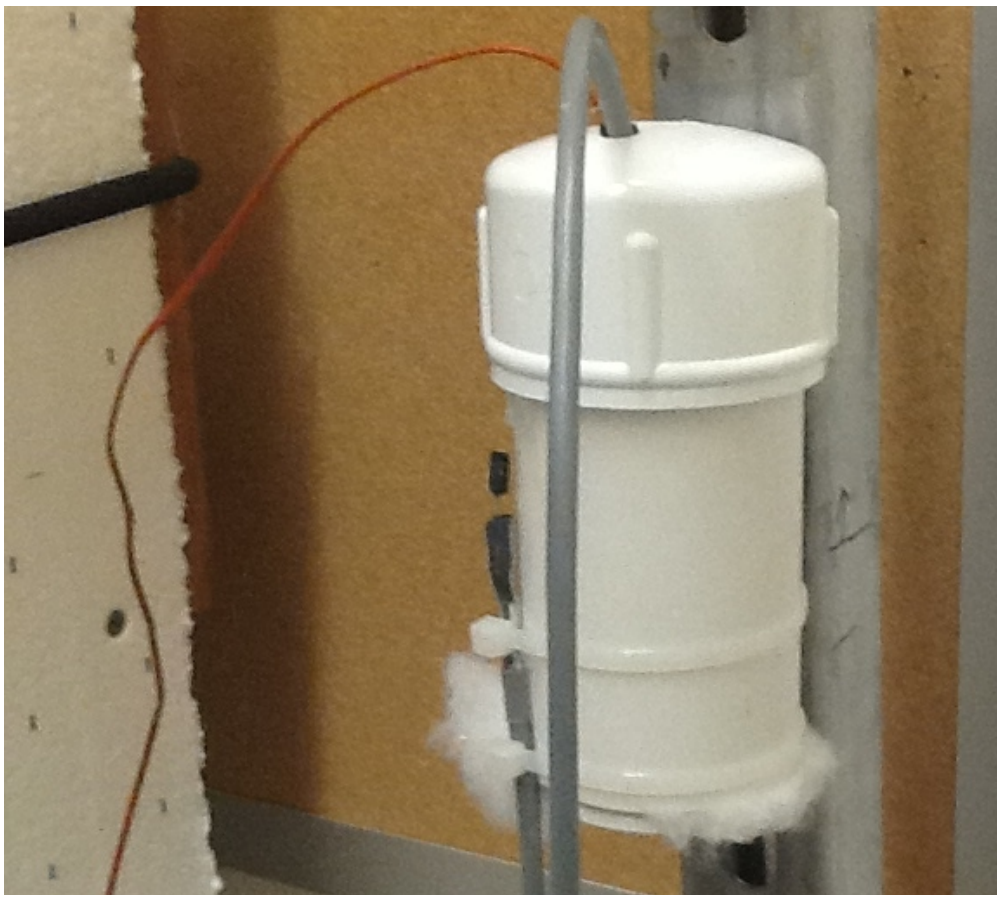

Figure J.1-2: Weather station used to test room conditions during the experiment. A thermocouple and barometer are located within this capped PVC chamber. The white "furry" substance at the bottom of the PVC tube is a layer of polyester upholstery batting that serves to damp out spurious air currents. A humidity sensor is seen attached to the outside of the column. Measurements are made in close proximity to the constant temperature box (seen on the left of the photo). Wires leads are connected to the data logger.

J.2 Measurements

A program was created in Campbell Scientific™ PC400 software to monitor all sensors during the experiment. A total of 25 sensors are monitored: 15 humidity sensors, 7 thermocouples, 1 barometer, 1 supply voltage, and 1 reference temperature housed within the data logger.

Measurements are made sequentially at five second intervals. Each minute, the average of these measurements is stored. Voltages recorded by the humidity sensors are used to convert to relative humidity (Appendix K). Voltages recorded by the barometer are used to convert to pressure in Kilopascals (Appendix K). The thermocouples give an output in degrees Celsius based on an internal reference temperature from the data logger.

APPENDIX K: SENSOR SPECIFICATIONS

K.1 Humidity Sensors – Honeywell™ HIH-4010

HIH-4010/4020/4021 Series

TABLE 1. PERFORMANCE SPECIFICATIONS (At 5 Vdc supply and 25 °C [77 °F] unless otherwise noted.)

Parameter	Minimum	Typical	Maximum	Unit	Specific Note
Interchangeability (first order curve)	–	–	–	–	–
0% RH to 59% RH	-5	–	5	% RH	–
60% RH to 100% RH	-8	–	8	% RH	–
Accuracy (best fit straight line)	-3.5	–	+3.5	% RH	1
Hysterisis	–	3	–	% RH	–
Repeatability	–	±0.5	–	% RH	–
Settling time	–	–	70	ms	–
Response time (1/e in slow moving air)	–	5	–	s	–
Stability (at 50 %RH in 1 year)	–	±1.2	–	% RH	2
Stability (at 50 %RH in 1 year)	–	±0.5	–	% RH	3
Voltage supply	4	–	5.8	Vdc	4
Current supply	–	200	500	µA	–
Voltage output (1st order curve fit)	$V_{OUT}=(V_{SUPPLY})(0.0062(\text{sensor RH}) + 0.16)$, typical at 25 °C				
Temperature compensation	True RH = (Sensor RH)/(1.0546 – 0.0026T), T in °C				
Output voltage temp. coefficient at 50% RH 5 V	–	-4	–	mV/°C	–
Operating temperature	-40[-40]	See Figure 1.	85[185]	°C[°F]	–
Operating humidity (HIH-4010)	0	See Figure 1.	100	% RH	5
Operating humidity (HIH-4020)	0	See Figure 1.	100	% RH	5
Operating humidity (HIH-4021)	0	See Figure 1.	100	% RH	–
Storage temperature	-50[-58]	–	125[257]	°C[°F]	–
Storage humidity	See Figure 2.			% RH	5

Specific Notes:

1. For HIH-40[*] 0/20/21-003/004 catalog listings only.
2. Includes testing outside of recommended operating zone.
3. Includes testing for recommended operating zone only.
4. Device is calibrated at 5 Vdc and 25 °C.
5. Non-condensing environment. When liquid water falls on the humidity sensor die, output goes to a low rail condition indicating no humidity.

General Notes:

- Sensor is ratiometric to supply voltage.
- Extended exposure to >90% RH causes a reversible shift of 3% RH.
- Sensor is light sensitive. For best performance, shield sensor from bright light.

FACTORY CALIBRATION DATA

HIH-40[*] 0/4020/402[*] Sensors may be ordered with a calibration and data printout. See Table 2 and the order guide on the back page.

TABLE 2. EXAMPLE DATA PRINTOUT

Model	HIH-40[*] 0-003
Channel	92
Wafer	030996M
MRP	337313
Calculated values at 5 V	
V_{OUT} at 0% RH	0.958 V
V_{OUT} at 75.3% RH	3.268 V
Linear output for 3.5% RH accuracy at 25 °C	
Zero offset	0.958 V
Slope	30.680 mV/%RH
Sensor RH	(V_{OUT} - zero offset)/slope (V_{OUT} - 0.958)/0.0307
Ratiometric response for 0% RH to 100% RH	
V_{OUT}	V_{SUPPLY} (0.1915 to 0.8130)

For HIH-40[*] 0-00[*] /002/003/004 catalog listings only.

For HIH-4020-00[*] /002/003/004 and HIH-4021-001/002/003/004 catalog listings only.

K.2 Thermocouples – Omega™ Type T

- 0.010” Diameter
- 72” long wire leads
- Teflon Insulation
- Copper-Constantan
- Item #5TC-TT-T-30-72

K.3 Barometer – Freescale Semiconductor™ MPX4115A

Table 2. Operating Characteristics
(V_S = 5.1 Vdc, T_A = 25°C unless otherwise noted, P1 > P2 Decoupling circuit shown in Figure 3 required to meet electrical specifications.)

Characteristic		Symbol	Min	Typ	Max	Unit
Pressure Range[1]		P_{OP}	15	-	115	kPa
Supply Voltage[2]		V_S	4.85	5.1	5.35	Vdc
Supply Current		I_o	—	7.0	10	mAdc
Minimum Pressure Offset[3] @ V_S = 5.1 Volts	(0 to 85°C)	V_{off}	0.135	0.204	0.273	Vdc
Full Scale Output[4] @ V_S = 5.1 Volts	(0 to 85°C)	V_{FSO}	4.725	4.794	4.863	Vdc
Full Scale Span[5] @ V_S = 5.1 Volts	(0 to 85°C)	V_{FSS}	—	4.59	—	Vdc
Accuracy[6]	(0 to 85°C)	—	—	—	±1.5	$\%V_{FSS}$
Sensitivity		V/P	—	46	—	mV/kPa
Response Time[7]		t_R	—	1.0	—	ms
Output Source Current at Full Scale Output		I_o+	—	0.1	—	mAdc
Warm-Up Time[8]		—	—	20	—	mSec
Offset Stability[9]		—	—	±0.5	—	$\%V_{FSS}$

1. 1.0kPa (kiloPascal) equals 0.145 psi.
2. Device is ratiometric within this specified excitation range.
3. Offset (V_{off}) is defined as the output voltage at the minimum rated pressure.
4. Full Scale Output (V_{FSO}) is defined as the output voltage at the maximum or full rated pressure.
5. Full Scale Span (V_{FSS}) is defined as the algebraic difference between the output voltage at full rated pressure and the output voltage at the minimum rated pressure.
6. Accuracy (error budget) consists of the following:
   Linearity:Output deviation from a straight line relationship with pressure, using end point method, over the specified pressure range.
   Temperature Hysteresis:Output deviation at any temperature within the operating temperature range, after the temperature is cycled to and from the minimum or maximum operating temperature points, with zero differential pressure applied.
   Pressure Hysteresis:Output deviation at any pressure within the specified range, when this pressure is cycled to and from the minimum or maximum rated pressure at 25°C.
   TcSpan:Output deviation over the temperature range of 0° to 85°C, relative to 25°C.
   TcOffset:Output deviation with minimum pressure applied, over the temperature range of 0° to 85°C, relative to 25°C.
   Variation from Nominal:The variation from nominal values, for Offset or Full Scale Span, as a percent of V_{FSS} at 25°C.
7. Response Time is defined as the time for the incremental change in the output to go from 10% to 90% of its final value when subjected to a specified step change in pressure.
8. Warm-up is defined as the time required for the product to meet the specified output voltage after the Pressure has been stabilized.
9. Offset stability is the product's output deviation when subjected to 1000 hours of Pulsed Pressure, Temperature Cycling with Bias Test.

Table 3. Mechanical Characteristics

Characteristic	Symbol	Min	Typ	Max	Unit
Weight, Basic Element (Case 867)	—	—	4.0	—	Grams
Common Mode Line Pressure[1]	—	—	—	690	kPa

1. Common mode pressures beyond what is specified may result in leakage at the case-to-lead interface.

APPENDIX L: HUMIDITY SENSOR CALIBRATION

L.1 Supersaturated salt solutions

Supersaturated salt solutions are useful for calibrating humidity sensors for two important reasons: 1) a saturated salt solution provides a fixed relative humidity at a given temperature, and 2) a supersaturated salt solution has the potential to remain saturated even when interacting with moisture in the air (Greenspan, 1976). Two salts were selected to create supersaturated salt solutions in order to perform a two-point calibration for each humidity sensor used in the experiment. The first salt, Sodium Chloride (NaCl), gives a relative humidity of 74.25% ± 0.32, and the second, Magnesium Chloride ($MgCl_2$), gives a relative humidity of 32.78% ± 0.16; both at the same temperature: 25 ^{o}C. These salts are easily accessible, disposable, and they provide a low and high relative humidity within the working range of the sensors (Appendix K).

L.2 Construction of apparatus

The supersaturated salt solution was made in a small compartment fabricated out of 4" PVC pipe. The compartment was created using the following steps:

1. A section piece of 4" PVC pipe was cut down to 2.5".
2. A 4" PVC knockout was attached to the bottom of the 2.5" section using Christy's Red Hot Blue Glue™ to create a leak free seal (Figure L.2-1).
3. The section was marked at intervals every 13/16" around the circumference of the piece (Figure L.2-2) for sensor placement (16 total markings for 16 sensors).
4. A center point for drilling was created 1-3/4" from the bottom of the section in line with each marking from step 3 (Figure L.2-2).

5. The PVC section was clamped into a vice and a 5/8” holes were drilled with a spade bit on the drill press (Figure L.2-3).
6. Loose ends from the drilling were removed and cleaned using a deburring tool.
7. 16 Pieces of Excelon™ RNT tubing (3/8 ID by 5/8 OD) were cut to lengths of 1 cm with wire cutters (Figure L.2-4). These pieces fit within the holes and allow a connection for sensor sockets (Appendix D)
8. Each piece of tubing was lightly sanded to rough up the exterior using #220 Al Oxide paper.
9. Christy’s Red Hot Blue Glue™ was used to cement in place each of the sections of tubing (Figure L.2-5).

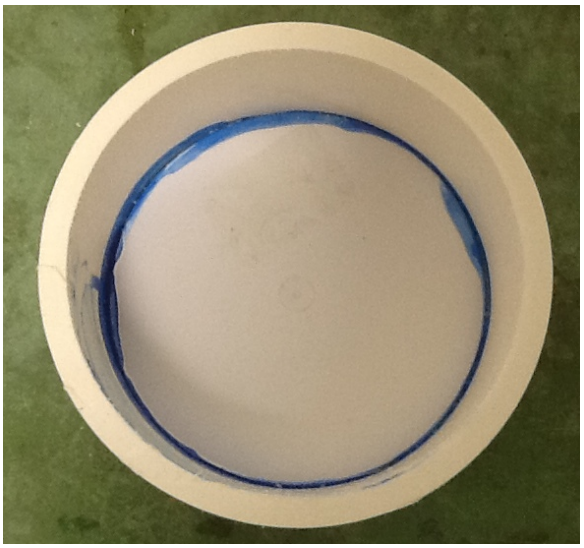

Figure L.2-1: Calibration apparatus step 1. A 4” PVC knockout is cemented onto a 2.5” long piece of 4” PVC pipe.

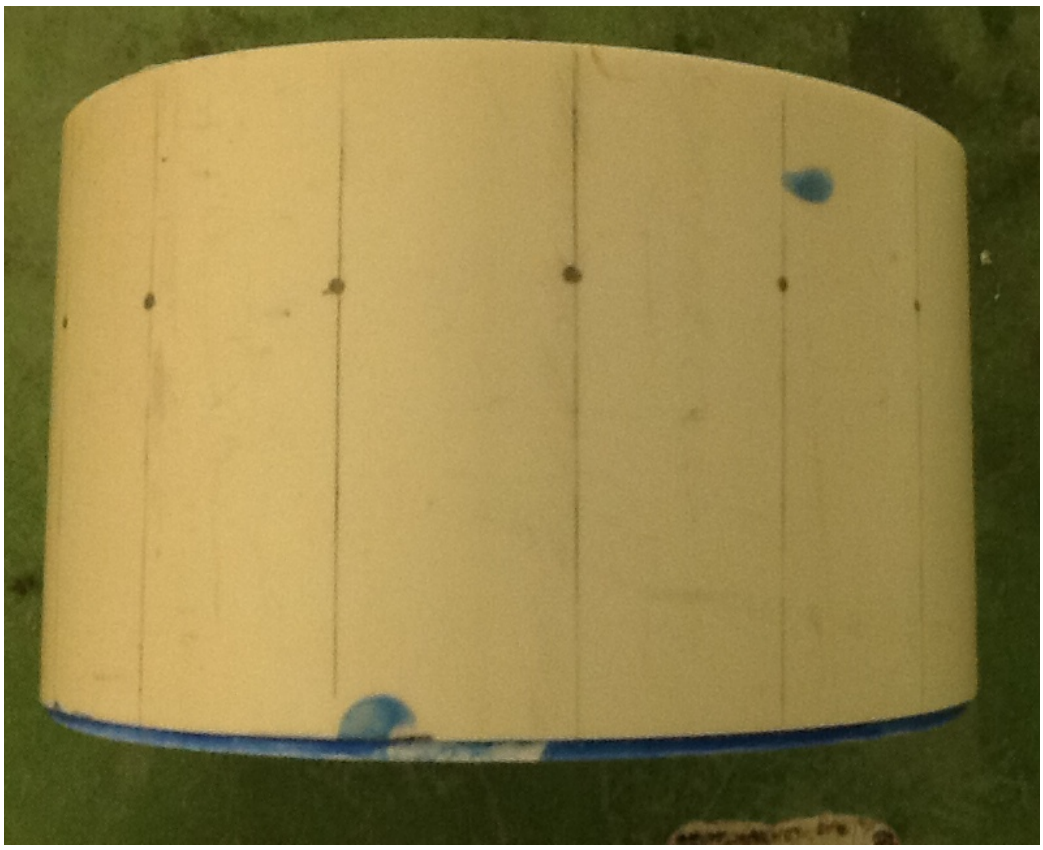

Figure L.2-2: Calibration apparatus step 2. Center points for drilling were created at regular intervals around the circumference of the PVC pipe.

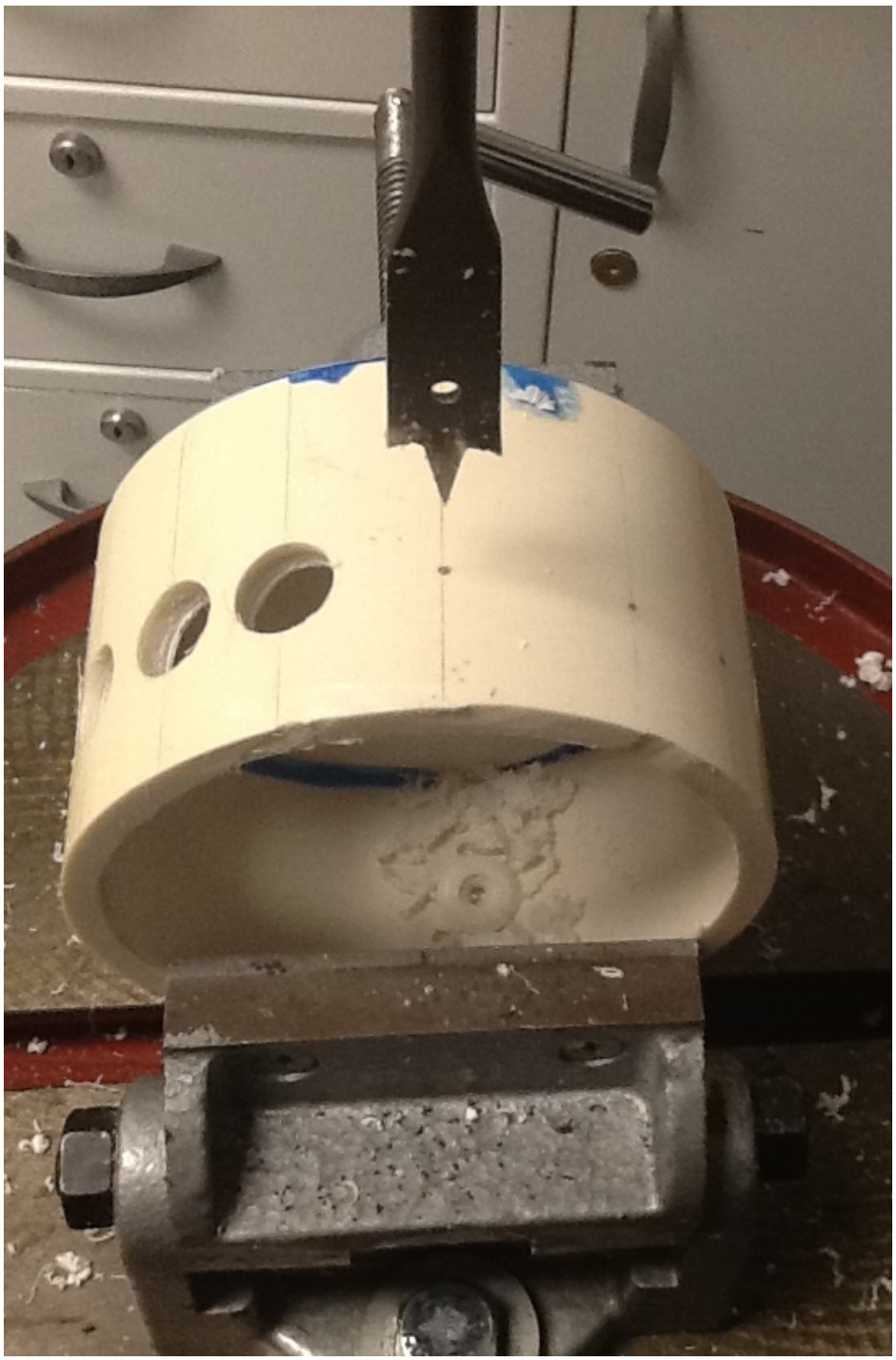

Figure L.2-3: Calibration apparatus step 3. A 5/8” spade bit was used to drill holes at regular intervals around the PVC pipe.

Figure L.2-4: Calibration apparatus step 4. Excelon™ RNT tubing (3/8 ID by 5/8 OD) was cut to lengths of 1 cm with wire cutters.

Figure L.2-5: Calibration apparatus step 5. Pieces of RNT tubing were permanently cemented to the PVC pipe.

L.3 Apparatus base

In order to prevent damage to the sensors during calibration, the apparatus used to hold the sensors and supersaturated solution needs to be sturdy. A base was constructed to hold the apparatus steady during calibration using the following steps:

1) A standard-sized brick was placed on top of a 4” PVC union fitting to mark its width (Figure L.3-1).
2) A PVC saw was used to cut down 1” on each side marked in step 1 of the PVC union fitting.
3) The PVC saw was used to completely remove a section of the PVC union fitting in order to create a tight fit on the brick (Figure L.3-2).

4) A total of six holes (three on each side) were drilled (Figure L.3-3) using a 5/8” spade bit (1” above where the union fitting sits on the brick) to allow airflow through the union fitting and to avoid any heating below the apparatus during calibration.
5) The completed base (Figure L.3-4) was put inside of the constant temperature box during calibration.

Figure L.3-1: Calibration apparatus step 6. A brick was placed on top of a 4” PVC Union fitting to remove a section of the union fitting.

Figure L.3-2: Calibration apparatus step 7. A PVC saw was used to remove the measured section of the union fitting.

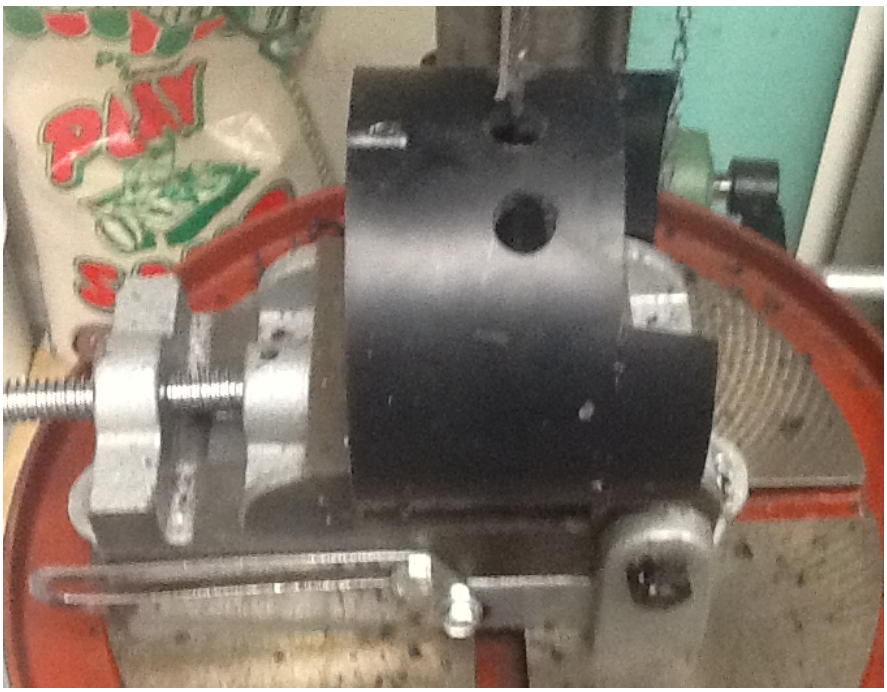

Figure L.3-3: Calibration apparatus step 8. A 5/8” spade bit was used to drill a total of six holes (3 on each side) to allow air to flow through the base.

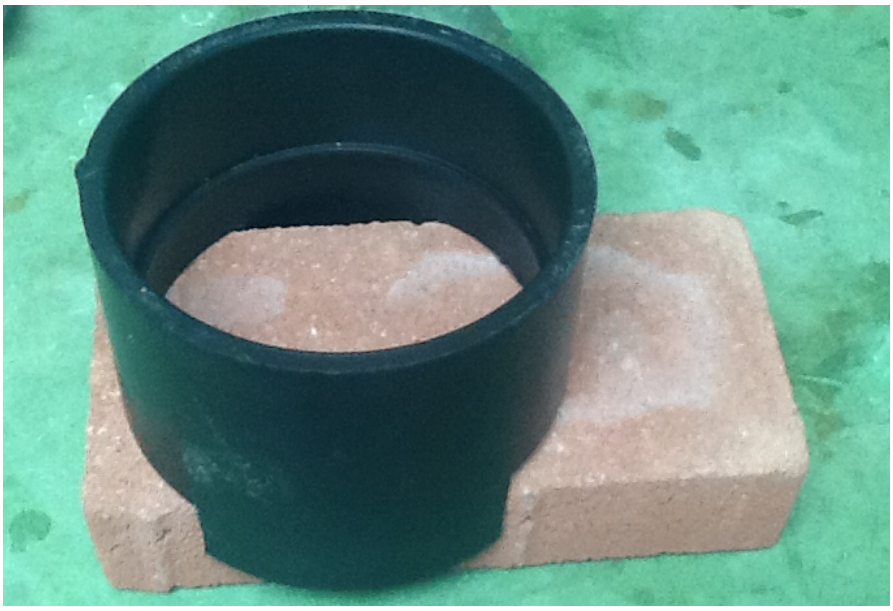

Figure L.3-4: Calibration apparatus step 9. The finished base sits snuggly on a brick for stability.

L.4 Sensor attachment

Sensors were attached to the apparatus in two different ways. Sensors that were permanently attached to socket plugs (Appendix D) connected directly to the RNT tubing and formed a tight connection. Unattached sensors (e.g., sensors monitoring humidity within the box) were fitted into the RNT tubing by first placing the sensor head through a small piece of Materflex® Norprene® food tubing (Precision size L/S 17 OD/0.25" ID). The extra space around the lead wires was filled using a smaller diameter Materflex® Norprene® food tubing (Precision size L/S 16 OD/0.12" ID) which formed a seal. Figure L.4-1 shows a side by side comparison of sensors prior to attachment. Figure L.4-2 shows a side view of the attached sensors to the apparatus, while Figure L.4-3 shows a view from above.

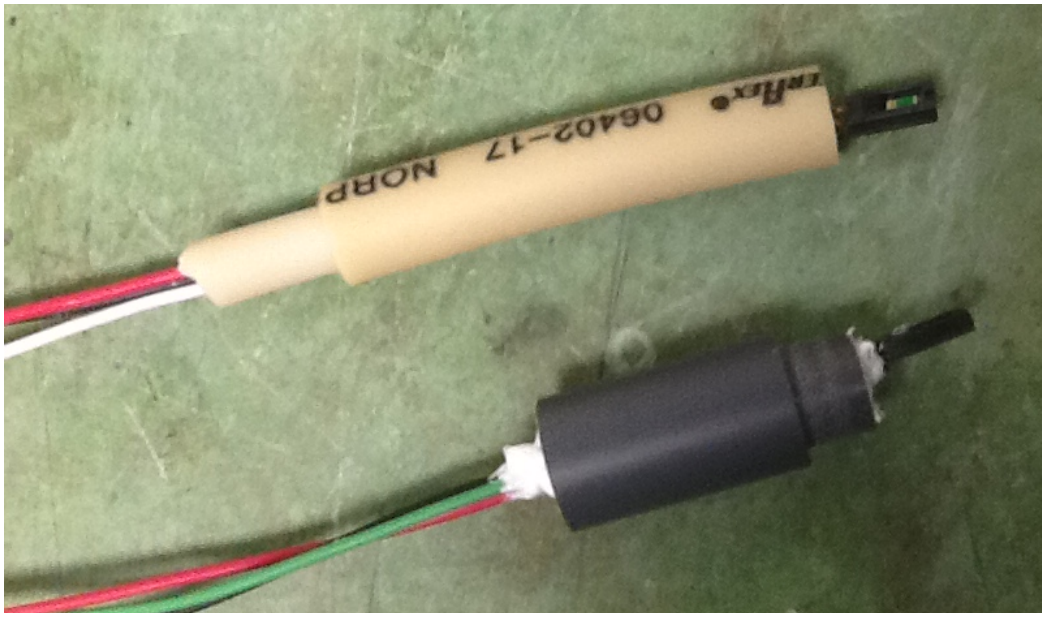

Figure L.4-1: A side by side comparison of sensors before they are attached to the calibration apparatus. Most sensors are already in a plug for later column attachment (bottom), while others are temporarily fitted with Norprene® food tubing.

Figure L.4-2: Sensor attachment. Sensors were attached directly to the RNT tubing.

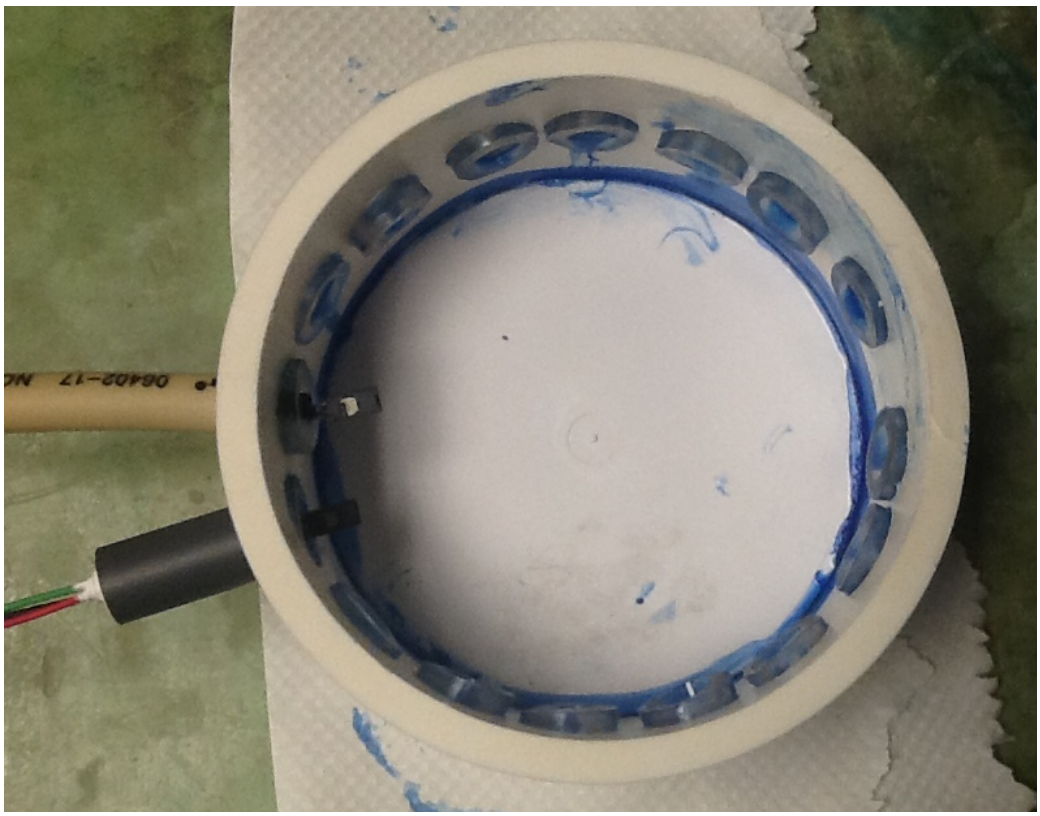

Figure L.4-3: Overhead view of sensor attachment. Sensor heads held in place directly above the supersaturated salt solution.

L.5 Calibration procedure

Sodium Chloride has a solubility of 35.7 g/100 mL water and Magnesium Chloride has a solubility of 54.6 g/100 mL water, both at 20 ^{o}C. In order to make a supersaturated solution for calibration, these values are important to consider. The following sensor calibration procedure was used to create a supersaturated solution for each salt:

1. Measure and add salt (25 g NaCl or 130 g $MgCl_2*6H_2O$) into the apparatus.

2. Set apparatus onto base within the constant temperature box (Appendix I) in order to avoid accidental spilling.
3. Attach all humidity sensors to the apparatus with sensor face pointing away from the salt (up).
4. Add 15 mL distilled water to the salt using a syringe. This will help avoid splashing and damage to the sensor heads. Using such a small volume of water is also important to make sure the solution becomes supersaturated.
5. Stir water and salt mixture with a small wooden stick. This is to be done carefully to avoid any splashing.
6. Put the lid (a 4" PVC Knockout) onto the apparatus and seal it shut with silicone tape.
7. Rotate each sensor from the outside about 180^{o} so that the sensor face is pointing toward the solution (down).
8. Seal and close up the constant temperature box. Let the temperature equilibrate to $25^{o}C$, and let the sensors monitor for 24 hours ($MgCl_2*6H_2O$) or 48 hours (NaCl).
9. The apparatus was washed with soap and distilled water between calibrations. The process was then repeated using the other salt.

APPENDIX M: TEST MATERIALS

M.1 Material selection

Multiple variables (pore size, tortuosity, surface area, and surface chemistry) are expected to play important roles in the advancement of water vapor into the test columns. Given the difficulty of systematically varying these properties individually, we elected to test materials with different particle size/shape and surface adsorptive properties. The first trials were run with the columns empty (100% porosity) to provide a reference for comparison to tests on porous media. The following porous media were tested, with each introducing additional complexity:

1. Softair USA ™ Ultrasonic 6 mm BB's (Appendix M.2)
2. Very fine grained gravel (Appendix M.3)
3. Medium grained sand (Appendix M.4)

Preparation of the materials, packing of the columns, estimation of porosity, and measurement of adsorption are described below.

M.2 Softair USA ™ Ultrasonic BB's

The first material tested consisted of 6 mm diameter Plastic BB's (Figure M.2-1). This material was selected to provide large uniform pores, relatively low tortuosity, and little to no adsorption. The mass and diameter of the BB's was measured to facilitate the estimation of porosity (M.2c-2). Because the mass of an individual BB (~0.11 g) is of similar order to the resolution of the scale (0.01 g), BB's were measured in randomly selected groups of 10, 25, 50, and 100 to estimate the average mass. From each of these groups, the diameter of five randomly selected BB's was measured to a precision of 0.01 mm using a dial caliper. The average of these

measurements (Table M.2.1) are both slightly less than the stated manufacturer's specifications of 0.12 g and 6 mm.

Figure M.2-1: A group of BB's next to a toothpick for scale.

# of BB's	Total group mass (g)	Mass per BB (g)	Avg. diameter (mm)
10	1.11	0.111	5.87
25	2.77	0.111	5.89
50	5.55	0.111	5.85
100	11.09	0.111	5.90
Average		0.111	5.88

Table M.2-1: BB mass and diameter. Random samples of BB's shows that the average BB mass is about 0.111 g, and the average BB diameter is 5.88 mm; both slightly less than specified by the manufacturer.

M.2a Preparation

Before use, the 6 mm BB's were washed in a Trisodium Phosphate (TSP) solution using the following procedure:

1. A sufficient amount of BB's to fill both columns to capacity was selected.
2. A TSP solution was made following the manufacturer's recommendations by adding roughly 0.5 ounces of TSP into 16 ounces of distilled water in a 32 ounce (1 quart) Kerr™ wide-mouth glass mason jar.
3. The BB's were added to the jars containing the TSP solution until full.
4. The glass jar was sealed and the mixture was shaken vigorously for 5 minutes.
5. The mixture was allowed to sit for roughly 2 minutes.
6. The water was drained, and the jar refilled with fresh distilled water.
7. The jar was shaken slightly and allowed to sit for roughly 2 minutes.
8. The contents of the jar were partially emptied onto a sieve (forming a thin layer).
9. Distilled water was liberally poured over the BB's to rinse them off.
10. The BB's were placed in a Pyrex™ 9"X13" glass cooking dish to air dry.
11. Steps 8 - 11 were repeated until the selected BB's were washed and rinsed.
12. The BB's were stirred occasionally during drying.
13. Throughout this process, the BB's were only in contact with clean plastic, glass, and talcum-free nitrile gloves.

M.2b Packing the columns

The BB's were added to the columns using a plastic funnel. Each column was filled halfway, gently shaken, and then filled to capacity.

M.2c Estimating porosity

Porosity for the column filled with BB's was estimated from gravimetric and dimensional measurements (Table M.2b-1). The first step was to estimate the number of BB's in each

column. This was done by taking the known mass of BB's in the filled column and dividing by the average mass of each BB. The estimated number of BB's within the column was multiplied by the average BB volume to get the volume occupied by solids within the column, which lead to the porosity (Table M.2b-2). Porosity estimates were compared to various packing arrangements of uniform spheres in order to gain insight on the packing arrangement of the BB's (Table M.2c-3). The actual packing arrangement is not possible to identify due to interference with the column wall.

Column	Empty mass (g)	Filled mass (g)	BB mass (g)	# of BB's
Upper	461.4	804.3	342.9	3089
Lower	370.1	712.0	341.9	3080

Table M.2c-1: Total BB estimate. Total number of BB's in each column was estimated by dividing the total mass of BB's (filled column wt. – empty column wt.) by the average BB mass. The difference in empty mass between upper and lower column occurs because the two columns were capped differently (Appendix F.1).

Column	# of BB's	Single BB volume (cm^3)	Total BB volume (cm^3)	Column volume (cm^3)	Pore volume (cm^3)	Estimated porosity
Upper	3089	0.106	327	551.3	224.3	0.41
Lower	3080	0.106	326	551.3	225.3	0.41

Table M.2c-2: BB-filled column porosity. Porosity is estimated by first calculating the total BB volume within the column, and then dividing by the total column volume.

Column	Estimate	Cubic*	Orthorhombic*	Tetragonal*	Tetrahedral*
Upper	41 %	48 %	40 %	30 %	26 %
Lower	41 %	48 %	40 %	30 %	26 %

Table M.2c-3: Porosity estimates compared with known porosity of different packing arrangements. The estimated porosity values for the test columns are similar to an Orthorhombic packing arrangement. The asterisk (*) indicates information obtained from Hillel, 1998.

M.2d Measuring adsorption

The pre-experiment weight of each column is subtracted from the post-experiment weight to estimate adsorption of water onto the particle surfaces within each column (Table M.2d-1).

Column	Pre-experiment weight (g)	Post-experiment weight (g)	Weight added due to adsorption (g)
Upper	804.3	804.5	0.2
Lower	712.0	712.2	0.2

Table M.2d-1: Adsorption onto BB's. Adsorption of water vapor onto material within the column is estimated by comparing pre- and post-experimental weights.

M.3 Very fine grained gravel

Quikrete™ All-Purpose Gravel with a size range conforming to ASTM-C33 grading specifications (150 μm to 9.5 mm) was dry sieved on US standard No. 5 and No. 10 mesh screens in order to retain grains with a diameter of 2-4 mm. The resulting material (Figure M.3-1) is classified as a very fine grained gravel. With respect to the BB's, the gravel adds in a small amount of adsorption, smaller pores, a wider range of pore sizes, and increased tortuosity, while maintaining a similar porosity (~43%). The gravel is well sorted and is comprised of sub-angular to sub-rounded particles with varying sphericity from high to low.

Figure M.3-1: Very fine grained gravel. Pieces of sorted gravel next to a toothpick and 6 mm diameter BB for scale.

M.3a Preparation

The gravel was washed and air dried in a manner similar to that described in Appendix M.2a.

M.3b Packing the columns

The gravel was added to the columns using a plastic funnel. Each column was shaken intermittently to allow the grains to settle.

M.3c Estimating porosity

Porosity within the gravel-filled columns was estimated (Table M.3c-1) by dividing the volume of water in the column voids by the total column volume. Two spare columns with the same dimensions as the test columns (Appendix F.1) were filled with gravel (Appendix M.3b). Water was then added to each column until the pore space was filled. The mass of water added to the column was then divided by the density of water (1 g/cm^3) to obtain the pore volume, which was then used to calculate the porosity. Water and gravel were removed from the spare columns. The gravel was then spread out flat in glass Pyrex™ cooking sheets and allowed to air dry with periodic stirring at room temperature for 1 week prior to use in experiments.

Column	Column and gravel (g)	Column, gravel, water (g)	Mass of water (g)	Volume of water (cm^3)	Tot. column volume (cm^3)	Estimated porosity
Upper	1280.2	1520.7	240.5	240.5	551.3	0.44
Lower	1281.6	1518.2	236.6	236.6	551.3	0.43

Table M.3c-1: Gravel-filled column porosity. Porosity within each column was estimated by dividing the volume of water in the voids by the total column volume in a spare test column.

The quantity of grains within each column was also estimated (Table M.3c-2) by weighing random groups of gravel particles (Figure M.3c-1). Small mounds were first created by slowing pouring gravel particles through a funnel. The mounds were then divided into eight sections. One of the eight sections was randomly selected, weighed on a scale with 0.01 g precision, and counted. This process was repeated five different times.

Column	Empty mass (g)	Filled mass (g)	Gravel mass (g)	Average wt. per Gravel (g)	Estimated Particles
Upper	461.4	1411.7	950.3	0.042	22,626
Lower	370.1	1324.2	954.1	0.042	22,716

Table M.3c-2: Total gravel estimate. The total number of particles in each column was estimated by dividing the total mass of the gravel inside each column by the average mass of each gravel particle. The difference in empty mass between upper and lower column occurs because the two columns were capped differently (Appendix F).

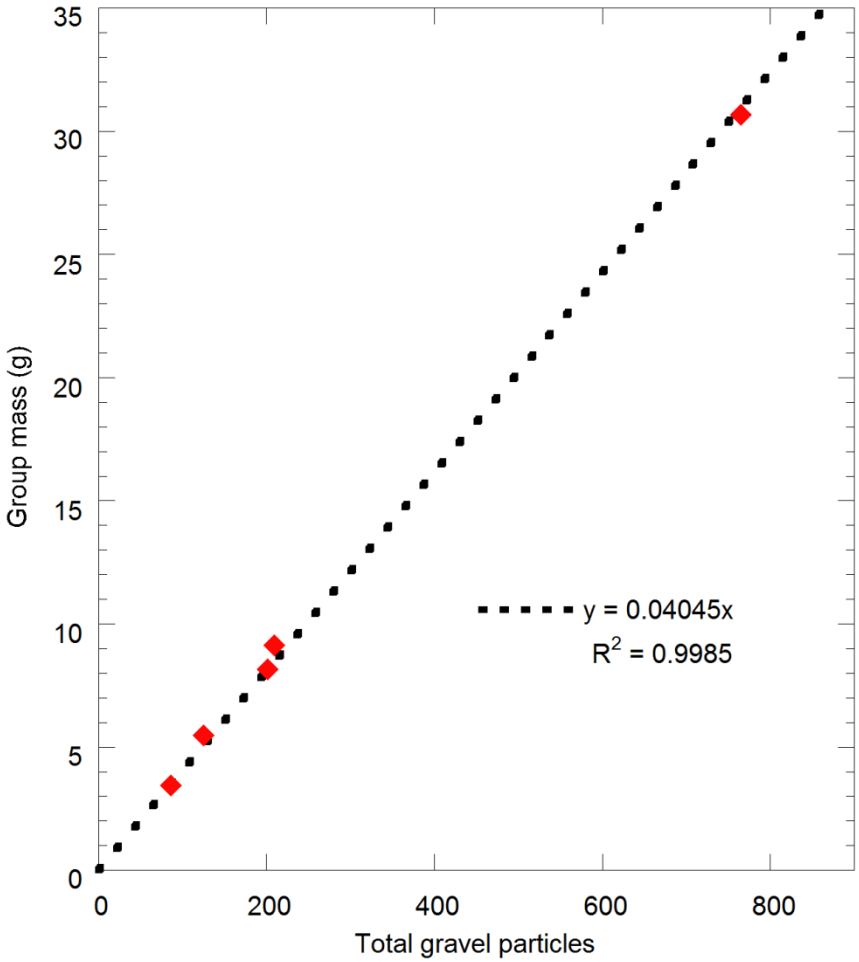

Figure M.3c-1: Comparison of the linear relationship between gravel particles and the mass of a randomly selected group.

M.3d Measuring adsorption

The pre-experiment weight of each column is subtracted from the post-experiment weight to estimate adsorption of water onto the particle surfaces within each column (Table M.3d-1).

Column	Pre-experiment weight (g)	Post-experiment weight (g)	Weight added due to adsorption (g)
Upper	1411.7	1412.1	0.4
Lower	1324.2	1324.4	0.2

Table M.3d-1: Adsorption of water vapor onto gravel. The additional weight in each column after the experiment ended is attributed to adsorption of water vapor onto the gravel particles. See Table M.2c-1 caption for an explanation of the weight difference between upper and lower columns.

M.4: 30-40 sand

A narrow distribution (30-40 mesh) sand (Figure M.4-1) was created by repeatedly washing and sieving commercial building sand. With respect to the very fine gravel, this material adds in an increased surface area for adsorption, increased tortuosity, and smaller pores, while maintaining a similar porosity (~42%).

M.4a Preparation

Quikrete™ medium sand, a 99.0 – 99.9 % by weight crystalline silica quartz sand, was wet sieved through a #30 sieve followed by a #40 sieve in order to retain the desired particle size (0.42 mm to 0.59 mm). This process was repeated a total of five times with the distilled wash water running clear after the third wash. This process removed any soluble minerals and most of the adhered ultra-fine particles (dust). For the first four washes, the sand was oven dried at 105 ^{o}C to eliminate any organic materials. After the fifth wash, the sand was allowed to dry at 75 ^{o}C for over 72 hours. The end result is a very well sorted, well rounded to sub-angular silica sand (Figure M.4-1).

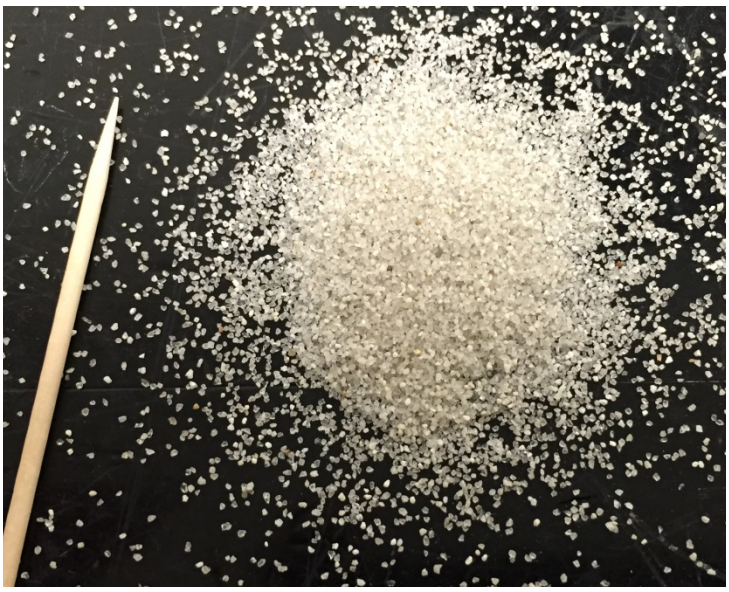

Figure M.4a-1: 30-40 Mesh medium sand next to a toothpick for scale.

M.4b Packing the columns

The medium grain sand was carefully packed into columns to avoid the effects of settling during the experiment. A series of preliminary tests using several different packing procedures (Table M.4b-1) yielded similar results (nearly identical column weights). This observation led to the conclusion that the manner in which the sand was packed into the columns was not as important as the fact that it needed to be packed. It was decided that the column would be packed by adding roughly 4 ounces of sand into the column using a measuring cup and funnel. A 2" brass weight was set on the sand to keep it stable. A plastic mallet attached to a hinge (Figure M.4b-1) was used as a drop hammer to hit the column 10 times from the same height. The column was rotated 180^{o} to avoid damaging the sensor housings (Appendix D), and the column was hit 10 more

times. The brass weight was removed, and the process was repeated until the column was filled to capacity.

Unpacked wt. (g)	Method 1 wt. (g)	Method 2 wt. (g)	Method 3 wt. (g)	Method 4 wt. (g)
1100.8	1194.1	1173.8	1190.9	1180.5

Table M.4b-1: Packing procedure 1. Weight comparison between a column filled with unpacked sand and a column packing using a variety of packing methods including: Adding 4 oz. of sand at a time, hitting the column 10 times, rotating the column 180^{o}, hitting 10 more times, repeat (Method 1); Adding 2 oz. of sand at a time, hitting the column 5 times, rotating the column 180^{o}, hitting 5 more times, repeat (Method 2); Adding 2 oz. of sand at a time, hitting the column 10 times, rotating the column 180^{o}, hitting 10 more times, patting the sand with an acrylic rod, repeat (Method 3); Adding 6 oz. of sand at a time, hitting the column 10 times, rotating the column 180^{o}, hitting 10 more times, repeat (Method 4). It was concluded that the way the column was packed was not as important as making sure that the column was packed.

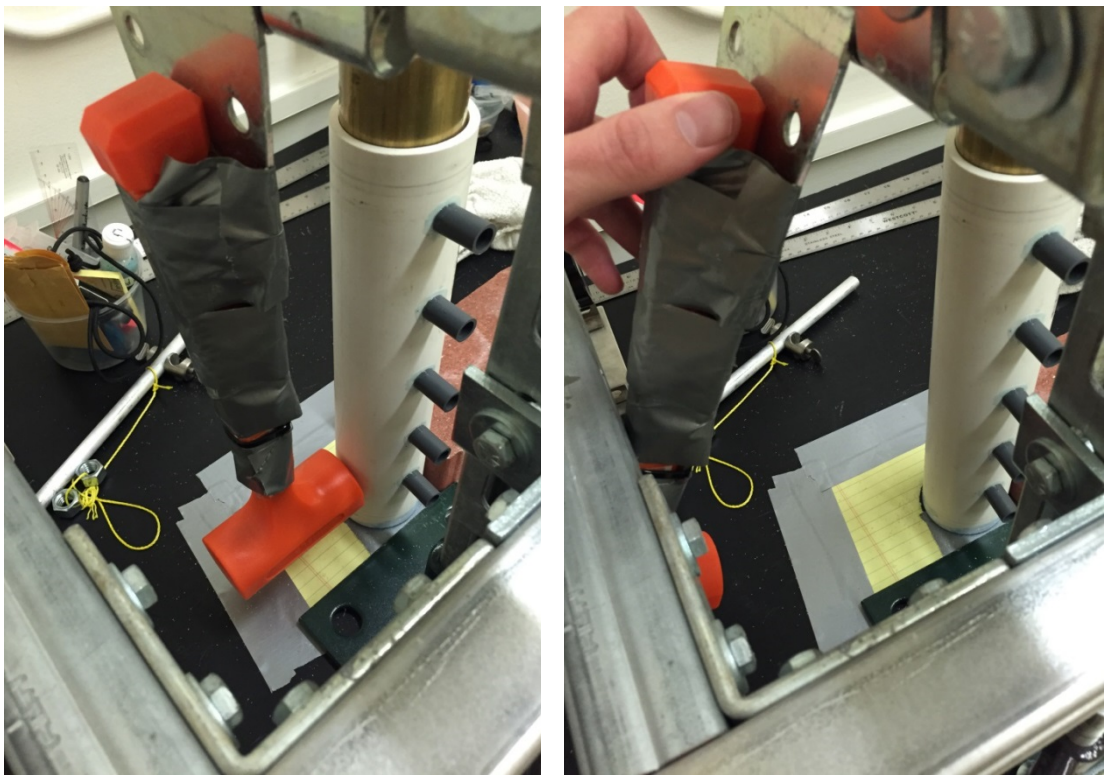

Figure M.4b-1: Packing procedure. The column was packed with medium sand by adding sand 4 ounces at a time into the column. A brass weight (shown in picture) was placed on top of the sand in the column, and a plastic mallet on a hinge was used to strike the column 10 times. The column was rotated 180^{o} and the process repeated until the column was filled to capacity. The paper below the column was used to place the column. The brick was used to make sure the column did not tip over when it was struck.

M.4c Estimating porosity

Porosity within the sand-filled column was estimated (Table M.4c-1) by dividing the mass of the sand in the packed columns by the known density of quartz sand (2.65 g/cm^3) to calculate the volume occupied by sand grains. Once this volume was obtained, it was first subtracted from the column volume to get the pore volume, and then divided by the column volume to determine porosity.

Column	Empty mass (g)	Filled mass (g)	Sand mass (g)	Qtz.density (g/cm^3)	Column vol. (cm^3)	Sand vol. (cm^3)	Estimated porosity
Upper	461.4	1313.2	851.8	2.65	551.3	321.4	0.42
Lower	370.1	1222.8	852.7	2.65	551.3	321.8	0.42

Table M.4c-1: Porosity of the sand-filled column. Porosity within each column was estimated by dividing the volume occupied by sand grains by the total column volume. Sand grain volume was determined by using the mass of the sand in the column and the density of quartz sand.

M.4d Measuring adsorption

The pre-experiment weight of each column is subtracted from the post-experiment weight to estimate adsorption of water onto the particle surfaces within each column (Table M.2d-1).

Column	Pre-experiment weight (g)	Post-experiment weight (g)	Weight added due to adsorption (g)
Upper	1313.2	1314.8	1.6
Lower	1222.8	1223.7	0.9

Table M.4d-1: Adsorption of water vapor onto sand particles. The additional weight in each column after the experiment ended is attributed to adsorption of water vapor onto the sand grains. See Table M.2c-1 caption for an explanation of the weight difference between upper and lower columns.

APPENDIX N: RESULTS

N.1: Introduction

This appendix documents the execution of all experiments that were performed for this thesis including: empty column (Appendix N.2), plastic BB-filled column (Appendix N.3), medium gravel-filled column (Appendix N.4), very fine gravel-filled column (Appendix N.5), and medium sand-filled column (Appendix N.6). Some of the experiments were performed a single time (e.g., medium sand), while others were repeated (e.g., empty column) in order to test different experimental procedures.

This appendix is organized according to the media that was used to fill the columns. Subsections are titled according to the name given to the .dat file collected from the data logger, and are organized by the configuration of sensor 5 position (upper and lower), which were: sealed (column is completely sealed and finite), open to the box (sensors in position 5 were removed, and the column was open to conditions within the constant temperature box), routed to bottles (sensors in position 5 were open to air within separate empty containers located within the box), and routed out (sensors in position 5 were open to air within the laboratory). Pre and post experimental column weights are included for all experiments except the empty column experiments, which did not consider adsorption due to absence of media. Additionally, each section contains two graphs containing relative humidity and temperature data collected. The relative humidity graphs have the following color structure: darker shades for the upper column, and lighter shades for the lower column: 1-H (red), 2-H (blue), 3-H (green), 4-H (purple), 5-H (orange), BC-1 (yellow), BC-2 (grey), Box1-H (blue), and Room1-H (black); the temperature

graphs also have a color structure: U4-T (dark green), U2-T (dark blue), BC1-T (black), L2-T (orange), L4-T (yellow), Room1-T (purple), Ptemp (light blue), and Box1-T (red).

N.2: Empty column

N.2.1 Empty_column_trial

This experiment was performed by initially connecting the humidity chamber to the humidity reservoir, and plugging in the ultrasonic fog generator for ~9 hours within the sealed constant temperature box. It was found that the ultrasonic fog generator created too much heat, which heated the box to temperatures above the desired 25 ^{o}C.

Description	Sealed
Ultrasonic fog generator plugged in	August 29, 2014 13:27
Ultrasonic fog generator unplugged	August 29, 2014 22:11
Column connection	August 29, 2014 13:27
End of experiment	August 30, 2014 13:16
Duration†	0 days, 23 hours, and 49 minutes

† The duration of the experiment is from the time that the humidity chamber is initially connected to the column, until the final data point is collected and the box is opened.

Table N.2.1-1: Empty_column_trial basic information. Basic information concerning the experiment performed.

Humidity Sensor	Initial‡		Final	
	Voltage (mV)	Calibrated % RH	Voltage (mV)	Calibrated % RH
U5-H	2492	52.07	3615	86.24
U4-H	2521	52.31	3653	87.56
U3-H	2543	54.96	3662	89.26
U2-H	2529	55.06	3644	89.65
U1-H	2632	55.55	3747	89.19
BC1-H	2881	65.46	3773	92.78
L1-H	2464	53.05	3576	87.48
L2-H	2428	48.00	3705	83.72
L3-H	2253	46.97	3533	87.42
L4-H	2256	44.98	3572	86.80
L5-H	2245	44.54	3610	87.83
BC2-H	3607	85.82	4175	103.22
ROOM1-H	1868	33.00	1716	28.40
BOX1-H	1876	35.21	1884	35.46

‡ Initial conditions are based on the time that the humidity chamber was connected to the humidity reservoir, and not initial conditions when the box was initially sealed.

Table N.2.1-2: Empty_column_trial RH data. Initial and final calibrated relative humidity data from the experiment.

Temperature Sensor	Initial‡	Final	Average ± 1 standard deviation
	°C	°C	°C
U4-T	24.41	25.14	25.18 ± 0.18
U2-T	24.39	25.14	25.17 ± 0.12
BC1-T	24.40	25.16	25.19 ± 0.11
L2-T	24.29	25.12	25.15 ± 0.11
L4-T	24.28	25.11	25.13 ± 0.09
ROOM1-T	23.84	26.32	26.01 ± 0.41
PTEMP	23.89	25.76	25.52 ± 0.40
BOX1-T	24.43	25.03	25.09 ± 0.10

‡ Initial conditions are based on the time that the humidity chamber was connected to the humidity reservoir, and not initial conditions when the box was initially sealed.

Table N.2.1-3: Empty_column_trial temperature data. Initial, final, and average temperature data from the experiment.

Pressure Sensor	Initial‡		Final		Average ± 1 st. dev.	
	mV	kPa	mV	kPa	mV	kPa
Room	3733	93.88	3722	93.63	3725 ± 3.42	93.70 ± 0.08

‡ Initial conditions are based on the time that the humidity chamber was connected to the humidity reservoir, and not initial conditions when the box was initially sealed.

Table N.2.1-4: Empty_column_trial pressure data. Initial, final, and average barometric pressure data from the experiment.

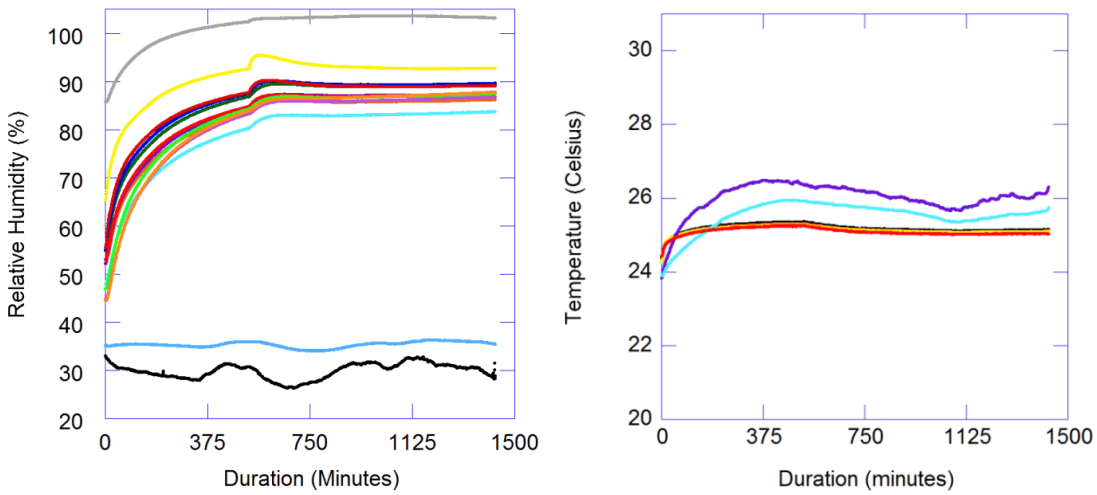

Figure N.2.1-1: Empty_column_trial graphs. Calibrated relative humidity data (left) and temperature data (right) collected during the experiment.

N.2.2 Empty_column_trial_2

This experiment was initiated with the ultrasonic fog generator turned on in the sealed humidity chamber, and the constant temperature box open. After ~1 hour, the chamber was connected to the humidity reservoir, the box was closed and sealed, and ~2 hours later the ultrasonic fog generator was unplugged.

Description	Sealed
Ultrasonic fog generator plugged in	September 12, 2014 13:10
Ultrasonic fog generator unplugged	September 12, 2014 14:17
Column connection	September 12, 2014 16:11
End of experiment	September 15, 2014 09:50
Duration†	2 days, 17 hours, and 39 minutes

† The duration of the experiment is from the time that the humidity chamber is initially connected to the column, until the final data point is collected and the box is opened.

Table N.2.2-1: Empty_column_trial_2 basic information. Basic information concerning the experiment performed.

Humidity Sensor	Initial‡		Final	
	Voltage (mV)	Calibrated % RH	Voltage (mV)	Calibrated % RH
U5-H	1976	35.58	3570	83.93
U4-H	2000	35.38	3622	85.12
U3-H	1951	35.85	3625	86.40
U2-H	1924	35.58	3601	87.08
U1-H	2003	35.83	3764	89.32
BC1-H	1991	37.55	3772	91.57
L1-H	1940	35.87	3713	89.51
L2-H	1996	35.18	3785	89.36
L3-H	1903	35.47	3622	88.14
L4-H	1981	35.68	3689	88.57
L5-H	1993	35.82	3716	87.91
BC2-H	4021	92.53	4077	94.10
ROOM1-H	1869	34.75	2130	43.21
BOX1-H	****	****	****	****

‡ Initial conditions are based on the time that the humidity chamber was connected to the humidity reservoir, and not initial conditions when the box was initially sealed.

**** indicates that unreliable data was obtained due to sensor error.

Table N.2.2-2: Empty_column_trial_2 RH data. Initial and final calibrated relative humidity data from the experiment.

Temperature Sensor	Initial‡	Final	Average ± 1 standard deviation
	^{o}C	^{o}C	^{o}C
U4-T	25.21	25.06	25.06 ± 0.03
U2-T	25.22	25.06	25.06 ± 0.03
BC1-T	25.36	25.07	25.06 ± 0.03
L2-T	25.23	25.05	25.05 ± 0.03
L4-T	25.18	25.05	25.05 ± 0.02
ROOM1-T	24.77	25.79	25.76 ± 0.45
PTEMP	24.18	24.98	25.27 ± 0.41
BOX1-T	25.16	25.42	24.98 ± 0.03

‡ Initial conditions are based on the time that the humidity chamber was connected to the humidity reservoir, and not initial conditions when the box was initially sealed.

Table N.2.2-3: Empty_column_trial_2 temperature data. Initial, final, and average temperature data from the experiment.

Pressure Sensor	Initial‡		Final		Average ± 1 st. dev.	
	mV	kPa	mV	kPa	mV	kPa
Room	3741	94.06	3741	94.06	3741 ± 0.00	94.06 ± 0.00

‡ Initial conditions are based on the time that the humidity chamber was connected to the humidity reservoir, and not initial conditions when the box was initially sealed.

Table N.2.2-4: Empty_column_trial_2 pressure data. Initial, final, and average barometric pressure data from the experiment.

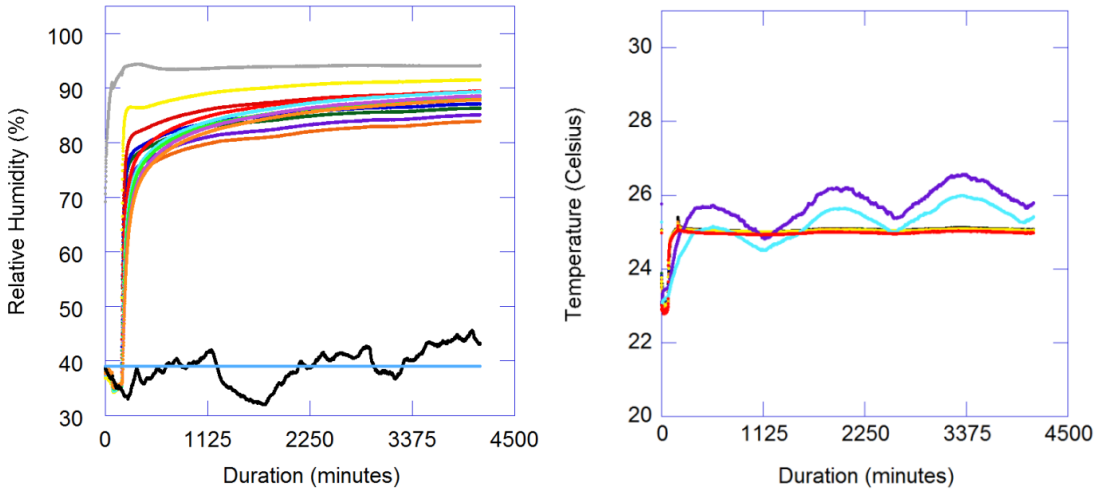

Figure N.2.2-1: Empty_column_trial_2 graphs. Calibrated relative humidity data (left) and temperature data (right) collected during the experiment.

N.2.3 Empty_column_trial_3

This experiment was initiated with the ultrasonic fog generator turned on in the sealed humidity chamber, and the constant temperature box closed. After ~2.5 hours, the ultrasonic fog generator was unplugged. Temperature was allowed to equilibrate for approximately 4 more hours, at which point the humidity chamber was connected to the humidity reservoir.

Description	Sealed
Ultrasonic fog generator plugged in	September 19, 2014 15:37
Ultrasonic fog generator unplugged	September 19, 2014 17:58
Column connection	September 19, 2014 21:39
End of experiment	September 22, 2014 09:33
Duration†	2 days, 11 hours, and 54 minutes

† The duration of the experiment is from the time that the humidity chamber is initially connected to the column, until the final data point is collected and the box is opened.

Table N.2.3-1: Empty_column_trial_3 basic information. Basic information concerning the experiment performed.

Humidity Sensor	Initial‡		Final	
	Voltage (mV)	Calibrated % RH	Voltage (mV)	Calibrated % RH
U5-H	2187	41.98	3565	83.78
U4-H	2243	42.83	3609	84.73
U3-H	2191	43.10	3603	85.73
U2-H	2124	41.72	3583	86.53
U1-H	2247	43.24	3744	88.72
BC1-H	2178	43.22	3743	90.69
L1-H	2193	43.52	3691	88.84
L2-H	2231	42.30	3760	88.60
L3-H	2152	43.10	3602	87.53
L4-H	2228	43.33	3670	87.98
L5-H	2255	43.74	3697	87.34
BC2-H	4176	96.87	4072	93.96
ROOM1-H	1819	31.08	2241	43.78
BOX1-H	2008	39.25	2300	48.71

‡ Initial conditions are based on the time that the humidity chamber was connected to the humidity reservoir, and not initial conditions when the box was initially sealed.

Table N.2.3-2: Empty_column_trial_3 RH data. Initial and final calibrated relative humidity data from the experiment.

Temperature Sensor	Initial‡	Final	Average ± 1 standard deviation
	^{o}C	^{o}C	^{o}C
U4-T	25.14	25.04	25.09 ± 0.03
U2-T	25.15	25.04	25.08 ± 0.03
BC1-T	25.19	25.04	25.08 ± 0.03
L2-T	25.11	25.03	25.07 ± 0.02
L4-T	25.11	25.03	25.06 ± 0.02
ROOM1-T	25.86	25.38	25.86 ± 0.27
PTEMP	25.26	24.94	25.37 ± 0.27
BOX1-T	25.14	24.96	25.01 ± 0.02

‡ Initial conditions are based on the time that the humidity chamber was connected to the humidity reservoir, and not initial conditions when the box was initially sealed.

Table N.2.3-3: Empty_column_trial_3 temperature data. Initial, final, and average temperature data from the experiment.

Pressure Sensor	Initial‡		Final		Average ± 1 st. dev.	
	mV	kPa	mV	kPa	mV	kPa
Room	3732	93.86	3760	94.48	3742 ± 8.37	94.07 ± 0.19

‡ Initial conditions are based on the time that the humidity chamber was connected to the humidity reservoir, and not initial conditions when the box was initially sealed.

Table N.2.3-4: Empty_column_trial_3 pressure data. Initial, final, and average barometric pressure data from the experiment.

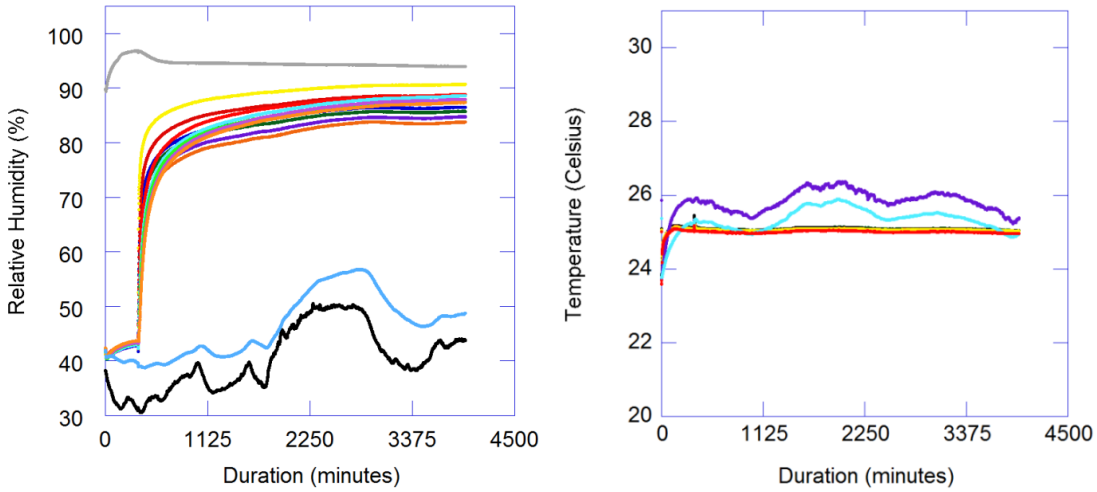

Figure N.2.3-1: Empty_column_trial_3 graphs. Calibrated relative humidity data (left) and temperature data (right) collected during the experiment.

N.2.4 Empty_column_trial_4

This experiment was initiated with the ultrasonic fog generator turned on in the sealed humidity chamber, and the constant temperature box closed. The ultrasonic fog generator was unplugged after a period of time (most likely ~2 hours). Temperature was allowed to equilibrate overnight (~12 – 14 hours), at which point the humidity chamber was connected to the humidity reservoir.

Description	Sealed
Ultrasonic fog generator plugged in	October 24, 2014 18:17
Ultrasonic fog generator unplugged	Not documented
Column connection	October 25, 2014 10:02
End of experiment	October 27, 2014 11:07
Duration†	2 days, 1 hour, and 5 minutes

† The duration of the experiment is from the time that the humidity chamber is initially connected to the column, until the final data point is collected and the box is opened.

Table N.2.4-1: Empty_column_trial_4 basic information. Basic information concerning the experiment performed.

Humidity Sensor	Initial‡		Final	
	Voltage (mV)	Calibrated % RH	Voltage (mV)	Calibrated % RH
U5-H	1884	32.82	3506	84.09
U4-H	1919	32.91	3576	83.52
U3-H	1849	32.82	3529	85.69
U2-H	1829	32.69	3503	85.99
U1-H	1903	32.84	3657	88.36
BC1-H	1838	32.94	3655	91.24
L1-H	1843	32.96	3579	87.43
L2-H	1915	32.74	3773	85.95
L3-H	1818	32.89	3500	86.88
L4-H	1888	32.82	3574	85.62
L5-H	1895	32.87	3580	84.88
BC2-H	4097	99.46	3975	95.79
ROOM1-H	1958	35.33	1600	24.33
BOX1-H	1838	32.23	1505	21.90

‡ Initial conditions are based on the time that the humidity chamber was connected to the humidity reservoir, and not initial conditions when the box was initially sealed.

Table N.2.4-2: Empty_column_trial_4 RH data. Initial and final calibrated relative humidity data from the experiment.

Temperature Sensor	Initial‡	Final	Average ± 1 standard deviation
	^{O}C	^{O}C	^{O}C
U4-T	24.90	24.90	24.93 ± 0.02
U2-T	24.89	24.91	24.93 ± 0.02
BC1-T	24.94	24.93	24.95 ± 0.02
L2-T	24.93	24.93	24.94 ± 0.02
L4-T	24.96	24.96	24.97 ± 0.01
ROOM1-T	23.38	23.58	24.05 ± 0.29
PTEMP	22.88	23.06	23.51 ± 0.27
BOX1-T	24.67	24.85	24.89 ± 0.02

‡ Initial conditions are based on the time that the humidity chamber was connected to the humidity reservoir, and not initial conditions when the box was initially sealed.

Table N.2.4-3: Empty_column_trial_4 temperature data. Initial, final, and average temperature data from the experiment.

Pressure Sensor	Initial‡		Final		Average ± 1 st. dev.	
	mV	kPa	mV	kPa	mV	kPa
Room	3758	94.45	3754	94.36	3739 ± 8.14	94.03 ± 0.18

‡ Initial conditions are based on the time that the humidity chamber was connected to the humidity reservoir, and not initial conditions when the box was initially sealed.

Table N.2.4-4: Empty_column_trial_4 pressure data. Initial, final, and average barometric pressure data from the experiment.

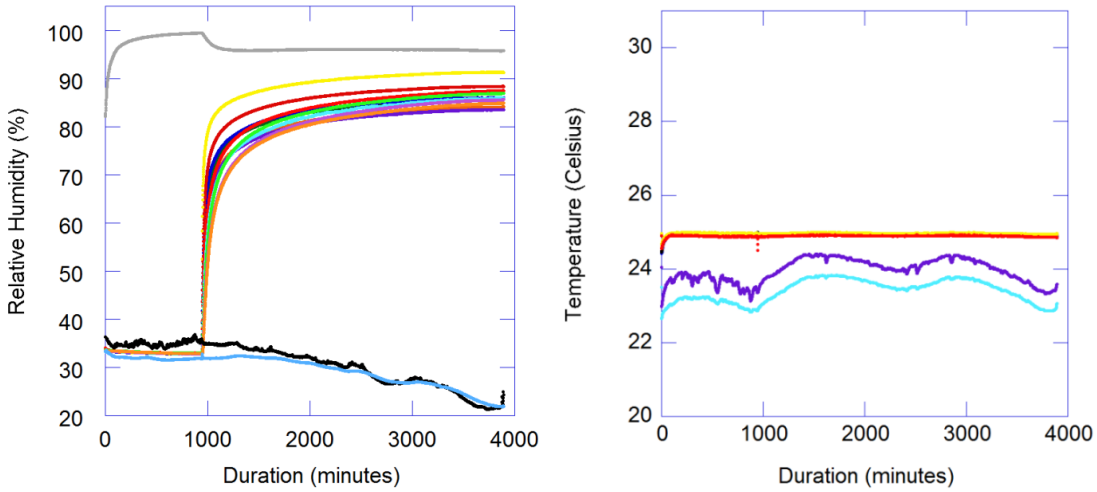

Figure N.2.4-1: Empty_column_trial_4 graphs. Calibrated relative humidity data (left) and temperature data (right) collected during the experiment.

N.2.5 2nd_empty_and_open

This experiment was initiated with the ultrasonic fog generator turned on in the sealed humidity chamber, and the constant temperature box closed. The ultrasonic fog generator was unplugged after a period of time (~2 hours). Temperature was allowed to equilibrate ~10 hours, at which point the humidity chamber was connected to the humidity reservoir. The relative humidity within the lower column of this experiment was significantly lower than in the upper column. This is attributed to interference by the fans located within the box. As a result, this data cannot be compared to other experiments.

Description	Open to the box
Ultrasonic fog generator plugged in	February 21, 2015 08:22
Ultrasonic fog generator unplugged	February 21, 2015 10:32
Column connection	February 21, 2015 20:10
End of experiment	February 24, 2015 14:34
Duration†	2 days, 18 hour, and 24 minutes

† The duration of the experiment is from the time that the humidity chamber is initially connected to the column, until the final data point is collected and the box is opened.

Table N.2.5-1: 2nd_empty_and_open basic information. Basic information concerning the experiment performed.

Humidity Sensor	Initial‡		Final	
	Voltage (mV)	Calibrated % RH	Voltage (mV)	Calibrated % RH
U5-H*	1298	15.75	1283	15.29
U4-H	1373	16.58	3446	81.11
U3-H	1315	17.31	3411	81.57
U2-H	1303	17.03	3397	81.99
U1-H	1361	17.21	3506	81.92
BC1-H	1290	16.73	3267	77.28
L1-H	1282	16.45	1767	31.47
L2-H	1324	17.12	1591	24.59
L3-H	1251	15.33	1387	19.63
L4-H	1308	14.85	1378	17.07
L5-H*	1303	14.67	1287	14.16
BC2-H	4138	102.09	3959	96.60
ROOM1-H	1284	15.32	1219	13.36
BOX1-H	1256	16.07	1244	15.70

‡ Initial conditions are based on the time that the humidity chamber was connected to the humidity reservoir, and not initial conditions when the box was initially sealed.

*Sensors U5-H and L5-H were not connected to the column during this experiment. The sensors laid within the constant temperature box below the lower column.

Table N.2.5-2: 2nd_empty_and_open RH data. Initial and final calibrated relative humidity data from the experiment.

Temperature Sensor	Initial‡	Final	Average ± 1 standard deviation
	°C	°C	°C
U4-T	25.00	25.00	25.09 ± 0.13
U2-T	25.00	25.01	25.08 ± 0.12
BC1-T	25.05	25.04	25.11 ± 0.10
L2-T	25.01	25.02	25.07 ± 0.08
L4-T	25.02	25.04	25.07 ± 0.06
ROOM1-T	24.96	25.17	26.57 ± 1.95
PTEMP	24.67	24.96	26.34 ± 2.02
BOX1-T	24.97	25.04	25.04 ± 0.13

‡ Initial conditions are based on the time that the humidity chamber was connected to the humidity reservoir, and not initial conditions when the box was initially sealed.

Table N.2.5-3: 2nd_empty_and_open temperature data. Initial, final, and average temperature data from the experiment.

Pressure Sensor	Initial‡		Final		Average ± 1 st. dev.	
	mV	kPa	mV	kPa	mV	kPa
Room	3710	93.35	3772	94.73	3750 ± 23.42	94.24 ± 0.52

‡ Initial conditions are based on the time that the humidity chamber was connected to the humidity reservoir, and not initial conditions when the box was initially sealed.

Table N.2.5-4: 2nd_empty_and_open pressure data. Initial, final, and average barometric pressure data from the experiment.

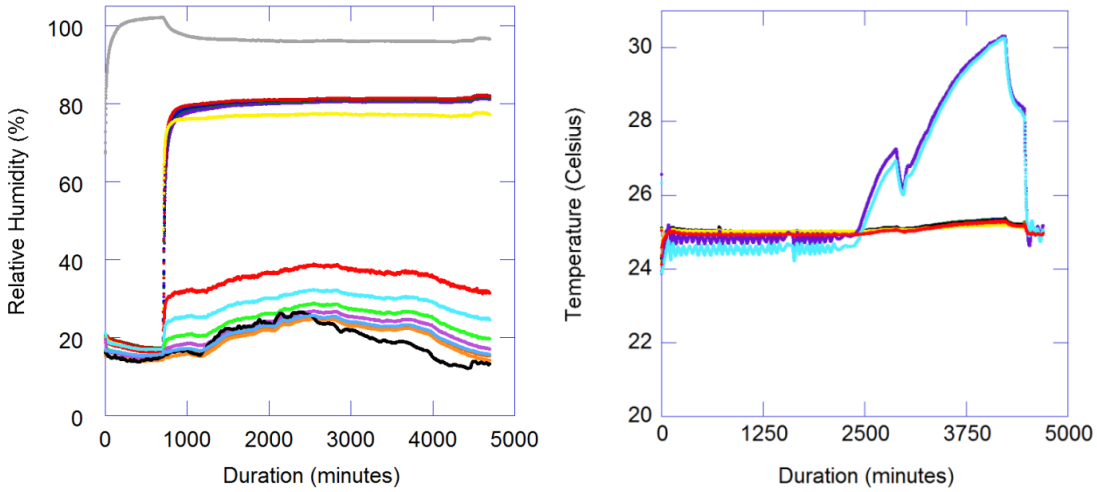

Figure N.2.5-1: 2nd_empty_and_open graphs. Calibrated relative humidity data (left) and temperature data (right) collected during the experiment.

N.2.6 2nd_empty_5routed_bottles

This experiment was initiated with the ultrasonic fog generator turned on in the sealed humidity chamber, and the constant temperature box closed. The ultrasonic fog generator was unplugged after a period of ~2 hours. Temperature was allowed to equilibrate overnight (~12 hours), at which point the humidity chamber was connected to the humidity reservoir. Sensors U5-H and L5-H were connected in the tubing that was used to connect the column to the bottles at a spot near close to its respective sensor socket.

Description	Routed to bottles
Ultrasonic fog generator plugged in	March 9, 2015 15:48
Ultrasonic fog generator unplugged	March 9, 2015 17:39
Column connection	March 10, 2015 08:15
End of experiment	March 12, 2015 15:09
Duration†	2 days, 6 hours, and 54 minutes

† The duration of the experiment is from the time that the humidity chamber is initially connected to the column, until the final data point is collected and the box is opened.

Table N.2.6-1: 2nd_empty_5routed_bottles basic information. Basic information concerning the experiment performed.

Humidity Sensor	Initial‡		Final	
	Voltage (mV)	Calibrated % RH	Voltage (mV)	Calibrated % RH
U5-H*	1415	19.30	2474	51.53
U4-H	1475	19.76	3567	84.88
U3-H	1417	20.44	3520	84.91
U2-H	1403	20.13	3504	85.31
U1-H	1466	20.37	3674	86.99
BC1-H	1404	20.22	3639	88.68
L1-H	1405	20.26	3494	84.94
L2-H	1459	20.89	3679	82.99
L3-H	1387	19.63	3378	82.53
L4-H	1445	19.20	3408	81.59
L5-H*	1384	17.24	2287	45.87
BC2-H	4100	100.92	3987	97.46
ROOM1-H	1405	18.99	1607	25.10
BOX1-H	1376	19.78	1546	25.03

‡ Initial conditions are based on the time that the humidity chamber was connected to the humidity reservoir, and not initial conditions when the box was initially sealed.

*Sensors U5-H and L5-H were not connected to the column during this experiment. The sensors laid within the constant temperature box below the lower column.

Table N.2.6-2: 2nd_empty_5routed_bottles RH data. Initial and final calibrated relative humidity data from the experiment.

Temperature Sensor	Initial‡	Final	Average ± 1 standard deviation
	°C	°C	°C
U4-T	25.04	24.96	24.97 ± 0.02
U2-T	25.03	24.96	24.97 ± 0.02
BC1-T	25.04	24.97	24.99 ± 0.01
L2-T	25.02	24.97	24.98 ± 0.01
L4-T	25.01	24.99	25.00 ± 0.01
ROOM1-T	25.60	24.86	24.89 ± 0.16
PTEMP	25.24	24.57	24.60 ± 0.14
BOX1-T	25.10	24.92	24.93 ± 0.01

‡ Initial conditions are based on the time that the humidity chamber was connected to the humidity reservoir, and not initial conditions when the box was initially sealed.

Table N.2.6-3: 2nd_empty_5routed_bottles temperature data. Initial, final, and average temperature data from the experiment.

Pressure Sensor	Initial‡		Final		Average ± 1 st. dev.	
	mV	kPa	mV	kPa	mV	kPa
Room	3762	94.51	3764	94.55	3764 ± 6.23	94.55 ± 0.14

‡ Initial conditions are based on the time that the humidity chamber was connected to the humidity reservoir, and not initial conditions when the box was initially sealed.

Table N.2.6-4: 2nd_empty_5routed_bottles pressure data. Initial, final, and average barometric pressure data from the experiment.

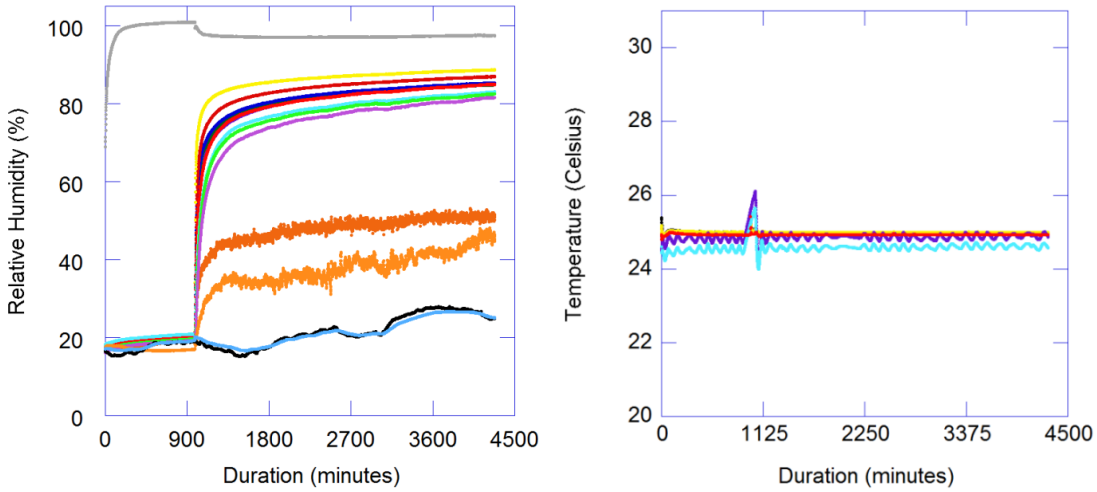

Figure N.2.6-1: 2nd_empty_5routed_bottles graphs. Calibrated relative humidity data (left) and temperature data (right) collected during the experiment.

N.2.7 2nd_empty_5routed_out

This experiment was initiated with the ultrasonic fog generator turned on in the sealed humidity chamber, and the constant temperature box closed. The ultrasonic fog generator was unplugged after a period of ~2 hours. Temperature was allowed to equilibrate overnight (~17 hours), at which point the humidity chamber was connected to the humidity reservoir. Sensors U5-H and L5-H were connected in the tubing that was used to connect the column to the bottles at a spot near close to its respective sensor socket.

Description	Routed out
Ultrasonic fog generator plugged in	February 25, 2015 13:29
Ultrasonic fog generator unplugged	February 25, 2015 15:27
Column connection	February 26, 2015 10:31
End of experiment	March 2, 2015 13:51
Duration†	4 days, 3 hours, and 20 minutes

† The duration of the experiment is from the time that the humidity chamber is initially connected to the column, until the final data point is collected and the box is opened.

Table N.2.7-1: 2nd_empty_5routed_out basic information. Basic information concerning the experiment performed.

Humidity Sensor	Initial‡		Final	
	Voltage (mV)	Calibrated % RH	Voltage (mV)	Calibrated % RH
U5-H	1467	20.89	1647	26.36
U4-H	1726	27.57	3670	88.08
U3-H	1670	28.20	3603	87.45
U2-H	1645	27.64	3611	88.62
U1-H	1720	28.04	3725	88.53
BC1-H	1646	27.63	3668	89.56
L1-H	1624	27.04	3440	83.27
L2-H	1686	27.24	3602	80.83
L3-H	1604	26.48	3250	78.48
L4-H	1657	25.94	3243	76.34
L5-H	1471	20.00	1653	25.77
BC2-H	4119	101.50	4007	98.07
ROOM1-H	1451	20.38	1589	24.55
BOX1-H	1421	21.17	1605	26.85

‡ Initial conditions are based on the time that the humidity chamber was connected to the humidity reservoir, and not initial conditions when the box was initially sealed.

Table N.2.7-2: 2nd_empty_5routed_out RH data. Initial and final calibrated relative humidity data from the experiment.

Temperature Sensor	Initial‡	Final	Average ± 1 standard deviation
	°C	°C	°C
U4-T	25.04	24.95	24.99 ± 0.04
U2-T	25.04	24.96	24.99 ± 0.03
BC1-T	25.08	24.98	25.01 ± 0.03
L2-T	25.03	24.97	25.00 ± 0.02
L4-T	25.05	24.99	25.01 ± 0.02
ROOM1-T	24.99	24.84	25.15 ± 0.55
PTEMP	24.76	24.60	24.87 ± 0.53
BOX1-T	25.21	24.91	24.94 ± 0.03

‡ Initial conditions are based on the time that the humidity chamber was connected to the humidity reservoir, and not initial conditions when the box was initially sealed.

Table N.2.7-3: 2nd_empty_5routed_out temperature data. Initial, final, and average temperature data from the experiment.

Pressure Sensor	Initial‡		Final		Average ± 1 st. dev.	
	mV	kPa	mV	kPa	mV	kPa
Room	3741	94.04	3719	93.55	3723 ± 18.60	93.63 ± 0.42

‡ Initial conditions are based on the time that the humidity chamber was connected to the humidity reservoir, and not initial conditions when the box was initially sealed.

Table N.2.7-4: 2nd_empty_5routed_out pressure data. Initial, final, and average barometric pressure data from the experiment.

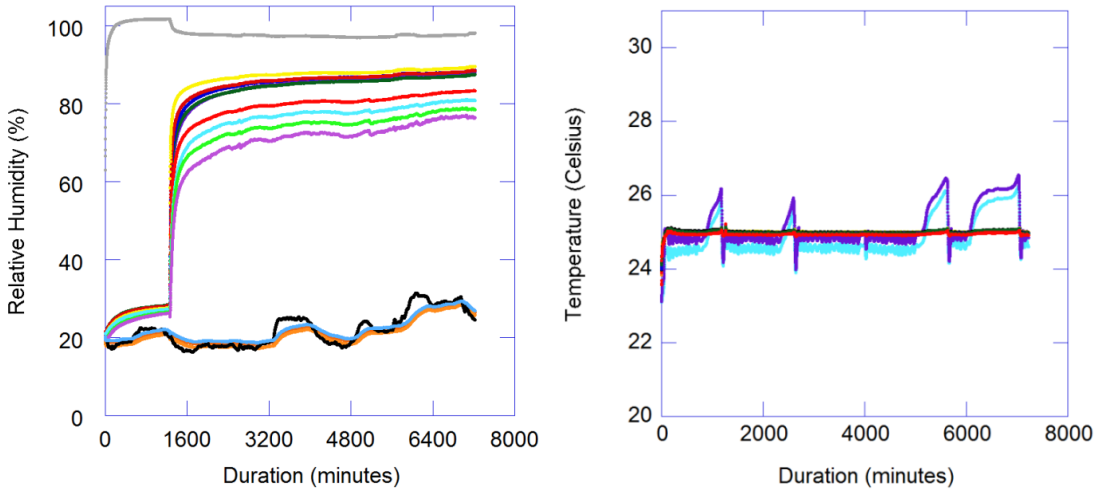

Figure N.2.7-1: 2nd_empty_5routed_out graphs. Calibrated relative humidity data (left) and temperature data (right) collected during the experiment.

N.3: Plastic spheres

N.3.1 BB_test1

This experiment was initiated with the ultrasonic fog generator turned on in the sealed humidity chamber, and the constant temperature box closed. The ultrasonic fog generator was unplugged after a period of ~3 hours. Temperature was allowed to equilibrate overnight (~17 hours), at which point the humidity chamber was connected to the humidity reservoir. Sensors U5-H and L5-H were connected to the column.

Description	Sealed
Ultrasonic fog generator plugged in	November 20, 2014 14:58
Ultrasonic fog generator unplugged	November 20, 2014 17:58
Column connection	November 21, 2014 12:19
End of experiment	December 1, 2014 13:05
Duration†	10 days, 0 hours, and 46 minutes

† The duration of the experiment is from the time that the humidity chamber is initially connected to the column, until the final data point is collected and the box is opened.

Table N.3.1-1: BB_test1 basic information. Basic information concerning the experiment performed.

Humidity Sensor	Initial‡		Final	
	Voltage (mV)	Calibrated % RH	Voltage (mV)	Calibrated % RH
U5-H	1471	19.76	1647	83.49
U4-H	1497	20.02	3670	83.03
U3-H	1438	19.89	3603	84.14
U2-H	1432	20.06	3611	87.48
U1-H	1504	20.21	3725	92.13
BC1-H	1453	20.59	3668	94.10
L1-H	1449	20.60	3440	89.19
L2-H	1499	20.83	3602	86.95
L3-H	1422	20.18	3250	85.37
L4-H	1487	20.27	3243	83.30
L5-H	1486	20.25	1653	82.66
BC2-H	4138	100.70	4007	97.20
ROOM1-H	1551	22.82	1589	30.08
BOX1-H	1431	19.61	1605	22.40

‡ Initial conditions are based on the time that the humidity chamber was connected to the humidity reservoir, and not initial conditions when the box was initially sealed.

Table N.3.1-2: BB_test1 RH data. Initial and final calibrated relative humidity data from the experiment.

Temperature Sensor	Initial‡	Final	Average ± 1 standard deviation
	°C	°C	°C
U4-T	24.74	24.79	24.81 ± 0.05
U2-T	24.75	24.79	24.81 ± 0.05
BC1-T	24.77	24.82	24.85 ± 0.05
L2-T	24.81	24.84	24.86 ± 0.04
L4-T	24.87	24.89	24.91 ± 0.03
ROOM1-T	21.04	21.88	21.83 ± 0.81
PTEMP	20.82	21.41	21.28 ± 0.72
BOX1-T	24.35	24.79	24.82 ± 0.04

‡ Initial conditions are based on the time that the humidity chamber was connected to the humidity reservoir, and not initial conditions when the box was initially sealed.

Table N.3.1-3: BB_test1 temperature data. Initial, final, and average temperature data from the experiment.

Pressure Sensor	Initial‡		Final		Average ± 1 st. dev.	
	mV	kPa	mV	kPa	mV	kPa
Room	3745	94.16	3775	94.83	3770 ± 29.91	94.73 ± 0.67

‡ Initial conditions are based on the time that the humidity chamber was connected to the humidity reservoir, and not initial conditions when the box was initially sealed.

Table N.3.1-4: BB_test1 pressure data. Initial, final, and average barometric pressure data from the experiment.

Column	Pre-experiment weight (g)	Post-experiment weight (g)	Weight added due to adsorption (g)
Upper	805.7	805.7	0.0
Lower	717.0	717.0	0.0

Table N.3.1-5: BB_test1 adsorption. Pre and post experimental weights used to consider the adsorption of water vapor onto the desiccated media.

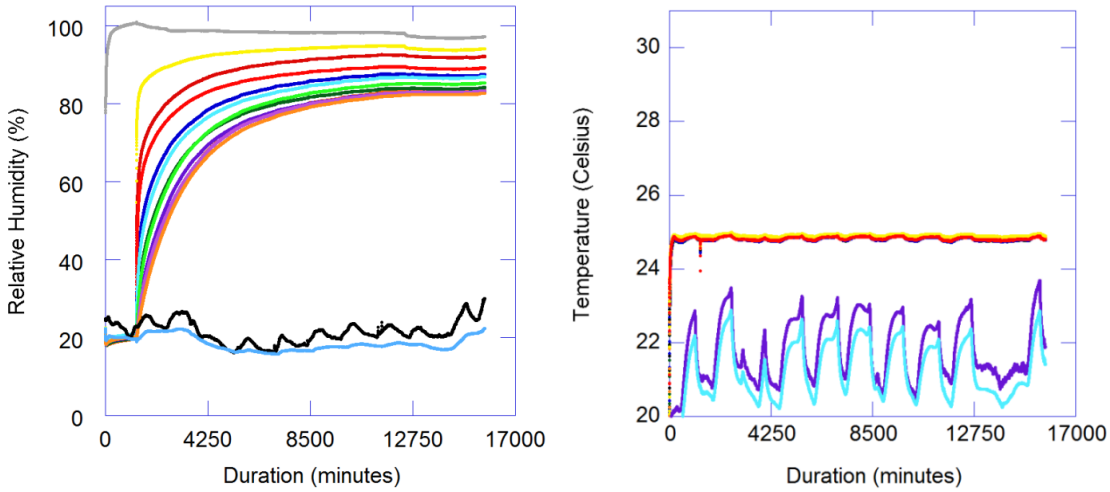

Figure N.3.1-1: BB_test1 graphs. Calibrated relative humidity data (left) and temperature data (right) collected during the experiment.

N.3.2 2nd_BB_routedout

This experiment was initiated with the ultrasonic fog generator turned on in the sealed humidity chamber, and the constant temperature box closed. The ultrasonic fog generator was unplugged after a period of ~2 hours. Temperature was allowed to equilibrate overnight (~11 hours), at which point the humidity chamber was connected to the humidity reservoir. Sensors U5-H and L5-H were connected in the tubing that was used to connect the column to the bottles at a spot near close to its respective sensor socket.

Description	Routed out
Ultrasonic fog generator plugged in	March 16, 2015 16:38
Ultrasonic fog generator unplugged	March 16, 2015 18:28
Column connection	March 17, 2015 07:29
End of experiment	March 23, 2015 13:45
Duration†	6 days, 6 hours, and 16 minutes

† The duration of the experiment is from the time that the humidity chamber is initially connected to the column, until the final data point is collected and the box is opened.

Table N.3.2-1: 2nd_BB_routedout basic information. Basic information concerning the experiment performed.

Humidity Sensor	Initial‡		Final	
	Voltage (mV)	Calibrated % RH	Voltage (mV)	Calibrated % RH
U5-H	1594	24.75	3069	69.63
U4-H	1655	25.36	3468	81.80
U3-H	1596	25.93	3447	82.67
U2-H	1580	25.62	3454	83.75
U1-H	1652	25.99	3673	86.96
BC1-H	1595	26.07	3625	88.25
L1-H	1584	25.80	3288	78.56
L2-H	1644	26.07	3131	67.66
L3-H	1565	25.25	2686	60.67
L4-H	1624	24.89	2501	52.76
L5-H	1567	23.04	1461	19.68
BC2-H	4189	103.65	4022	98.53
ROOM1-H	1568	23.92	1446	20.23
BOX1-H	1529	24.50	1414	20.95

‡ Initial conditions are based on the time that the humidity chamber was connected to the humidity reservoir, and not initial conditions when the box was initially sealed.

Table N.3.2-2: 2nd_BB_routedout RH data. Initial and final calibrated relative humidity data from the experiment.

Temperature Sensor	Initial‡	Final	Average ± 1 standard deviation
	^{O}C	^{O}C	^{O}C
U4-T	24.98	24.96	24.96 ± 0.01
U2-T	24.99	24.96	24.96 ± 0.01
BC1-T	25.00	24.98	24.98 ± 0.01
L2-T	24.99	24.97	24.98 ± 0.01
L4-T	25.01	25.00	25.00 ± 0.01
ROOM1-T	24.82	24.89	24.82 ± 0.09
PTEMP	24.56	24.59	24.52 ± 0.08
BOX1-T	25.00	24.92	24.92 ± 0.01

‡ Initial conditions are based on the time that the humidity chamber was connected to the humidity reservoir, and not initial conditions when the box was initially sealed.

Table N.3.2-3: 2nd_BB_routedout temperature data. Initial, final, and average temperature data from the experiment.

Pressure Sensor	Initial‡		Final		Average ± 1 st. dev.	
	mV	kPa	mV	kPa	mV	kPa
Room	3748	94.20	3751	94.26	3750 ± 9.96	94.25 ± 0.22

‡ Initial conditions are based on the time that the humidity chamber was connected to the humidity reservoir, and not initial conditions when the box was initially sealed.

Table N.3.2-4: 2nd_BB_routedout pressure data. Initial, final, and average barometric pressure data from the experiment.

Column	Pre-experiment weight (g)	Post-experiment weight (g)	Weight added due to adsorption (g)
Upper	804.3	804.5	0.2
Lower	712.0	712.2	0.2

Table N.3.2-5: 2nd_BB_routedout adsorption. Pre and post experimental weights used to consider the adsorption of water vapor onto the desiccated media.

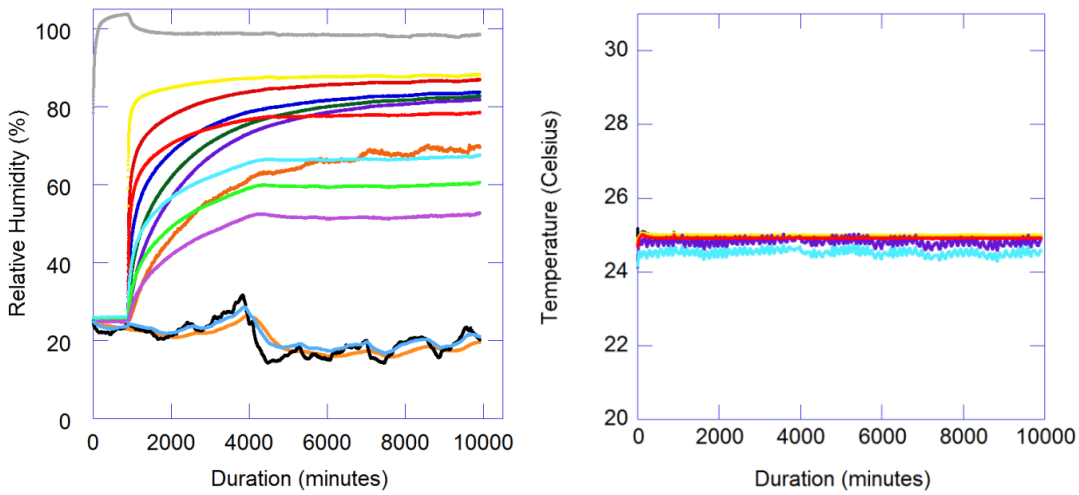

Figure N.3.2-1: 2nd_BB_routedout graphs. Calibrated relative humidity data (left) and temperature data (right) collected during the experiment.

N.4: Medium gravel

N.4.1 Gravel_test1

This experiment was initiated with the ultrasonic fog generator turned on in the sealed humidity chamber, and the constant temperature box closed. The ultrasonic fog generator was unplugged after a period of ~2.5 hours. Temperature was allowed to equilibrate overnight (~21.5 hours), at which point the humidity chamber was connected to the humidity reservoir. Sensors U5-H and L5-H were connected directly to the column.

Description	Sealed
Ultrasonic fog generator plugged in	December 2, 2014 12:22
Ultrasonic fog generator unplugged	December 2, 2014 14:49
Column connection	December 3, 2014 12:16
End of experiment	December 12, 2014 15:27
Duration†	9 days, 3 hours, and 11 minutes

† The duration of the experiment is from the time that the humidity chamber is initially connected to the column, until the final data point is collected and the box is opened.

Table N.4.1-1: Gravel_test1 basic information. Basic information concerning the experiment performed.

Humidity Sensor	Initial‡		Final	
	Voltage (mV)	Calibrated % RH	Voltage (mV)	Calibrated % RH
U5-H	1884	32.82	3388	80.36
U4-H	1913	32.73	3477	80.50
U3-H	1840	32.54	3445	83.04
U2-H	1830	32.73	3487	85.48
U1-H	1909	33.03	3733	90.77
BC1-H	1848	33.26	3733	93.75
L1-H	1853	33.28	3603	88.18
L2-H	1906	32.48	3715	84.29
L3-H	1813	32.73	3253	78.95
L4-H	1879	32.54	3374	79.36
L5-H	1894	32.84	3352	77.84
BC2-H	4173	101.75	4038	97.68
ROOM1-H	1997	36.53	1855	32.17
BOX1-H	1860	32.91	1766	29.99

‡ Initial conditions are based on the time that the humidity chamber was connected to the humidity reservoir, and not initial conditions when the box was initially sealed.

Table N.4.1-2: Gravel_test1 RH data. Initial and final calibrated relative humidity data from the experiment.

Temperature Sensor	Initial‡	Final	Average ± 1 standard deviation
	°C	°C	°C
U4-T	25.00	25.00	25.16 ± 0.05
U2-T	25.00	25.00	25.15 ± 0.05
BC1-T	25.04	25.02	25.17 ± 0.05
L2-T	25.02	25.00	25.11 ± 0.04
L4-T	25.02	25.02	25.10 ± 0.03
ROOM1-T	25.10	25.22	27.38 ± 0.70
PTEMP	24.43	24.71	26.95 ± 0.76
BOX1-T	24.97	24.93	25.04 ± 0.04

‡ Initial conditions are based on the time that the humidity chamber was connected to the humidity reservoir, and not initial conditions when the box was initially sealed.

Table N.4.1-3: Gravel_test1 temperature data. Initial, final, and average temperature data from the experiment.

Pressure Sensor	Initial‡		Final		Average ± 1 st. dev.	
	mV	kPa	mV	kPa	mV	kPa
Room	3759	94.47	3776	94.85	3759 ± 11.60	94.47 ± 0.26

‡ Initial conditions are based on the time that the humidity chamber was connected to the humidity reservoir, and not initial conditions when the box was initially sealed.

Table N.4.1-4: Gravel_test1 pressure data. Initial, final, and average barometric pressure data from the experiment.

Column	Pre-experiment weight (g)	Post-experiment weight (g)	Weight added due to adsorption (g)
Upper	1353.1	1353.4	0.3
Lower	1270.1	1270.5	0.4

Table N.4.1-5: Gravel_test1 adsorption. Pre and post experimental weights used to consider the adsorption of water vapor onto the desiccated media.

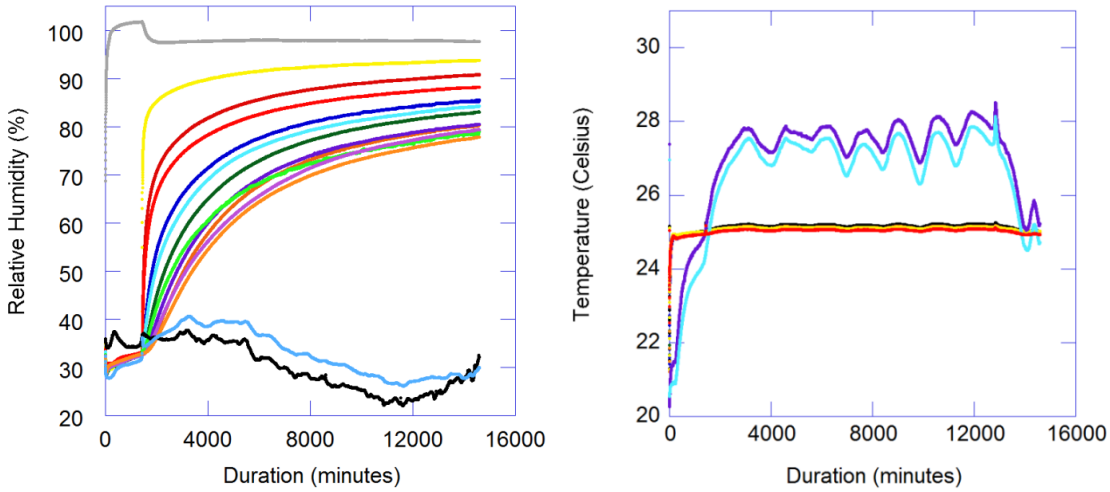

Figure N.4.1-1: Gravel_test1 graphs. Calibrated relative humidity data (left) and temperature data (right) collected during the experiment.

N.5: Very fine gravel

N.5.1 2nd_gravel_routedout

This experiment was initiated with the ultrasonic fog generator turned on in the sealed humidity chamber, and the constant temperature box closed. The ultrasonic fog generator was unplugged after a period of ~2.5 hours. Temperature was allowed to equilibrate overnight (~13 hours), at which point the humidity chamber was connected to the humidity reservoir. Sensors U5-H and L5-H were connected in the tubing that was used to connect the column to the bottles at a spot near close to its respective sensor socket.

Description	Routed out
Ultrasonic fog generator plugged in	March 24, 2015 14:10
Ultrasonic fog generator unplugged	March 24, 2015 16:44
Column connection	March 25, 2015 07:32
End of experiment	April 6, 2015 10:29
Duration†	12 days, 2 hours, and 57 minutes

† The duration of the experiment is from the time that the humidity chamber is initially connected to the column, until the final data point is collected and the box is opened.

Table N.5.1-1: 2nd_gravel_routedout basic information. Basic information concerning the experiment performed.

Humidity Sensor	Initial‡		Final	
	Voltage (mV)	Calibrated % RH	Voltage (mV)	Calibrated % RH
U5-H	1475	21.13	2420	49.88
U4-H	1589	23.31	3342	77.87
U3-H	1542	24.27	3349	79.67
U2-H	1549	24.66	3443	83.41
U1-H	1644	25.74	3645	86.11
BC1-H	1594	26.04	3619	88.06
L1-H	1585	25.83	3259	77.66
L2-H	1614	25.23	3037	65.03
L3-H	1512	23.58	2570	57.00
L4-H	1558	22.79	2389	49.20
L5-H	1445	19.17	1338	15.78
BC2-H	4187	103.59	4006	98.04
ROOM1-H	1434	19.86	1397	18.74
BOX1-H	1379	19.87	1312	17.80

‡ Initial conditions are based on the time that the humidity chamber was connected to the humidity reservoir, and not initial conditions when the box was initially sealed.

Table N.5.1-2: 2nd_gravel_routedout RH data. Initial and final calibrated relative humidity data from the experiment.

Temperature Sensor	Initial‡	Final	Average ± 1 standard deviation
	°C	°C	°C
U4-T	24.97	24.97	24.97 ± 0.01
U2-T	24.97	24.97	24.97 ± 0.01
BC1-T	24.98	24.99	24.98 ± 0.01
L2-T	24.99	24.98	24.98 ± 0.01
L4-T	25.00	25.00	25.00 ± 0.01
ROOM1-T	24.80	24.89	24.88 ± 0.21
PTEMP	24.53	24.61	24.60 ± 0.19
BOX1-T	24.92	24.92	24.92 ± 0.01

‡ Initial conditions are based on the time that the humidity chamber was connected to the humidity reservoir, and not initial conditions when the box was initially sealed.

Table N.5.1-3: 2nd_gravel_routedout temperature data. Initial, final, and average temperature data from the experiment.

Pressure Sensor	Initial‡		Final		Average ± 1 st. dev.	
	mV	kPa	mV	kPa	mV	kPa
Room	3773	94.75	3728	93.75	3750 ± 23.53	94.25 ± 0.53

‡ Initial conditions are based on the time that the humidity chamber was connected to the humidity reservoir, and not initial conditions when the box was initially sealed.

Table N.5.1-4: 2nd_gravel_routedout pressure data. Initial, final, and average barometric pressure data from the experiment.

Column	Pre-experiment weight (g)	Post-experiment weight (g)	Weight added due to adsorption (g)
Upper	1411.7	1412.1	0.4
Lower	1324.2	1324.4	0.2

Table N.5.1-5: 2nd_gravel_routedout adsorption. Pre and post experimental weights used to consider the adsorption of water vapor onto the desiccated media.

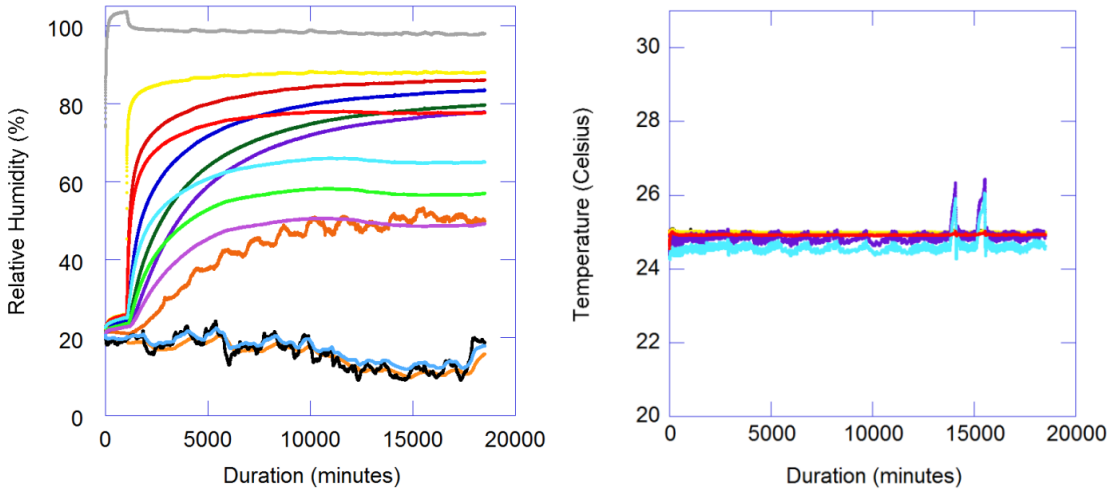

Figure N.5.1-1: 2nd_gravel_routedout graphs. Calibrated relative humidity data (left) and temperature data (right) collected during the experiment.

N.6: 30-40 sand

N.6.1 Sand_routedout

This experiment was initiated with the ultrasonic fog generator turned on in the sealed humidity chamber, and the constant temperature box closed. The ultrasonic fog generator was unplugged after a period of ~2.5 hours. Temperature was allowed to equilibrate overnight (~12 hours), at which point the humidity chamber was connected to the humidity reservoir. Sensors U5-H and L5-H were connected in the tubing that was used to connect the column to the bottles at a spot near close to its respective sensor socket.

Description	Routed out
Ultrasonic fog generator plugged in	April 8, 2015 14:50
Ultrasonic fog generator unplugged	April 8, 2015 17:30
Column connection	April 9, 2015 07:20
End of experiment	July 9, 2015 15:10
Duration†	91 days, 7 hours, and 50 minutes

† The duration of the experiment is from the time that the humidity chamber is initially connected to the column, until the final data point is collected and the box is opened.

Table N.6.1-1: Sand_routedout basic information. Basic information concerning the experiment performed.

Humidity Sensor	Initial‡		Final	
	Voltage (mV)	Calibrated % RH	Voltage (mV)	Calibrated % RH
U5-H	1195	12.61	2319	46.81
U4-H	1000	4.97	3500	82.79
U3-H	923	5.30	3497	84.20
U2-H	921	5.18	3587	87.88
U1-H	1019	6.89	3793	90.58
BC1-H	1029	8.73	3771	92.72
L1-H	985	7.26	3647	89.68
L2-H	983	7.58	3765	85.39
L3-H	916	4.75	3390	82.91
L4-H	964	3.92	3422	82.03
L5-H	1185	10.93	2231	44.10
BC2-H	4210	104.29	4092	100.68
ROOM1-H	1271	14.93	1739	29.09
BOX1-H	1237	15.49	1780	32.25

‡ Initial conditions are based on the time that the humidity chamber was connected to the humidity reservoir, and not initial conditions when the box was initially sealed.

Table N.6.1-2: Sand_routedout RH data. Initial and final calibrated relative humidity data from the experiment.

Temperature Sensor	Initial‡	Final	Average ± 1 standard deviation
	°C	°C	°C
U4-T	25.01	25.00	24.97 ± 0.01
U2-T	25.01	25.00	24.97 ± 0.01
BC1-T	25.02	25.00	24.98 ± 0.01
L2-T	25.01	25.00	24.98 ± 0.01
L4-T	25.01	25.01	25.00 ± 0.01
ROOM1-T	25.37	24.86	24.85 ± 0.15
PTEMP	25.00	24.53	24.48 ± 0.15
BOX1-T	24.94	24.96	24.93 ± 0.01

‡ Initial conditions are based on the time that the humidity chamber was connected to the humidity reservoir, and not initial conditions when the box was initially sealed.

Table N.6.1-3: Sand_routedout temperature data. Initial, final, and average temperature data from the experiment.

Pressure Sensor	Initial‡		Final		Average ± 1 st. dev.	
	mV	kPa	mV	kPa	mV	kPa
Room	3759	94.44	3707	93.28	3729 ± 13.84	93.77 ± 0.31

‡ Initial conditions are based on the time that the humidity chamber was connected to the humidity reservoir, and not initial conditions when the box was initially sealed.

Table N.6.1-4: Sand_routedout pressure data. Initial, final, and average barometric pressure data from the experiment.

Column	Pre-experiment weight (g)	Post-experiment weight (g)	Weight added due to adsorption (g)
Upper	1313.2	1314.8	1.6
Lower	1222.8	1223.7	0.9

Table N.6.1-5: Sand_routedout adsorption. Pre and post experimental weights used to consider the adsorption of water vapor onto the desiccated media.

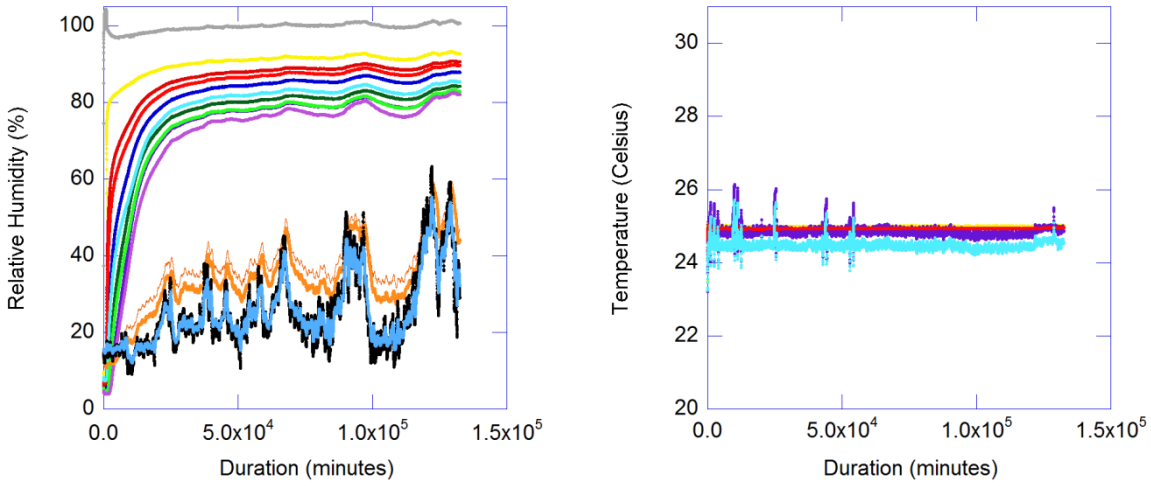

Figure N.6.1-1: Sand_routedout graphs. Calibrated relative humidity data (left) and temperature data (right) collected during the experiment.

REFERENCES CITED

Abtew, W., and Melesse, A., 2013, Evaporation and evapotranspiration: Measurements and estimations, Springer Science, DOI 10.1007/978-94-007-4737-1_5, p. 53-62.

Baehr, Arthur L., 1987, Selective transport of hydrocarbons in the unsaturated zone due to aqueous and vapor phase partitioning, Water Resources Research, v. 23, no. 10, p. 1926-1938.

Bouwer, Herman, 1991, Simple derivation of the retardation equation and application to preferential flow and macrodispersion, Groundwater, v. 29, No. 1, p. 41-46.

Department of Energy, 2008, Deep vadose zone treatability test plan for the Hanford Central Plateau, DOE/RL-2007-56.

Falta, R. W., Javandel, I., Pruess, K., and Witherspoon, P. A., 1989, Density-driven flow of gas in the unsaturated zone due to the evaporation of volatile organic compounds, Water Resources Research, v. 25, no. 10, p. 2159-2169.

Fluor Hanford, INC, 2006, Evaluation of vadose zone treatment technologies to immobilize Technetium-99, WMP-27397.

Ho and Webb, 2006, Gas transport in porous media, Springer, v. 20.

Hillel, Daniel, 1998, Environmental Soil Physics, Academic Press, p. 103-104.

Kreamer, David K., Weeks, Edwin P., and Thompson, Glenn M., 1988, A field technique to measure the tortuosity and sorption-affected porosity for gaseous diffusion of materials in the unsaturated zone with experimental results from near Barnwell, South Carolina, Water Resources Research, v. 24, no. 3, p. 331-341.

Lawrence, Mark, G., 2005, The relationship between relative humidity and the dew point temperature in moist air, American Meteorological Society, February, p. 225-233.

Lide, David R., ed. (2005), CRC Handbook of Chemistry and Physics, Boca Raton, Florida, CRC Press.

Millington, R. J., and Quirk, J. P., 1960, Permeability of porous solids, Transactions of the Faraday Society, v. 57, issue 8, p. 1200-1207.

Nield, Donald A., and Bejan, Adrian, 2006, Convection in Porous Media, Springer Science and Business Media, Inc., p. 6-7, 52.

Oostrom, M., Wietsma, T. W., Dane, J. H., Truex, M. J., and Ward, A.L., 2009, Desiccation of unsaturated porous media: Intermediate-scale experiments and numerical simulation, Vadose Zone Journal, v. 8, no. 3, p. 643-650.

Richards, L. A., 1931, Capillary conduction of liquids through porous mediums, Journal of Applied Physics, v. 1, p. 318-333.

Roy, P.D., Josenhans, W.T., and Miller, C.H., 1970, Variations in air viscosity due to changes in water vapor pressure for isothermal conditions at temperatures below 40 ^{o}C, Canadian Journal of Physiology and Pharmacology, v. 48, p. 50-53.

Ruiz, J., Bilbao, R., and Murillo, M., 1998, Adsorption of different VOC onto soil minerals from gas phase: Influence of mineral, type of VOC, and air humidity, Environmental Science and Technology, v. 32, no. 8, p. 1079-1084.

Truex, M. J., Oostrom, M., Strickland, C. E., Benecke, M. W., and Johnson, C. D., 2011, Field-scale assessment of desiccation implementation for deep vadose zone contaminants, Vadose Zone Journal, v. 10, Special Section: Contaminants in the vadose zone.

Ward, A. L., Oostrom, M., and Bacon, D.H., 2008, Experimental and numerical investigations of soil desiccation for vadose zone remediation: Summary report for fiscal year 2007, PNNL-17274.

CURRICULUM VITAE

Taylor Arland Ball

Taylor.arland.ball@gmail.com 951-235-0027 6223 Ordaz Ave. #101 Henderson, NV 89011

EDUCATION

University of Nevada, Las Vegas

January 2013 to present

MS Geoscience emphasis: Hydrogeology - Current GPA: 3.95/4.0

Thesis: Rewetting of artificially desiccated soil: Effect of gravity on vapor phase diffusion.

Brigham Young University

June 2006 to August 2012

BS Geology - GPA: 3.42/4.0

EMPLOYMENT HISTORY

Broadbent and Associates – Henderson, Nevada

August 2015 to present

Staff Geologist

Perform a variety of field work including groundwater sampling and core logging.

Oversee excavation of contaminated soil, and other remediation efforts.

Desert Research Institute – Las Vegas, Nevada

June 2014 to present

Design an experiment to monitor Radon gas in the soil.

Write CRBasic programs for a CR1000 data logger for use in the experiment.

Complete a variety of field based projects.

Graduate Teaching Assistantship – Las Vegas, Nevada

Geography Teaching Assistant/Head T.A.

January 2013 to present

Lead weekly meetings to prepare fellow TA's for teaching responsibilities.

First Service Residential – Las Vegas, Nevada

Customer Care Representative

October 2012 – December 2013

Work in a call center environment assisting customers access Home Owner's Association information from an online database.

BYU Electric Shop – Provo, Utah

Elevator Technician

May 2010 – August 2012

Repair and maintain elevator equipment. All experience gained on the job.

RELEVANT COURSEWORK

Engineering Geology

Application of physical geology to construction and engineering. Focus on slope stability, factor of safety, stability testing, and methods to test rock strength.

Geologic Methods and Research

Discussion on the methods of scientific research and research design. Presentation preparation and presentation practices.

Geology Field Camp (8 weeks)

Geologic Mapping, Groundwater & Hydrological Analysis, Well Coring, Seismic Analysis, GPR, Structural Geology, Creating Stratigraphic Columns, Geologic Hazard Interpretation, Creation of Geologic Cross Sections.

Geochemistry

Mathematically describing geochemical fractionation, kinetics, mixing, transport, and equilibrium with regards to climate, solid earth, rives, and other planets.

Stable Isotope Geochemistry

Use of stable isotopes as geothermometers and to help with a variety of environmental issues. Presented information on the use of isotopes to determine evaporation in the vadose zone.

Hydrogeology

Developed an in-depth understanding of physical hydrogeology. Developed a working use of the methods of hydrogeology to enhance problem-solving techniques. Wrote weekly reports on water related problems and solutions.

Structural Geology

A structural analysis of the Wasatch Fault was required using field data that was collected over several weeks.

Mineral Analysis of Utah Lake Sediments

Researched minerals found in Utah Lake Sediments to help indicate their watershed origin. Research was conducted by X-ray diffraction data and computer analysis. Study also included the effect of sediments on local biology.

Geology of Metallic Ores

Experience identifying rocks and alteration commonly found in the Porphyry, Carlin, Epithermal, and Skarn deposits that are common in Nevada.

Rock/Soil Analysis of the Carmel Formation

A team field project consisting of measuring, describing, and mapping the Carmel Formation in Eastern Utah. Included grain size analysis, rock classification, color, bedform structures, thickness, fossil identification, bounding surfaces, etc. A stratigraphic column and report were created to provide a geologic summary of the area.

Groundwater Analysis of Pilot Valley, NV

A group field study of the hydrogeological system in Pilot Valley, Nevada. A report was produced describing the groundwater system in two aquifers. Field work consisted of well construction, well monitoring, and spring reconnaissance.

Topics in Advanced Geochemistry

Focused on the requirements for habitability on Earth and throughout the solar system. Course required discussions on scientific papers written on a variety of topics related to habitability, student led papers, and presentations.

Principles of Hydrology and Hydraulics

Discussion of modern concepts in Hydrology and Hydraulics. Students were required to develop a model and attempt to answer a question with the model developed.

GIS: Theory and Applications

Developed a working knowledge on how different GIS technologies were developed and how they are applied. Course required an individual project that used Arc GIS to solve a problem or answer a question. Weekly labs provided regular exposure to GIS software to achieve proficiency.

Sedimentology and Stratigraphy

Developed a basic understanding of a variety of topics such as erosion, sediment transport and deposition, depositional systems, and facies analysis.

Geophysics

Basic principles related to the physics of the earth. Seismology, gravity, seismic, magnetic, electrical, and heat flow properties.

Structural Geology

Basic principles related to structural geology. Mapping and measuring structures in the field. Developing cross sections and geologic interpretations of structures. Developed a regional tectonic interpretation based on structural evidence found locally in individual outcrops.

HONORS AND ACHIEVEMENTS

- **2014 1st place in graduate poster competition at the UNLV Geosymposium.**
- **2014 Sponsored member of the International Association of Hydrogeologists (IAH).**
- **2013-2014 Graduate Assistantship.**
- **Eagle Scout (Boy Scouts of America)**

SPECIAL SKILLS

Language

Fluent in speaking, writing, and reading Portuguese.

Basic Spanish skills.

Computer

Arc GIS

MS Office Suite

Adobe Illustrator and Photoshop

CRBasic to program Campbell Dataloggers (self-taught)

SERVICE

July 2007 to July 2009 – Rio Grande do Sul, Brazil

Two years of service spent in Southern Brazil. On a daily basis, I was meeting new people and engaging them in conversation and discussion. I also held different positions of responsibility, which included organizing, and leading meetings of 6 to 8 other people as well as training new arrivals. During this period, I spent time helping various people with physical jobs like building houses and teaching English.

INTERESTS

Basketball, Hiking, Camping, and spending time with my wife and daughter. A recent interest I have is geocaching.